Optimal Planning and Operation of AC-DC Hybrid Distribution Systems

by

Haytham Mohamed Abdelrahman Mohamed Ahmed

A thesis
presented to the University of Waterloo
in fulfillment of the
thesis requirement for the degree of
Doctor of Philosophy
in
Electrical and Computer Engineering

Waterloo, Ontario, Canada, 2017

© Haytham Mohamed Abdelrahman Mohamed Ahmed 2017

Examining Committee Membership

The following served on the Examining Committee for this thesis. The decision of the Examining Committee is by majority vote.

Supervisor	Prof. Magdy Salama
External Examiner	Prof. Mohamed E. El-Hawary
Internal Member	Prof. Mohamed Oussama Damen
Internal Member	Prof. Tarek Abdelgalil
Internal-external Member	Prof. Eihab Abdel-Rahman

AUTHOR'S DECLARATION

I hereby declare that I am the sole author of this thesis. This is a true copy of the thesis, including any required final revisions, as accepted by my examiners.

I understand that my thesis may be made electronically available to the public.

Abstract

Recent years have been marked by a significant increase in interest in green technologies, which have led to radical changes in the way electric power is generated and utilized. These changes have been accompanied by greater utilization of DC-based distributed generators (DGs), such as photovoltaic (PV) panels and fuel cells, as well as DC-based load demands, such as electric vehicles (EVs) and modern electronic loads. In addition to accommodating these technologies, future distribution systems (DSs) will also need to support the integration of additional battery storage systems with renewable DGs. A further factor is the number of policies that have been implemented in Ontario, Canada, with the goal of encouraging the use of clean energy. The first, the feed-in-tariff (FIT) program, was introduced to promote the application of renewable DGs, including PV panels and wind DGs, and a second, new program that offers incentives for switching to EVs has been announced recently. The result is that future DSs must include additional DC loads and DC-based DGs along with their present AC loads and energy resources. Future DSs should thus become AC-DC hybrids if they are to provide optimal accommodation of all types of AC and DC loads and DGs. These considerations accentuate the need for reliable techniques appropriate for the planning and operation of future hybrid DSs.

This thesis presents new directions for the planning and operation of AC-DC hybrid DSs. The main target of the research presented in this thesis is to optimally accommodate the expected high penetration of DC loads and DC-based DGs in future DSs. Achieving this target entailed the completion of four consecutive parts: 1) developing a unified load flow (LF) model for AC-DC hybrid DSs, 2) introducing an energy management scheme (EMS) for the optimal operation of AC-DC hybrid DSs, 3) introducing a planning model to determine the optimal AC-DC network configuration that minimizes the costs of the hybrid DS, and 4) developing a reliability-based planning technique for the simultaneous optimization of the DS costs and reliability.

The first part of this research introduces a novel unified LF model for AC-DC hybrid DSs. The LF model can be applied in hybrid DSs with a variety of configurations for AC/DC buses and AC/DC lines. A new classification of DS buses is introduced for LF analysis. Three binary matrices, which are used as a means of describing the configuration of the AC and DC buses and lines, have been employed in the construction of the unified power equations. The LF model is generic and can be used for both grid-connected and isolated hybrid DSs. The new model has been tested using several case studies of hybrid DSs that include different operational modes for the AC and DC DGs. The effectiveness

and accuracy of the developed LF model has been verified against the steady-state solution produced by PSCAD/EMTDC software.

The second part presents a two-stage EMS that can achieve optimal and reliable operation for AC-DC hybrid DSs. The first stage introduces a network reconfiguration algorithm to determine the optimal day-ahead reconfiguration schedule for a hybrid DS, while considering the forecasted data for load demands and renewable DGs. The objective of the reconfiguration algorithm is the minimization of DS energy losses. The second stage introduces a real-time optimal power flow (OPF) algorithm that minimizes the DS operation costs. In addition, a load-curtailment-management (LCM) technique is integrated with the OPF algorithm in order to guarantee optimal and reliable DS operation in the case of abnormal operating conditions.

The third part presents a novel stochastic planning model for AC-DC hybrid DSs. Taking into account the possibility of each line/bus being AC or DC, the model finds the optimal AC-DC hybrid configuration of buses and lines in the DS. It incorporates consideration of the stochastic behavior of load demands and renewable DGs. The stochastic variations are addressed using a Monte-Carlo simulation (MCS). The objective of the planning model is the minimization of DS investment and operation costs. The developed planning model has been employed for finding the optimal configuration for a suggested case study that included PV panels, wind DGs, and EV charging stations. The same case study was also solved using a traditional AC planning technique in order to evaluate the effectiveness of the hybrid planning model and the associated cost-savings.

The last part of this research introduces a stochastic multi-objective optimization model for the planning of AC-DC hybrid DSs. The introduced model determines the optimal AC-DC network configuration that achieves two objectives: 1) minimizing system costs, and 2) maximizing system reliability. Network buses and lines can become either AC or DC in order to achieve the planning objectives. The model features an MCS technique for addressing stochastic variations related to load demands and renewable DGs. The developed model has been tested using a case study involving a hybrid DS that included a variety of types of loads and DGs. Solving the same case study using a traditional AC planning technique provided verification of the benefits offered by the developed model, whose efficacy was confirmed through a comparison of the AC and hybrid Pareto fronts. The developed planning framework represents an effective technique that can be used by DS operators to identify the optimal AC-DC network configuration of future hybrid DSs.

Acknowledgements

First and foremost, all praise and thanks are due to Allah Almighty for granting me the strength and knowledge to achieve this work.

I would like to express my deepest gratitude to my advisor, Professor Magdy Salama, for his continuous support, encouragement, and valuable advice throughout the course of my research. His excellent guidance was crucial for the completeness of this thesis.

My appreciation and thanks are also extended to my PhD committee members: Professor Mohamed El-Hawary, Professor Mohamed Oussama Damen, Professor Tarek Abdelgalil, and Professor Eihab Abdel-Rahman for investing time in reading and providing many valuable comments on my thesis.

My sincere thanks go to my dear friend Dr. Ayman Eltantawy, whose valuable discussions, advice, and support inspired me and helped me during my PhD period.

I would like to express my deepest gratitude and respect to my parents, Mohamed Abdelrahman and Hamida Mohamed, for their continuous encouragement, support, patience, and prayers. I would like also to thank my brother Hossam Mohamed for his support and encouragement. Also, my sincere thanks and respect go to my wife's parents, Moheyeldin Abdeen and Sahar Alantary, for their unlimited support, encouragement, and prayers.

Finally, I would like to express my special thanks to my wife, Eman Abdeen, for her endless love, patience, understanding, and support during my PhD journey. Also, I would like to thank my daughter Salma and my son Ali for giving me the happiness and strength. Without my family, I would have never been able to finish this work.

Dedication

To my parents,
my wife's parents,
my wife Eman,
my daughter Salma,
and my son Ali ...

Table of Contents

List of Tables

List of Figures

Nomenclature

Acronyms

AC	Alternating current
ACB	AC breaker
DC	Direct current
DCB	DC breaker
DG	Distributed generator
DNLP	Nonlinear programming problem with discontinuous derivatives
DS	Distribution system
DSM	Demand-side management
DSS	Distribution substation
EENS	Expected energy not supplied
EMS	Energy management scheme
EV	Electric vehicle
EVS	Electric vehicle station
FIT	Feed-in-tariff program

GA	Genetic algorithm
GAMS	General algebraic modeling system
GRG	Generalized reduced gradient method
HVDC	High voltage direct current
LCM	Load curtailment management
LF	Load flow
MCS	Monte-Carlo Simulation
NSGA	Non-dominated sorting genetic algorithm
OPF	Optimal power flow
PV	Photovoltaic
VSC	Voltage source converter

Parameters

α_f^{min}	The minimum permissible number of feasible OPF solutions as a percentage of the total number of solutions for different MCS scenarios.
$\alpha_{L_{i,ac}}$	Maximum allowable curtailment ratio for AC load i, as a %.
$\alpha_{L_{k,dc}}$	Maximum allowable curtailment ratio for DC load k, as a %.
β_m	Annual maintenance cost, as a percentage of the investment costs.
Δt	Duration of each time interval, equal to 1 h.
$\eta_{c\text{-}n\text{-}i}$	Efficiency of an interfacing inverter at bus n, as a %.
$\eta_{c\text{-}n\text{-}r}$	Efficiency of an interfacing rectifier at bus n, as a %.
$\eta_{c\text{-}nm\text{-}i}$	Efficiency of the VSC (c) that functions as an inverter at bus n, between buses n and m, as a %.

$\eta_{c\text{-}nm\text{-}r}$	Efficiency of the VSC (c) that functions as a rectifier at bus n, between buses n and m, as a %.
λ_f	Failure rate of a DS component, in f/year.
$\lambda_{L_{i,ac}}$	Load-curtailment cost for AC load i.
$\lambda_{L_{k,dc}}$	Load-curtailment cost for DC load k.
ω^*	Nominal frequency.
ω_0	No-load frequency for an AC DG.
ψ_p^{ac}	Active power droop-gain for an AC DG.
ψ_p^{dc}	DC Power droop-gain for a DC DG.
ψ_q^{ac}	Reactive power droop-gain for an AC DG.
ε	A selected small tolerance.
B_{nm}	Susceptance of the AC line connecting buses n and m, p.u.
$C_{acb\text{-}G_n^{ac}}$	Cost of an AC breaker for the AC DG at bus n.
$C_{acb\text{-}L_n^{ac}}$	Cost of an AC breaker for the AC load at bus n.
$C_{acb\text{-}n\text{-}i}$	Cost of an AC breaker for an inverter at bus n.
$C_{acb\text{-}n\text{-}r}$	Cost of an AC breaker for a rectifier at bus n.
$C_{acb\text{-}nm}$	Cost of an AC breaker connected in line nm.
C_{acl}	Cost of AC lines, in k$/mile.
$C_{dcb\text{-}G_n^{dc}}$	Cost of a DC breaker for the DC DG at bus n.
$C_{dcb\text{-}L_n^{dc}}$	Cost of a DC breaker for the DC load at bus n.
$C_{dcb\text{-}n\text{-}i}$	Cost of a DC breaker for an inverter at bus n.

$C_{dcb\text{-}n\text{-}r}$	Cost of a DC breaker for a rectifier at bus n.
$C_{dcb\text{-}nm}$	Cost of a DC breaker connected in line nm.
C_{dcl}	Cost of DC lines, in k$/mile.
$C^{ac}_{G_j}$	Energy cost of the AC generator j, in $/MWh.
$C^{dc}_{G_l}$	Energy cost of the DC generator l, in $/MWh.
$C_{i\text{-}G^{dc}_n}$	Cost of an inverter for the DC DG at bus n.
$C_{i\text{-}L^{ac}_n}$	Cost of an inverter for the AC load at bus n.
$C_{r\text{-}G^{ac}_n}$	Cost of a rectifier for the AC DG at bus n.
$C_{r\text{-}L^{dc}_n}$	Cost of a rectifier for the DC load at bus n.
$C_{vsc\text{-}nm}$	Cost of a VSC connected in line nm.
d	Discount rate, as a %.
G_{nm}	Conductance of the AC line connecting buses n and m, p.u.
G^{dc}_{nm}	Conductance of the DC line connecting buses n and m, p.u.
K_c	Constant of the voltage source converter.
L_{nm}	Inductance of the AC line connecting buses n and m.
$N^{max}_{l,n}$	Maximum permissible number of lines that can be connected to bus n.
$N^{min}_{l,n}$	Minimum permissible number of lines that can be connected to bus n.
$N^{max}_{SW,s}$	Maximum number of daily switching actions for each controlled switch s.
$N^{max}_{SW,t}$	Maximum number of switching actions at time t.
P^{ac}_{Ln}	Active power demand for the AC load at bus n.
P^{dc}_{Ln}	Power demand for the DC load at bus n.

P_{TD} Total active power demand for the system loads.

$PF_{L_{i,ac}}$ Constant power factor for AC load i.

$Pr_{f,k}$ Probability of the failure of DS component k. Component k can be an AC breaker (acb), a DC breaker (dcb), an AC line (acl), a DC line (dcl), an inverter (c-i), a rectifier (c-r), or a VSC (vsc).

Q_{Ln}^{ac} Reactive power demand for the AC load at bus n.

R^{dc} Resistance of a DC line, equal to $(1/G^{dc})$.

R_{nm} Resistance of the AC line connecting buses n and m.

S_{base} Base power for the AC-DC network, in MVA.

t_f Failure duration (or mean repair time), in h/f.

$U_{f,k}$ Unavailability of DS component k, in h/year. Component k can be an AC breaker (acb), a DC breaker (dcb), an AC line (acl), a DC line (dcl), an inverter (c-i), a rectifier (c-r), or a VSC (vsc).

V_0^{ac} No-load voltage for an AC DG.

V_0^{dc} No-load voltage for a DC DG.

V_{base}^{ac} Base value of the AC voltage, in kV.

V_{base}^{dc} Base value of the DC voltage, in kV.

X_{nm} Minimum available distance between bus n and bus m, in miles.

$\blacklozenge^{max}$ Maximum limit of the variable $\blacklozenge$.

$\blacklozenge^{min}$ Minimum limit of the variable $\blacklozenge$.

Sets

$\mathbb{S}$ Set of available network sections that have the flexibility to be either open or closed.

$\mathbb{S}_c$	Set of network sections that are permanently closed.
$\mathcal{N}_{LCM}^{ac}$	Set of AC loads participating in the load-curtailment program.
$\mathcal{N}_{LCM}^{dc}$	Set of DC loads participating in the load-curtailment program.
$\mathcal{N}_{MCS}$	Set of MCS scenarios.
$\mathfrak{B}_G^{ac}$	Set of AC generators in the system.
$\mathfrak{B}_G^{dc}$	Set of DC generators in the system.
N_b	Set of network buses.
N_c	Set of AC-DC converters in the system.
T	Set of time intervals of the next day.
T_P	Planning period (or planning horizon), in years.

Variables

$\Delta P_{L_i}^{ac}$	Curtailed active power for AC load i.
$\Delta P_{L_k}^{dc}$	Curtailed power for DC load k.
$\Delta Q_{L_i}^{ac}$	Curtailed reactive power for AC load i.
$\mathbb{E}\,(\,\blacklozenge\,)$	Expected value of the stochastic variable $\blacklozenge$.
$\mathcal{P}_{loss,t}$	Active power losses at time t.
ω	Operating frequency.
$\overline{D_{nm}}$	Logical inverse of D_{nm}, equal to $(1 - D_{nm})$.
$\overline{W_n}$	Logical inverse of W_n, equal to $(1 - W_n)$.
$\sigma(C_{OPF})$	Standard deviation of the variable C_{OPF}.
θ_{nm}	Voltage angle difference (i.e., $\theta_{nm} = \theta_n - \theta_m$).

θ_n	Voltage angle at bus n, in rad or degrees.
$\varphi_{c\text{-}nm}$	Power factor angle of the VSC (c) connected at bus n between buses n and m.
$\widehat{\omega}$	Normalized frequency.
$\widehat{V}^{dc}$	Normalized DC voltage.
$C_{OPF,s,t}$	Stochastic variable representing the optimal operation cost for an MCS scenario s, at year t.
C_{OPF}	Optimal operation cost of the DS.
$C_{AOM,t}$	Annual operation and maintenance costs for year t.
C_{INV}	Investment costs of lines, breakers, and converters.
C_{NPV}	Net present value of the DS costs.
D_{nm}	Binary element of line nm in the line matrix D.
$EENS$	Total expected energy not supplied, in MWh.
$ENS_{s,t}$	Energy not supplied for an MCS scenario s, at year t.
IC	Investment costs of lines and converters.
M_{nm}	Modulation index of the VSC connected at bus n, between buses n and m.
P_c	Active power at the AC side of the VSC (c).
P_n^{cal}	Calculated active power at bus n.
P_n^{inj}	Injected active power at bus n.
P_{Gn}^{ac}	Active power of the AC generator at bus n.
P_{Gn}^{dc}	Output power of the DC generator at bus n.
P_{nm}	Active power transmitted from bus n to bus m.

P_{TG}	Total active power generated from the energy resources in the system.
Q_c	Reactive power at the AC side of the VSC (c).
Q_n^{cal}	Calculated reactive power at bus n.
Q_n^{inj}	Injected reactive power at bus n.
$Q_{Gn\text{-}c}^{dc}$	Reactive power injected at AC bus n from the converter of the DC generator connected at that bus.
Q_{Gn}^{ac}	Reactive power of the AC generator at bus n.
$Q_{Ln\text{-}c}^{dc}$	Reactive power absorbed at AC bus n from the converter of the DC load connected at that bus.
Q_{nm}	Reactive power transmitted from bus n to bus m.
RC	Running cost of the DS.
S_c	Apparent power of the VSC (c).
S_{nm}	Apparent power transmitted from bus n to bus m.
$U_{f,bus\text{-}n}$	Unavailability of electric power at bus n, in h/year.
U_{nm}	Binary element of line nm in the connection matrix U.
V_n	Voltage magnitude at bus n, in kV or p.u.
W_n	Binary element of bus n in the bus-type vector W.

Chapter 1

Introduction

1.1 Preface

The electric energy debate between AC (alternating current) and DC (direct current) was started in New York in the 19th century [1]. The battle was won by AC, which has been the main type of the electric power generation, transmission, and distribution. The AC power became the dominant because of different reasons, including the utilization of power transformers that can be used to step the AC voltage up for lower transmission losses and step it down for power distribution purposes. Since the beginning of the 21st century, the manner in which electric power is generated and utilized has changed significantly. Heightened environmental concerns have led many countries to be interested in green technologies, such as electric vehicles (EVs), photovoltaic (PV) energy, and other renewable distributed generators (DGs). The DC power is therefore making a comeback to satisfy the needs of the present and future power networks. The DC system can offer several benefits for the electric grid, such as greater power line capacity, higher efficiency, lower system costs, and less design complexity [2–4]. However, the benefits of both AC and DC power systems can be gained by integrating them into an AC-DC hybrid structure [5–8].

1.2 Motivation

Increased exploration of the use of DC architectures in distribution systems (DSs) has been prompted by the growing trend toward greater utilization of DC-based energy resources,

such as PV panels and battery storage systems [9], as well as the expanded DC-based load demand related to components such as EVs and modern home appliances. On one hand, the global installed capacity of solar PV energy increases dramatically every year, and is expected to reach more than 600 GW by 2020, as shown in Figure 1.1 [10]. In Canada, solar PV energy has grown substantially, reaching 1210 MW in 2013 [11]. The significant increase started in 2009 with the installation of 62 MW of solar PV energy and continued with 186 MW in 2010, 216 MW in 2011, 268 MW in 2012, and 445 MW in 2013 [11]. The vast majority of this growth occurred in the province of Ontario. Canadian solar industries association expects that Canada's solar PV capacity will reach 6300 MW by 2020 [12]. On the other hand, the worldwide market sales of EVs increased by 70% between 2014 and 2015, and are expected to reach 20 million cars by 2020 [13]. Figure 1.2 shows that the global EV sales are significantly increased over the years [13]. A further factor is the number of energy policies directed at encouraging the use of green technologies. Examples of these policies in Ontario, Canada, include 1) the feed-in-tariff (FIT) program that was developed to increase the installation of renewable-based DGs (e.g., PV and wind DGs) [14], and 2) the incentive program that promotes the use of EVs [15].

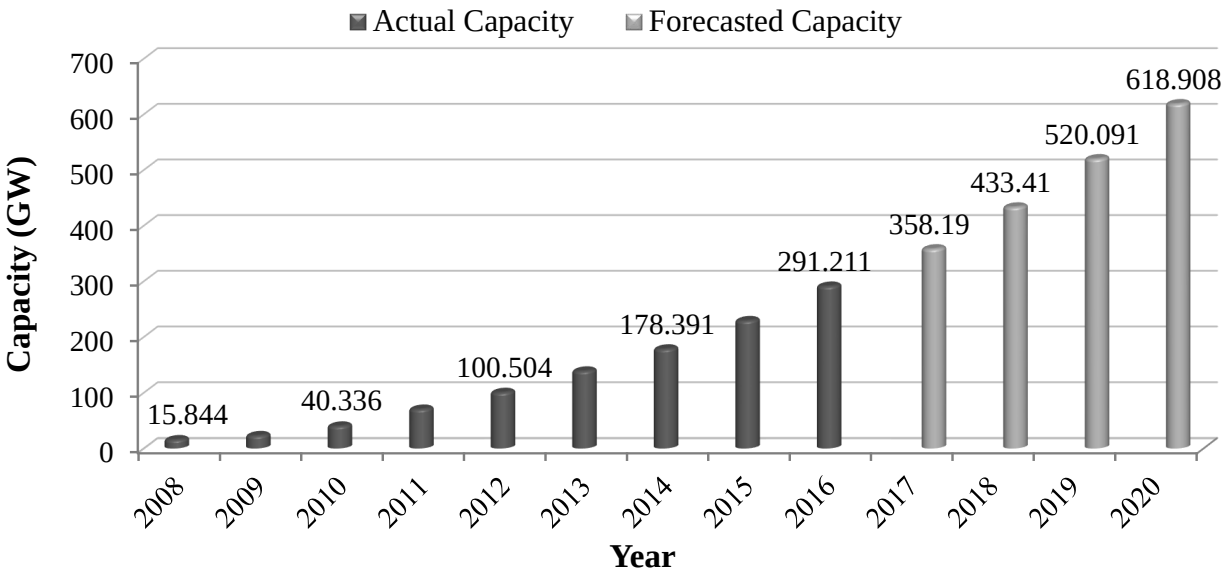

Figure 1.1: Global growth of solar PV electric energy.

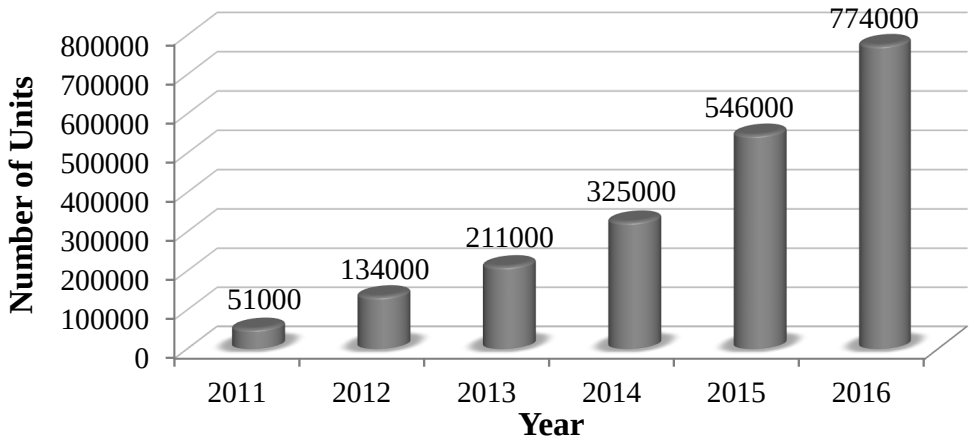

Figure 1.2: Global sales of electric vehicles.

Based on the aforementioned discussion, it is obvious that the current and future DSs include additional DC loads and DC-based DGs along with the traditional AC loads and generators [2]. Future DSs should thus become AC-DC hybrids if they are to provide optimal accommodation of all types (AC and DC) of loads and DGs. However, there is a lack of research conducted in the area of AC-DC hybrid DSs, where many points related to the planning and operation of such hybrid DSs are not well covered in the literature. Therefore, the work presented in this thesis aims to fill gaps evident in the available literature through the development of effective techniques appropriate for the planning and operation of future hybrid DSs.

1.3 Research Objectives

The primary goal of this research is to optimally accommodate the expected high penetration of DC loads and DC-based DGs in future DSs. To achieve this goal, new methodologies for the planning and operation of AC-DC hybrid DSs are developed in this thesis. The objectives of the research presented in this thesis are shown in Figure 1.3, and can be summarized as follows:

1. The development of a unified load flow (LF) model that is flexible, versatile, and suitable for the planning and operation of AC-DC hybrid DSs.

2. The development of an energy management scheme (EMS) that can be used for guaranteeing optimal and reliable operation of AC-DC hybrid DSs.

3. The development of a stochastic planning model for AC-DC hybrid DSs. The model must be capable of determining the optimal AC-DC network configuration that minimizes the DS investment and operation costs. The model should incorporate consideration of the stochastic behavior of load demands and renewable DGs.

4. The development of a reliability-based stochastic planning model for AC-DC hybrid DSs. The proposed model should be formulated to achieve two objectives: 1) minimizing system costs, and 2) maximizing system reliability. The stochastic variations related to load demands and renewable DGs should be addressed in the model.

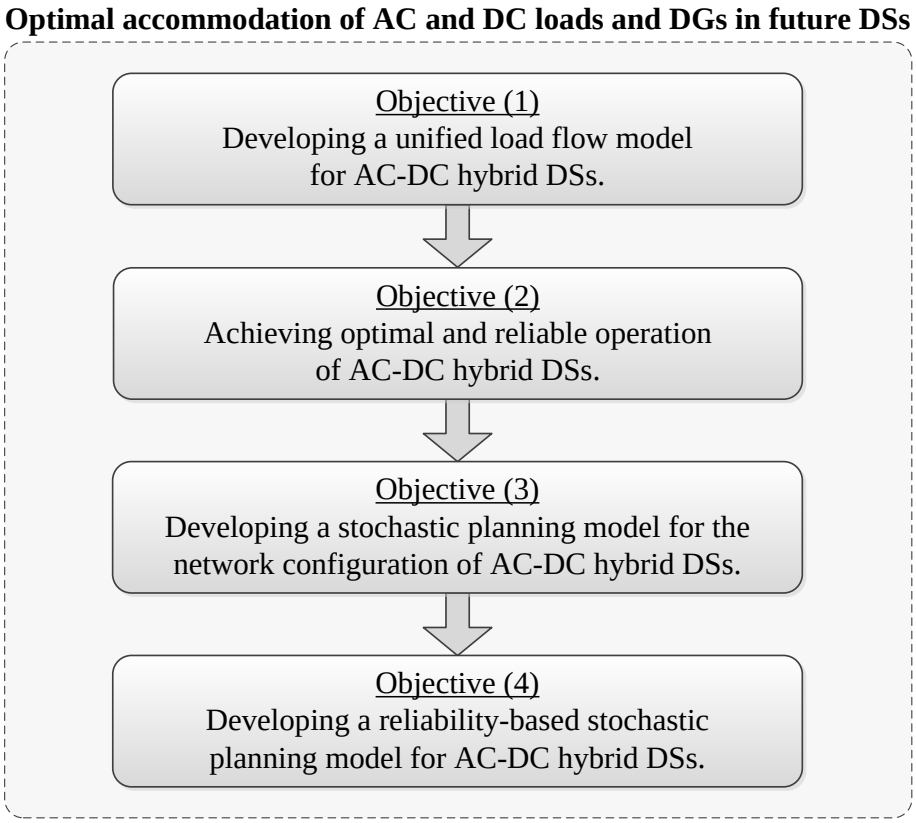

Figure 1.3: Research objectives.

1.4 Thesis Outline

The remainder of this thesis is organized as follows:

Chapter 2 provides the required background and literature survey on the previous work conducted in the area of AC-DC hybrid systems, including AC-DC LF analysis as well as the planning and operation of AC-DC hybrid power systems.

Chapter 3 introduces a unified model for solving the LF problem of AC-DC hybrid DSs. The proposed model is generic and can be used for the planning and operation of different hybrid power systems. The proposed model can be applied in hybrid DSs with mixed configurations for AC/DC buses and AC/DC lines. A set of generic LF equations has been derived based on comprehensive analysis of the possible AC-DC hybrid system configurations.

Chapter 4 presents a two-stage EMS for the optimal operation of AC-DC hybrid DSs. In the first stage, a proposed network reconfiguration algorithm determines the optimal day-ahead reconfiguration schedule that includes consideration of the forecasted data for load demands and renewable DGs. In the second stage, a proposed real-time OPF-LCM algorithm guarantees reliable and optimal operation of the hybrid DS.

Chapter 5 presents a novel stochastic planning model for AC-DC hybrid DSs. A connectivity profile has been introduced as a means of representing possible AC-DC hybrid bus and line configurations. The model searches for the optimal AC-DC network configuration that minimizes the DS costs. The model incorporates consideration of the stochastic behavior of load demands and renewable DGs.

Chapter 6 introduces a reliability-based stochastic planning model for AC-DC hybrid DSs. The proposed model is formulated as a multi-objective optimization problem that has two objectives: 1) minimizing system costs, and 2) maximizing system reliability. The second objective is achieved through the minimization of the expected energy not supplied (EENS) in the system. Network buses and lines can become either AC or DC in order to achieve the planning objectives.

Chapter 7 sets out the thesis conclusions and contributions as well as recommendations for future research studies.

Chapter 2

Background and Literature Survey

2.1 Introduction

As mentioned in Chapter 1, future DSs should become AC-DC hybrids if they are to provide optimal accommodation of all types (AC and DC) of the anticipated loads and DGs. This belief accentuates the need for reliable techniques appropriate for the planning and operation of future hybrid DSs, as highlighted in the research objectives in the previous chapter. This chapter presents the required background and literature survey pertaining to the objectives of this thesis. The first section, Section 2.2, presents an overview of the different types of the AC-DC hybrid power systems that have been discussed in the literature. Section 2.3 discusses the AC-DC hybrid LF methods presented in previous research studies. A review of the operation and planning techniques used for AC-DC hybrid power systems is introduced in Sections 2.4 and 2.5. Finally, the conclusions and discussions of this chapter are presented in Section 2.6.

2.2 AC-DC Hybrid Power Systems

Different types of AC-DC hybrid power systems are discussed in the literature, such as high-voltage direct current (HVDC) systems, AC-DC hybrid microgrids, and low voltage

direct current (LVDC) systems. An overview of the network topologies of those hybrid systems is presented in the following subsections.

2.2.1 HVDC Transmission Systems

HVDC transmission system is a well-known application of AC-DC hybrid power systems because it has been proven that transmitting DC power for very long distances can achieve more benefits compared to the conventional AC transmission [16]. As shown in Figure 2.1, two types of HVDC connections are presented in the literature: two-terminal and multi-terminal DC transmission systems [17, 18].

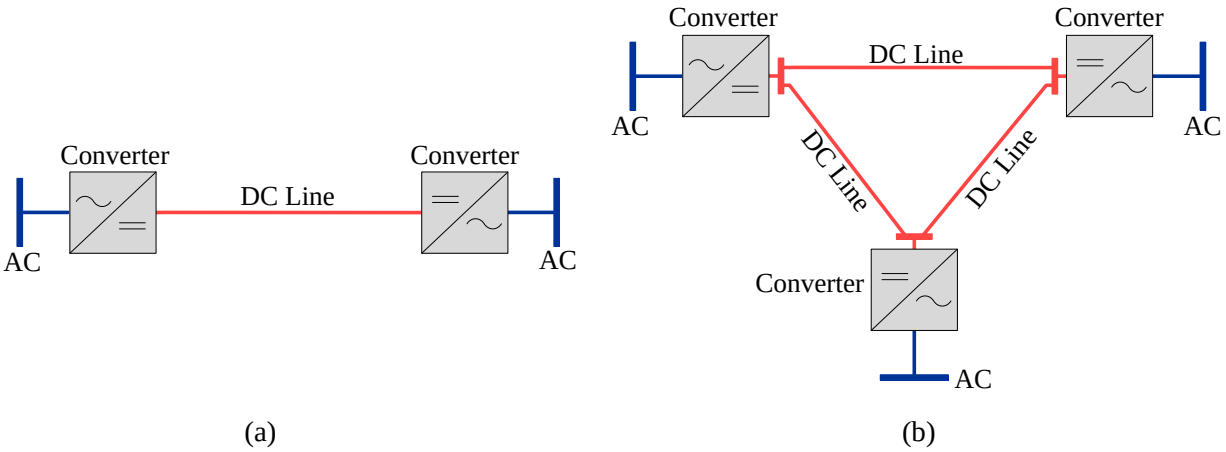

Figure 2.1: HVDC connections: (a) two-terminal HVDC, (b) multi-terminal HVDC.

2.2.2 AC-DC Hybrid Microgrids

AC-DC Hybrid microgrids represent one of the future distribution networks to achieve the merits of both AC and DC power. Several research studies have discussed the technology and power management strategies of AC-DC hybrid microgrids [19–21]. In the general architecture of the hybrid microgrid, all system components are clustered into AC and DC subgrids, which are interconnected by an interlinking converter, as shown in Figure 2.2. These components include AC/DC loads, AC/DC renewable-based DGs, dispatchable DGs, and energy storage systems.

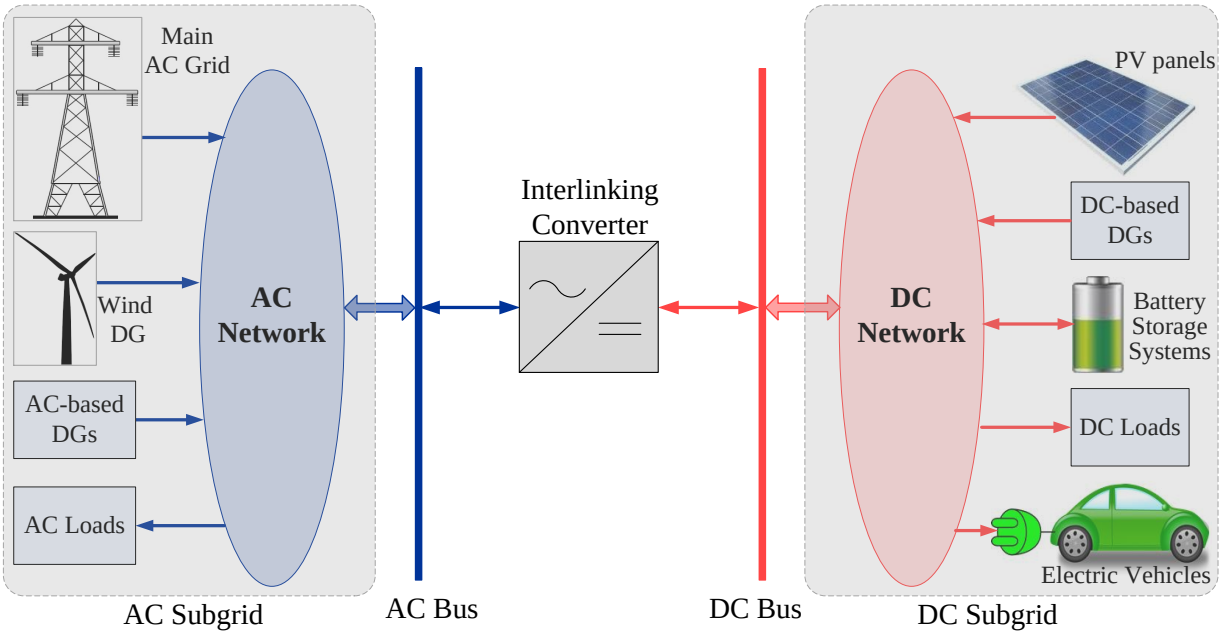

Figure 2.2: General architecture of AC-DC hybrid microgrids.

The clustering topology of the hybrid microgrid is suitable for special applications (e.g. small and remote areas). From the network connection perspective, AC-DC hybrid microgrids represent the most obvious way to interlink different types (AC and DC) of system components. However, this approach does not represent the most economical hybrid connection for large power systems, such as the typical distribution systems.

2.2.3 LVDC Distribution Systems

The techno-economic analysis of LVDC systems has been discussed in [3, 4, 22]. With respect to the location of the DC links and DC/AC converters, two main topologies are investigated in [22]: 1) LVDC link style (Figure 2.3-a), and 2) wide LVDC distribution district style (Figure 2.3-b), in which the DC/AC converters are installed at the customer ends.

The results in [3, 4, 22] showed that although the operation and protection of LVDC distribution network are more complex compared to the conventional AC grid, the LVDC system can provide higher transmission capacity, better power quality, and lower power

losses compared to the AC system. However, there are some demerits of the DC distribution system are mentioned in [3]. These demerits are related to the lifetime, power losses, and voltage harmonics of the AC-DC converters.

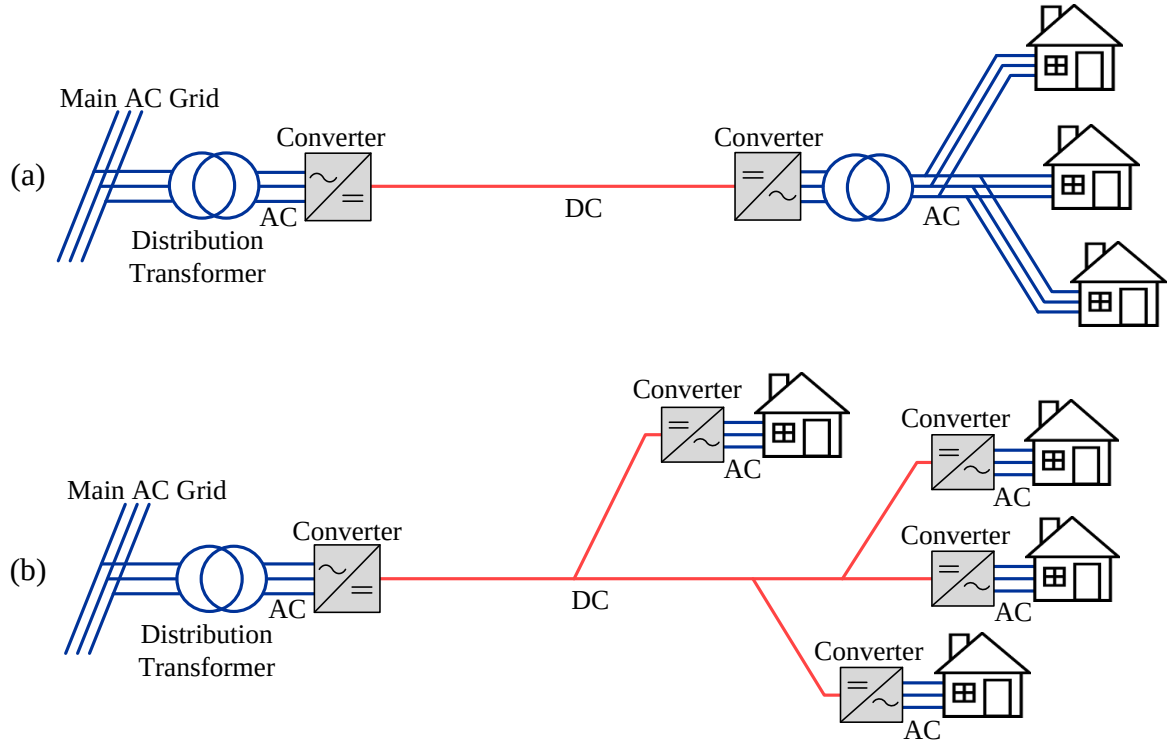

Figure 2.3: LVDC topologies presented in [22] - (a) LVDC link style, and (b) wide LVDC distribution district.

An AC-DC bilayer DS was introduced in another research study [7]. The bilayer DS is based on installing a DC layer parallel to the conventional AC layer, as shown in Figure 2.4. The two layers plus an interlinking converter are integrated to supply the electric power to the system AC loads as well as to accommodate the presence of plug-in hybrid electric vehicles and PV arrays. A case study revealed that the bilayer DS can reduce the overloading of the secondary distribution transformer, and avoid distribution transformer upgrades as a consequence.

Other researchers [23–26] have also demonstrated the benefits of using DC power in residential and commercial buildings. For example, a new energy management strategy

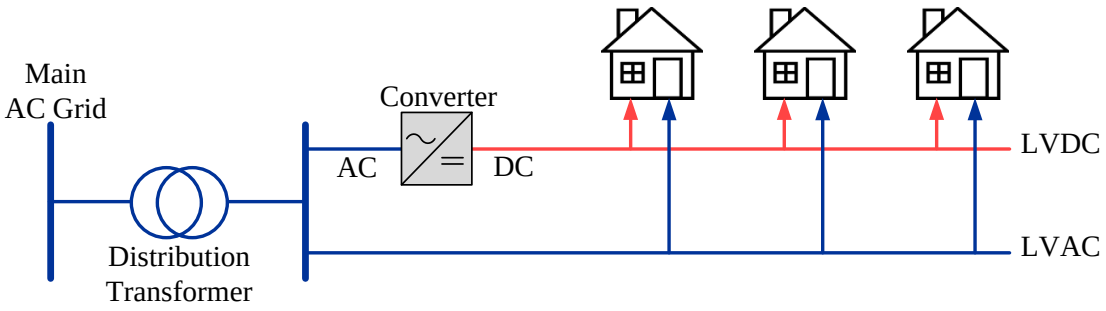

Figure 2.4: The bilayer DS proposed in [7].

for a DC DS in buildings is proposed in [23] to minimize the building energy costs and to provide benefits to EV owners. In another research [24], a DC nanogrid has been presented as a means of integrating the residential electronic loads with the renewable-based DGs and energy storage batteries. The study in [25] proposes an LVDC DS to supply sensitive electronic loads in buildings. The laboratory measurements showed that the use of the suggested DC system led to lower power losses than occur in a purely AC system. The feasibility of using DC power in commercial facilities was discussed in [26]. A techno-economic comparison was carried out between the traditional AC system and the proposed DC architecture. The study revealed that the DC system can achieve less voltage drop, less power losses, and less installation and operation costs compared to the AC system.

Although the aforementioned research studies have investigated the benefits associated with the use of DC power alongside AC power in DSs, the determination of the optimal AC-DC hybrid DS configuration considering all possible combinations of AC and DC buses and lines has not been addressed before in the literature.

2.3 AC-DC Hybrid Load Flow Analysis

The load flow (or power flow) problem is the problem of computing the steady-state flow of electrical power in the power networks. The LF analysis represents the most important network computation in power systems. The LF problem arises in many power system applications, and has been extensively discussed in the literature [27, 28]. The main parameters obtained from the LF study are the magnitude and phase angle of the voltage

at each bus, as well as the active and reactive power flowing in each line in the network. The LF study is important for planning of future power systems as well as for the optimal operation of existing systems.

2.3.1 AC Load Flow

In AC LF analysis, there are four parameters associated with any AC bus in the power network. These parameters are: the active power (P), the reactive power (Q), the voltage magnitude (V), and the voltage angle (θ). For the AC power network shown in Figure 2.5, the AC power flow can be calculated for the AC bus i using (2.1) and (2.2) [29].

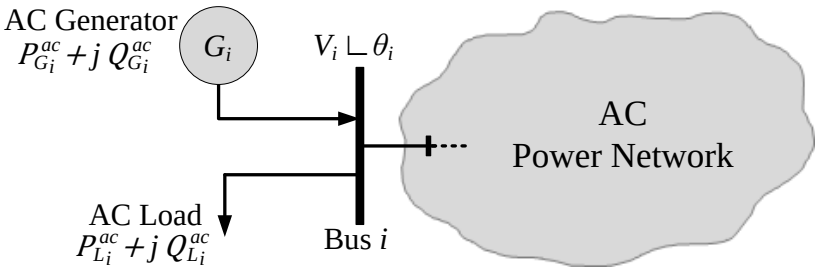

Figure 2.5: Typical AC-bus representation for power flow analysis.

$$P_{G_i}^{ac} - P_{L_i}^{ac} = \sum_{j=1}^{N_b^{ac}} V_i\, V_j \left(G_{ij}^{\backprime} \cos(\theta_i - \theta_j) + B_{ij}^{\backprime} \sin(\theta_i - \theta_j) \right) \tag{2.1}$$

$$Q_{G_i}^{ac} - Q_{L_i}^{ac} = \sum_{j=1}^{N_b^{ac}} V_i\, V_j \left(G_{ij}^{\backprime} \sin(\theta_i - \theta_j) - B_{ij}^{\backprime} \cos(\theta_i - \theta_j) \right) \tag{2.2}$$

where N_b^{ac} is the number of AC buses in the system; $P_{G_i}^{ac}$ and $Q_{G_i}^{ac}$ are the active and reactive power of the AC generator at bus i, respectively; $P_{L_i}^{ac}$ and $Q_{L_i}^{ac}$ are the active and reactive power demand for the AC load at bus i, respectively; V_i and θ_i are the magnitude and angle of the bus i voltage, respectively; and $(G_{ij}^{\backprime} + j\ B_{ij}^{\backprime})$ is the complex element (i, j) in the bus admittance matrix Y_{bus}.

One of the most well-known LF methods discussed in the literature is the Newton Raphson (NR) method. The NR method uses the active and reactive power equations described in (2.1) and (2.2). The NR method is based on the solving of the matrix equation (2.3) in each iteration until a convergence criterion is satisfied [30].

$$\begin{bmatrix} \Delta P \\ \Delta Q \end{bmatrix} = [J] \begin{bmatrix} \Delta\theta \\ \Delta V \end{bmatrix} = \begin{bmatrix} \frac{\partial P}{\partial \theta} & \frac{\partial P}{\partial V} \\ \frac{\partial Q}{\partial \theta} & \frac{\partial Q}{\partial V} \end{bmatrix} \begin{bmatrix} \Delta\theta \\ \Delta V \end{bmatrix} \tag{2.3}$$

where ΔP and ΔQ are the active and reactive power mismatches, respectively; and ΔV and $\Delta\theta$ are the variation in the voltage magnitude and angle at each iteration, respectively. The Jacopian matrix $[J]$ represents the matrix of partial derivatives, which must be constructed at each iteration.

Due to its quadratic convergence characteristics, the NR method is considered as an efficient algorithm for solving the LF problem of highly meshed power systems (e.g., power transmission systems) [31, 32]. However, the NR method may diverge in the case of DSs due to the high R/X ratio [33]. In addition, the Jacobian matrix in the NR method has to be constructed and inverted in each iteration. Therefore, the NR method may take a huge amount of computational time in the case of large DSs.

Another method that can be used in DS is the Forward/Backward (F/B) method [34, 35]. The F/B method is based on two steps: 1) The backward sweep, in which Kirchhoff's current law (KCL) is applied for the calculation of the branch currents, starting from the last branches in the DS, and 2) The forward sweep, in which the Kirchhoff's voltage law (KVL) is applied for the calculation of the bus voltages, using the source bus voltage and the calculated branch currents. This process is iteratively repeated until a convergence criterion is satisfied. The convergence criterion is satisfied if the active and reactive power mismatches at all system buses become less than a selected small tolerance. The KCL and KVL equations for the line portion shown in Figure 2.6 are expressed in (2.4) and (2.5), respectively.

$$\overline{I_{12}} = \overline{I_{L2}} + \overline{I_{23}} \tag{2.4}$$

$$\overline{V_2} = \overline{V_1} - \overline{Z_{12}}\ \ \overline{I_{12}} \tag{2.5}$$

where $\overline{I_{12}}$ and $\overline{I_{23}}$ are the branch currents of lines 1-2 and 2-3, respectively; $\overline{V_1}$ and $\overline{V_2}$ are the voltages of bus 1 and bus 2, respectively; $\overline{Z_{12}}$ is the impedance of line 1-2; and $\overline{I_{L2}}$ is the current of the load connected at bus 2.

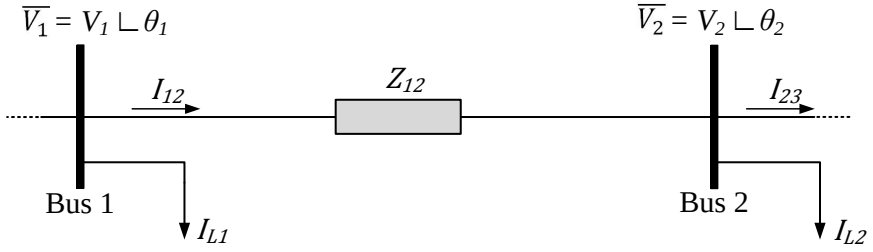

Figure 2.6: Line section in a radial DS.

The F/B method has two main advantages: simple calculation procedures and high-speed convergence. However, the method is not suitable for meshed distribution networks.

2.3.2 DC Load Flow

In DC LF analysis, the two parameters associated with any DC bus in the power network are the DC power and the DC voltage. For the DC power network shown in Figure 2.7, the DC power flow can be calculated for the DC bus k using (2.6) [36].

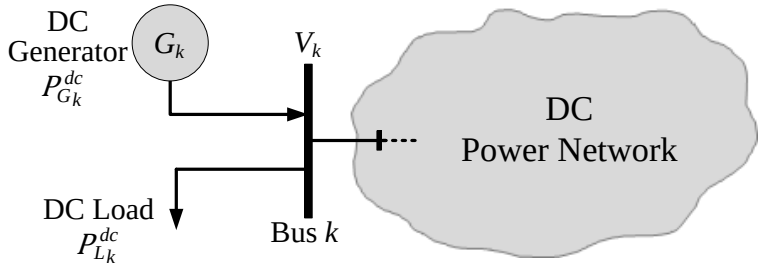

Figure 2.7: Typical DC-bus representation for power flow analysis.

$$P_{G_k}^{dc} - P_{L_k}^{dc} = \sum_{j=1}^{N_b^{dc}} V_k \, V_j \, G_{kj}^{\wedge} \tag{2.6}$$

where N_b^{dc} is the number of DC buses in the network; $P_{G_k}^{dc}$ is the output power of the DC generator at bus k; $P_{L_k}^{dc}$ is the power demand of the DC load at bus k; V_k is the bus k voltage; and $G_{kj}^{\backprime}$ is the element (k, j) in the bus conductance matrix G_{bus}.

2.3.3 AC-DC Hybrid Load Flow

Several researchers [36–40] have discussed LF analysis for AC-DC hybrid power systems, and most have focused on HVDC systems. For example, the authors of [37] provide a detailed analysis of a VSC-based HVDC model and introduce an equivalent injected power approach for calculating the AC-DC power flow. In [36] and [38], the LF calculation for AC-DC hybrid power systems is performed using a sequential approach, in which the AC and DC LF equations are solved independently at each iteration until the convergence criteria in the AC and DC subnetworks are satisfied, as shown in Figure 2.8. Because the sequential method is complicated and time-consuming [39], an integrated approach is presented in two further studies [39, 40]. In the integrated method, both AC and DC LF equations are solved together at each iteration in order to overcome the drawbacks associated with the sequential method. However, both the sequential and integrated LF methods presented in [36–40] are based on decoupled analysis; i.e., the AC and DC networks have separate power equations. In this type of analysis, the main hybrid grid is divided into several AC and DC subgrids that have to be solved iteratively until convergence is reached. Traditionally, these methods are suitable for HVDC systems, in which the number of DC nodes is limited. The authors of [41–44] have presented hybrid LF equations in the formulation of the OPF problem. However, their models are limited only for HVDC system configurations, and in an effort to simplify the LF calculations, most of them [42–44] have ignored the power losses of the AC-DC converters.

From the aforementioned discussion, it is obvious that the results of the research related to AC-DC hybrid LF analysis are still inconclusive and address very limited AC-DC network configurations. The hybrid LF methods presented in [36–44] have focused on grid-connected systems. These methods cannot deal with isolated hybrid DSs, since they do not include consideration of the unavailability of a slack bus or the frequency variation in the AC subnetworks. In addition, the AC-DC LF algorithms presented in the literature (e.g., [36–40]) are based on decoupled LF analysis, in which the main hybrid network is

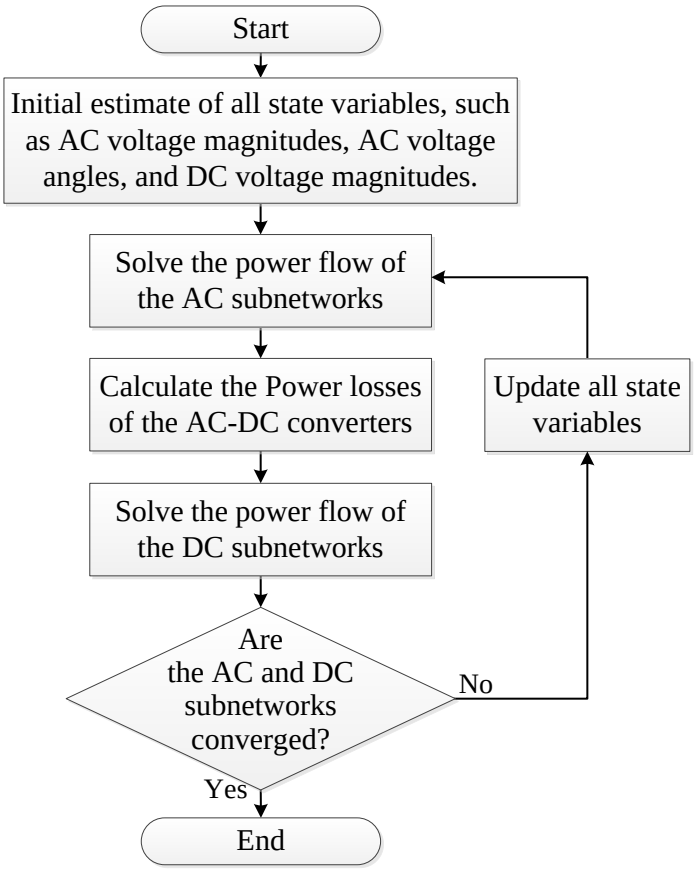

Figure 2.8: Procedures of the sequential load flow analysis.

divided into several AC and DC subnetworks that have to be solved iteratively. In the smart grid era, future hybrid DSs are expected to include i) a variety of types of AC and DC loads and DGs, and ii) huge numbers of AC and DC buses and lines that are merging together and cannot be easily clustered to fit the LF methods discussed in the literature. Such methods are expected to suffer from computational complexity and numerical solution instability if they are used for large highly-coupled hybrid DSs. Other studies have introduced LF methods for AC-DC hybrid microgrids [45–47]. These methods, however, are designed for hybrid microgrid topologies and are also based on decoupled LF analysis. In addition, the decoupled-analysis-based methods can only be used for predetermined network configurations. These methods therefore cannot be used in hybrid planning studies to determine the optimal network configurations of future hybrid DSs.

2.4 Optimal Operation of AC-DC Hybrid Smart DSs

Hybrid smart DSs are characterized by the availability of information and communication technologies that allow intelligent energy management techniques to be used for the optimal operation scheduling of such hybrid systems. Hybrid smart DSs will host a variety of types of loads and DGs, including modern controllable loads and renewable-based DGs. Although renewable DGs can provide economic and environmental benefits for the DS, their intermittent nature also adds greater complexity to DS operation. Robust and reliable forecasting techniques are therefore needed in order to reduce the stochastic risk associated with renewable DGs. A lower level of stochastic risk can also be guaranteed if fast OPF algorithms are used for the online operation of smart DSs. Hybrid smart DSs will also include bidirectional relays and remotely controlled switches, both of which will enable the application of network-reconfiguration techniques. In this context, the characteristics and components that will accompany hybrid smart DSs in the future have accentuated the need for effective energy management techniques that can guarantee the reliable and optimal operation of AC-DC hybrid smart DSs.

2.4.1 Network Reconfiguration

Network reconfiguration is the process of controlling the open/closed status of the sectionalized (or tie) switches in order to achieve an optimal DS operation schedule. Several studies have involved the examination of DS reconfiguration techniques for traditional AC DSs. For example, the authors of [48] proposed an operational planning strategy for smart active DSs. The objective of the strategy was to minimize day-ahead operation costs based on consideration of the hourly reconfiguration capability of the DS network. In two further studies [49, 50], the authors proposed reconfiguration algorithms for distribution networks. These studies revealed that the use of a reconfiguration strategy provides a number of benefits, including a reduction in DS power losses and improvement in the DS voltage profile. In [51] and [52], simultaneous reconfiguration and DG allocation algorithms were proposed as a means of minimizing DS power losses and improving the voltage profile. The authors of [53–55] also proposed optimal reconfiguration strategies for minimizing power losses in distribution networks. Although these studies [48–55] introduced reconfiguration techniques for traditional AC DSs, the AC-DC hybrid reconfiguration problem has yet to

be tackled. Reconfiguration of an AC-DC hybrid network will be more complicated than the traditional AC version.

2.4.2 Demand-Side Management

Demand-side management (DSM) includes load-curtailment management (LCM) and other demand response programs. Taken together, they represent an important practice available for efficient DS operation because they can lower operating costs and provide an appropriate degree of system reliability [56, 57]. Several studies have investigated the benefits associated with the application of DSM programs. For example, the authors of [58] proposed a demand-response strategy that includes hourly load shifting and curtailment techniques. The proposed strategy allows better scheduling of the energy resources available in the system. In [48], an optimal energy management framework was presented as a means of minimizing the day-ahead operation costs of smart DSs, taking into account reconfiguration and load control techniques. To achieve optimal scheduling of transmission outages and to maintain system security and reliability, the authors of [59] introduced a security-constrained optimal scheduling model that uses a load shedding technique. In another study [60], dynamic contracts for load curtailment were designed to guarantee suitable benefits for both the utility operator and the customers. However, all of these techniques [48, 58–60] were applied on traditional AC DSs.

2.4.3 Energy Management of AC-DC Hybrid Systems

Few researchers have discussed the energy management of AC-DC hybrid systems. For example, the authors of [61] suggested a stochastic centralized dispatch technique for an AC-DC hybrid smart grid. The objective of the proposed technique was to minimize the day-ahead operation costs, while taking into consideration different stochastic scenarios that could occur during the next day. In [6], a power management strategy was proposed for controlling the active and reactive power exchange between the converters and the AC feeders in an AC DS with DC-grid interconnections. The objective of the strategy was to increase power handling capacity and improve the voltage profile of the DS feeders. Another study [62] described a management strategy for the optimal operation of an AC-

DC hybrid grid composed of two clustered subgrids: AC and DC. The proposed strategy was based on two levels of operation: system level and device level. In the system level, a mixed-integer optimization model was proposed to minimize the day-ahead operation costs of the AC-DC hybrid grid considering the uncertainties associated with load demands and renewable DGs. In the device level, the voltage variations were controlled in both AC and DC subgrids through the controlling of the DG converters.

However, to the best of the author's knowledge, no studies have proposed network reconfiguration and LCM techniques for the energy management of AC-DC hybrid DSs.

2.5 Planning of AC-DC Hybrid DSs

The primary purpose of DS planning is to ensure reliable and optimal satisfaction of the growing electricity demand. To achieve this goal, several methods have been targeted at the formulation of the AC planning problem, as discussed in [63–71]. With respect to planning stages, two approaches are presented in the literature: 1) stage-by-stage planning; in which the planning periods are optimized separately [63–65], and 2) Multi-stage planning; in which all planning stages are integrated and considered simultaneously [66–70]. With respect to planning objectives, two main objectives have been adopted: 1) minimizing investment and operation costs [65–67], and 2) maximizing system reliability. DS planners currently consider these two objectives simultaneously by formulating the planning problem as a multi-objective optimization problem [69–71]. For future smart DSs, an AC-DC hybrid structure constitutes the most likely optimal solution for supplying AC/DC loads from available AC/DC energy resources [5–8]. Because the new hybrid structure will encompass additional DS components, such as AC/DC buses, AC/DC lines, and AC-DC converters, consideration of their installation costs and failure rates must be included in the planning problem. Further factors that should also be taken into account are the stochastic variations associated with the different types (AC and DC) of load demands and renewable-based DGs. The hybrid planning problem is consequently much more complicated than the traditional AC version. DS planners will therefore require suitable techniques for the planning of these new hybrid systems. However, research in the area of AC-DC hybrid DSs is in the infant stage and still lacks an effective methodology for the planning of such hybrid DSs.

Recent papers [17, 72–75] have examined the optimal planning of AC-DC hybrid power systems in general: most have focused on HVDC systems. For example, an algorithm for the expansion planning of AC-DC hybrid transmission systems was proposed in [17]. The algorithm selects the optimal combination of AC-DC transmission links from a predefined set of candidates. The model has two main disadvantages: 1) it is based on the solving of a specific number of scenarios; 2) it ignores the power losses associated with AC-DC converters and DC lines. In [72], a smart targeted planning algorithm was introduced as a means of improving the economic dispatch efficiency of an HVDC system that incorporates VSCs. The algorithm prioritizes potential DC line locations in an existing transmission system in order to establish which of the scenarios solved provides the optimal solution. In [73], a multi-objective optimization algorithm was proposed to solve the transmission expansion planning problem, considering candidate AC/DC lines to minimize two objective functions: the total investment costs and the active power losses. In another study [74], the authors proposed an OPF method that incorporates a VSC-based multi-terminal DC (VSC-MTDC) model. The model was used for solving a number of scenarios related to the installation of MTDC in an existing AC network, and then for determining which scenario is the optimal one.

Since, the studies reported in [17, 72–74] are based on the solving of specific predefined scenarios, only a limited number of candidate DC links are examined. This approach does not allow the inclusion of all possible AC-DC configurations, thereby limiting the chances of finding superior solutions. The hybrid planning methods presented in the literature are unsuitable for use with complicated hybrid DSs, which include a variety of types of AC and DC loads and DGs. These methods do not have the flexibility required for including consideration of all possible AC-DC configuration scenarios or of the variety of conditions encountered in the operation of future hybrid DSs.

2.6 Conclusions and Discussions

According to the surveyed literature in this chapter, the idea of hybrid DSs represents a promising technique to incorporate the benefits of both AC and DC power. Due to the increased penetration rate of DC loads and DC-based DGs, the current belief is that the future DSs will be AC-DC hybrid systems. Therefore, more research works in the area of

AC-DC hybrid DSs are required to face all challenges associated with the planning and operation of such hybrid systems. The gaps in the literature can be addressed from many perspectives. From the LF perspective, most researchers have solved the LF problem of hybrid power systems based on decoupled LF analysis (i.e. DC LF analysis and AC LF analysis have separate power equations). However, a unified hybrid LF model is needed for the planning of AC-DC hybrid DSs. In order to address this requirement, Chapter 3 introduces a unified AC-DC LF model that can solve the AC and DC portions of the hybrid network simultaneously based on generic AC-DC power equations. In addition, no studies have been conducted for the optimal operation of AC-DC hybrid DSs considering the network reconfiguration capabilities. To fill this gap, a two-stage EMS is presented in Chapter 4 for determining the optimal day-ahead reconfiguration schedule as well as for guaranteeing reliable and optimal online operation for AC-DC hybrid DSs. From the hybrid planning perspective, most hybrid planning methods presented in the literature have focused on HVDC systems. These methods are dependent on prioritization of the solutions of a limited number of candidate scenarios. This approach does not allow the inclusion of all possible AC-DC configurations, thereby limiting the chances of finding superior solutions. Therefore, a novel planning model is proposed in Chapter 5 to determine the optimal AC-DC network configuration that minimizes the DS investment and operation costs. In order to incorporate the DS reliability in the planning problem, a reliability-based stochastic planning model is introduced in Chapter 6. The model aims to optimize the DS costs and reliability, considering the stochastic variations associated with load demands and renewable-based DGs.

Chapter 3

A Generalized Approach for the Load Flow Analysis of AC-DC Hybrid DSs

3.1 Introduction

This chapter presents a unified LF model that can be applied to hybrid DSs with varied AC-DC configurations. A new classification of hybrid DS buses is also introduced for LF analysis. Unified AC-DC power equations are constructed based on comprehensive analysis of the possible hybrid DS configurations. The proposed LF model employs three binary matrices to describe the AC-DC configuration of any hybrid DS. These matrices enable a single configuration at a time to be activated in the unified power equations. VSCs are used in the proposed model for AC-DC power conversions. In this model, the AC and DC portions of the hybrid network are solved simultaneously considering different operational modes for system DGs. The proposed model can be applied to i) radial or meshed; ii) isolated or grid-connected; and iii) easily clustered or highly-coupled hybrid DSs. The new model has been used for solving the LF problem of several case studies of grid-connected and isolated hybrid systems. As a means of evaluating the effectiveness and the accuracy of the proposed model, the LF solution was compared to the solution produced by PSCAD/EMTDC. A comparison of the results reveals the efficacy of the proposed LF model. The developed LF model is flexible, versatile, and suitable for the planning of AC-DC hybrid DSs, as discussed in Chapters 5 and 6.

This chapter is organized as follows: Section 3.2 details the modeling and analysis of power equations for an AC-DC hybrid system that incorporates a VSC model. The formulation of the proposed LF model, including the unified AC-DC power equations, is explained in Section 3.3. The case studies as well as the validation of the proposed LF model are described in Section 3.4. The final section presents the summary and conclusion of this chapter.

3.2 Modeling and Analysis of AC-DC Hybrid DSs

Hybrid DSs consist of a variety of AC and DC components, including loads, generating units, lines, and buses. These components can be interconnected in different hybrid configurations. This section explains the classification of AC/DC buses and discusses the VSC steady-state model used in the proposed LF model. The proposed classification of the AC-DC hybrid configurations that was used for deriving the unified AC-DC power equations is also presented and analyzed.

3.2.1 Classification of AC and DC Buses

As depicted in Figure 3.1, hybrid DS buses can be either AC or DC. Hybrid DSs include DC loads and DC DGs alongside the conventional AC loads and AC generators. Examples of DC DGs include PV panels and fuel cells. EVs and modern elevators represent examples of DC loads. In the case of AC buses, AC-DC converters are necessary for connecting DC loads and DC DGs to an AC bus, as shown in Figure 3.1(a). This arrangement is reversed in the case of DC buses, as shown in Figure 3.1(b).

In the proposed LF model, AC buses are classified as follows [76]:

1. AC slack (or reference) bus: The voltage magnitude and voltage angle of the bus are known, while the active and reactive powers generated at the bus are unknown.

2. AC load (or P-Q) bus: The active and reactive powers of the loads connected at the bus are known, while the voltage magnitude and voltage angle of the bus are unknown.

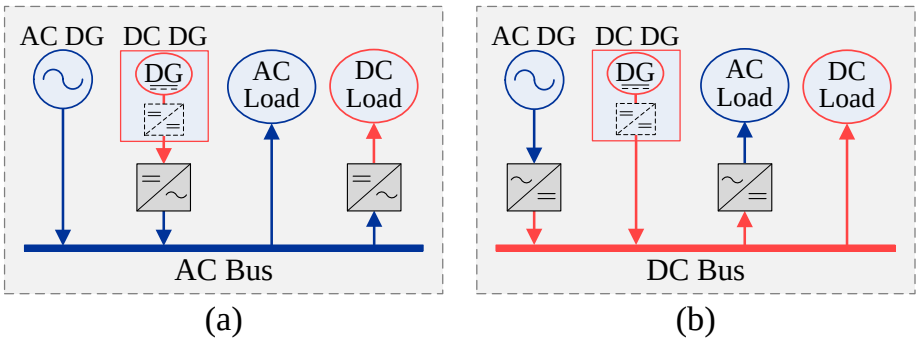

Figure 3.1: Connection of loads and DGs to (a) an AC bus and (b) a DC bus.

3. AC voltage-controlled (or P-V) bus: The active power generated at the bus and the voltage magnitude of the bus are known, while the bus voltage angle and the generated reactive power are unknown. In this case, if the generated reactive power violates the minimum or maximum limits, the bus would be converted to a P-Q bus, with the reactive power then being set to equal the limit that was violated.

4. AC droop-based DG bus: This type is used in isolated hybrid DSs for power sharing among AC DGs [77]. The frequency and the voltage magnitude of the AC DG are regulated based on the generated active and reactive powers, respectively.

The two main parameters for each DC bus are the DC voltage and the DC power, and there is only one DC power balance equation that can be defined for each DC bus. Therefore, the following classification of DC buses is introduced:

1. DC load (or P^{dc}) bus: The net DC power (from the loads and/or DGs) injected into the bus is known, while the DC bus voltage is unknown.

2. DC voltage-controlled (or V^{dc}) bus: The DC bus voltage is known, and the power generated at the bus is unknown. However, if the generated power violates the minimum or maximum limits, the bus would be converted to a P^{dc} bus, with the power then being set to equal the limit that was violated.

3. DC droop-based DG bus: This type is used in isolated hybrid DSs for power sharing among DC DGs [77]. The DC voltage is regulated based on the generated DC power.

For the LF analysis proposed in this study, the specified parameters and the unknown variables for each type of the hybrid DS buses are presented in Section 3.3 – Table 3.1.

3.2.2 AC-DC Converter Model

VSCs can be used in hybrid DSs for two reasons: 1) VSCs can provide fast and independent control of the active and reactive power, and 2) the power flow can be easily reversed by reversing the direction of the current [39]. These two features are suitable for use in active DSs, in which the power flow can be controlled in both directions. VSCs are therefore employed for AC-DC power conversions in the proposed LF model. The DC side of the VSC is a unipolar circuit that has two DC lines, as shown in Figure 3.2. The converter impedance Z_c shown in Figure 3.2 includes the elements connected between the point of common coupling (PCC) and the AC bus of the VSC, such as power transformers, phase reactors, or low pass filters. Since Z_c is connected between two AC buses, it can be modeled as described in Case 1 discussed in Section 3.2.3.

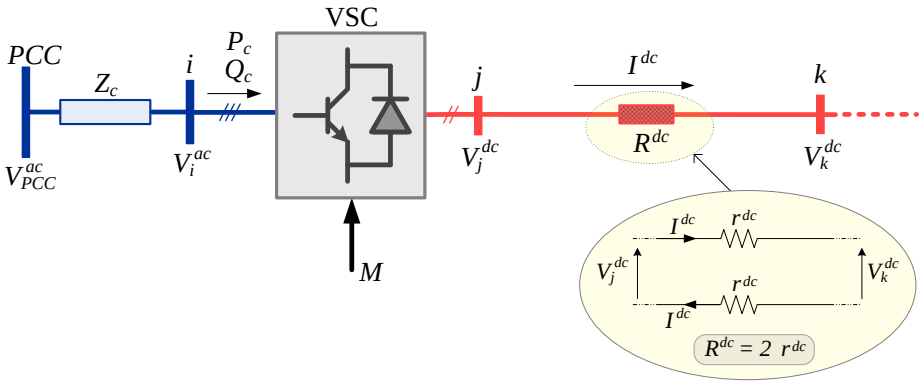

Figure 3.2: Model of a voltage source converter.

The steady-state model of the VSC can be represented by the following equations. First, the AC-side voltage V_i^{ac} is related to the DC-side voltage V_j^{dc} as follows [78]:

$$V_{i,LL_{rms}}^{ac} = K_c\ M\ V_j^{dc} \tag{3.1}$$

where M is the modulation index of the VSC. The value of the converter constant K_c

is dependent on the type of the VSC as well as the type of the pulse width modulation (PWM) strategy. For the three-phase sinusoidal PWM converter used in this study, the value of K_c is equal to ($\sqrt{3}/2\sqrt{2}$) [78].

The relation between the AC voltage base and the DC voltage base is given by

$$V_{base}^{ac} = K_c \; V_{base}^{dc} \tag{3.2}$$

Accordingly, a 1 p.u. AC voltage is equivalent to a 1 p.u. DC voltage at a unity modulation index, as expressed in (3.3).

$$V_{i,p.u.}^{ac} = M \; V_{j,p.u.}^{dc} \tag{3.3}$$

The relation between the DC power and the AC active power is a function of the efficiency η_c of the converter, as follows:

$$P_c = P_c^{dc}/\eta_c = (V_j^{dc} \; I^{dc})/\eta_c \tag{3.4}$$

where the DC current I^{dc} is given by

$$I^{dc} = G^{dc}\left(V_j^{dc} - V_k^{dc}\right) \tag{3.5}$$

Substituting (3.3) and (3.5) in (3.4) gives

$$P_c = \frac{G_{p.u.}^{dc}}{\eta_c}\Big(M^{-2} \; (V_{i,p.u.}^{ac})^2 - M^{-1} \; V_{i,p.u.}^{ac} \; V_{k,p.u.}^{dc}\Big) \tag{3.6}$$

The reactive power Q_c at the AC side of the VSC can be either controlled using a direct set point or calculated as follows:

$$Q_c = P_c \; \tan\varphi_c \tag{3.7}$$

Regarding the operation of the VSC, two parameters need to be specified. The first parameter can be the AC active power, the DC power, the modulation index, or the DC-side voltage. The second parameter can be the converter reactive power, the AC-side voltage, or the power factor angle. For isolated DSs (e.g., AC-DC hybrid microgrids), the

VSC can be controlled autonomously to achieve power sharing between the AC and DC subgrids without the need to specify the aforementioned two parameters. In this case, the frequency ω and the DC voltage V^{dc} are used as loading indicators for the AC and DC subgrids, respectively. In order to equalize the loading of the AC and DC subgrids, the active power flow between the two subgrids can be determined using (3.8) [77]. The VSC in an isolated DS can also support the reactive power when the active power flows from the DC side to the AC side [77]. The converter reactive power can then be controlled using the same reactive power droop of an AC DG (equation (3.32) in Section 3.3) unless the capacity limit of the VSC is reached [47]. It should be noted that the upper and lower limits of the modulation index should be taken into consideration in order to avoid overmodulation and excessive harmonics [36].

$$\widehat{\omega} = \widehat{V}^{dc} \tag{3.8}$$

where

$$\widehat{\omega} = \frac{\omega - 0.5\left(\omega^{max} + \omega^{min}\right)}{0.5\left(\omega^{max} - \omega^{min}\right)} \tag{3.9}$$

$$\widehat{V}^{dc} = \frac{V^{dc} - 0.5\left(V^{dc,max} + V^{dc,min}\right)}{0.5\left(V^{dc,max} - V^{dc,min}\right)} \tag{3.10}$$

3.2.3 Classification of AC-DC Hybrid Configurations

This subsection presents the proposed classification and the comprehensive analysis of the possible cases of AC-DC connections. AC/DC buses can be interconnected via AC/DC lines and AC-DC converters according to one of the following cases:

3.2.3.1 Connection between Two AC Buses

A connection between two AC buses can be achieved using the method exemplified by either Case 1 or Case 2. In Case 1, two AC buses are connected via an AC line, as shown in Figure 3.3(a). In this case, the active and reactive power equations are given by

$$P_{nm}^{(\mathbf{a})} = V_n^2 G_{nm} - V_n V_m \left(G_{nm}\cos\theta_{nm} + B_{nm}\sin\theta_{nm}\right) \tag{3.11}$$

$$Q_{nm}^{(\mathbf{a})} = -V_n^2 B_{nm} - V_n V_m \left(G_{nm}\sin\theta_{nm} - B_{nm}\cos\theta_{nm}\right) \tag{3.12}$$

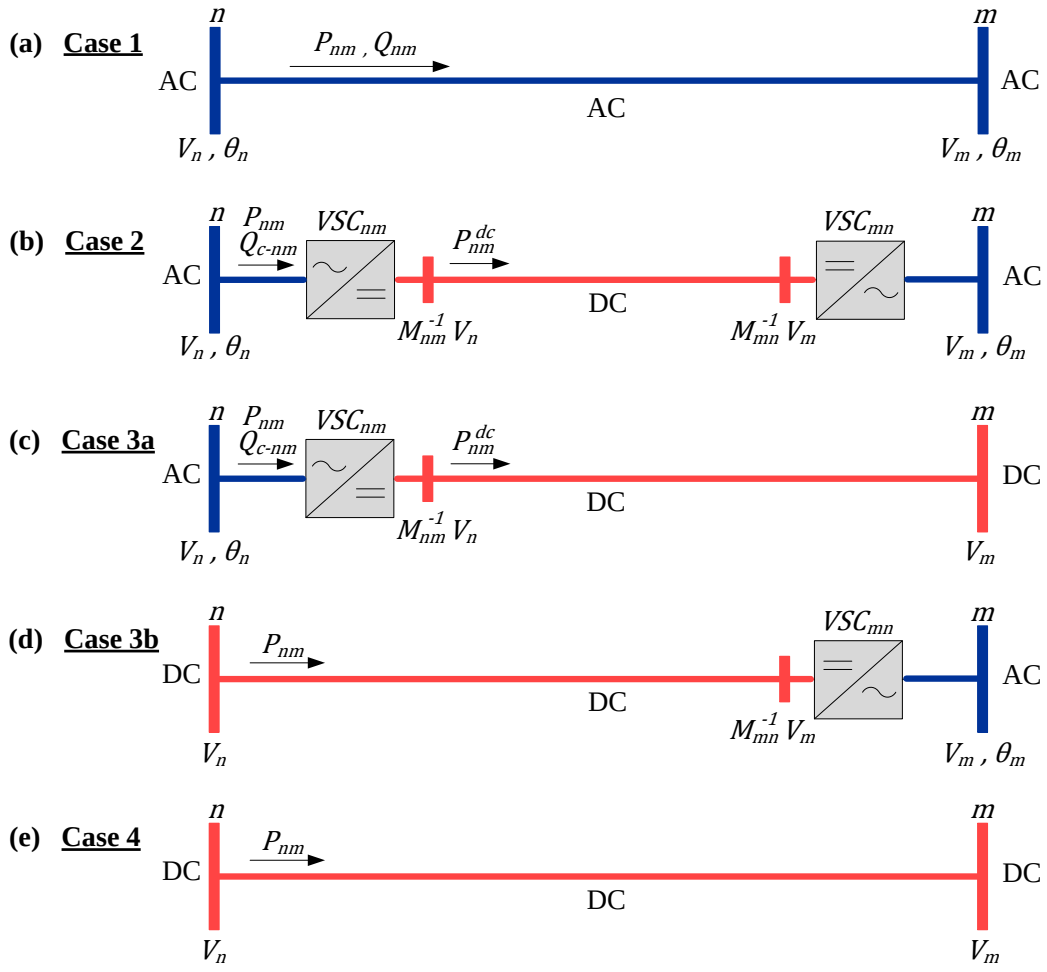

Figure 3.3: Possible cases of AC-DC connections.

In Case 2, a DC line connects the two AC buses via two AC-DC converters, as shown in Figure 3.3(b). The active and reactive power equations are expressed as (3.13) and (3.14), respectively. The values of a_1 and b_1, obtained from (3.15) and (3.16), respectively, are dependent on the direction of the power flow. If the power flows from bus n to bus m, the VSC at bus n functions as a rectifier, while the VSC at bus m functions as an inverter. In this case, the values of a_1 and b_1 become 1 and 0, respectively. In contrast, if the power flows from bus m to bus n, the values of a_1 and b_1 become 0 and 1, respectively.

$$P_{nm}^{\mathbf{(b)}} = G_{nm}^{dc}\left(M_{nm}^{-2}V_n^2 - M_{nm}^{-1}V_nM_{mn}^{-1}V_m\right)\left(\frac{a_1}{\eta_{c\text{-}nm\text{-}r}} + b_1\,\eta_{c\text{-}nm\text{-}i}\right) \tag{3.13}$$

$$Q_{c\text{-}nm}^{\mathbf{(b)}} = P_{nm}^{\mathbf{(b)}}\ \tan\varphi_{c\text{-}nm} \tag{3.14}$$

where

$$a_1 = 0.5(1 + \text{sign}(M_{nm}^{-1}V_n - M_{mn}^{-1}V_m)) \tag{3.15}$$

$$b_1 = 0.5(1 - \text{sign}(M_{nm}^{-1}V_n - M_{mn}^{-1}V_m)) \tag{3.16}$$

$$\text{sign}(x) = \begin{cases} 1 & \text{if } x > 0\,, \\ -1 & \text{if } x < 0\,, \\ 0 & \text{if } x = 0\,. \end{cases} \tag{3.17}$$

3.2.3.2 Connection between AC and DC Buses

The connection between two different types of buses (AC and DC) can be accomplished through the installation of a DC line and a VSC. Since this case involves two different types of buses (AC and DC), the formulation of the power flow equations at one side differs from that at the other side. Consideration of the following two cases facilitates the formulation of the power flow equations: 1) Case 3a entails the study of the power flow from the AC side, and 2) Case 3b involves the examination of the power flow from the DC side. Cases 3a and 3b are illustrated in Figure 3.3(c) and Figure 3.3(d), respectively. In Case 3a, the power equations (3.18)-(3.21) for the AC bus are formulated in the same manner as in Case 2.

$$P_{nm}^{\mathbf{(c)}} = G_{nm}^{dc}\left(M_{nm}^{-2}V_n^2 - M_{nm}^{-1}V_nV_m\right)\left(\frac{a_2}{\eta_{c\text{-}nm\text{-}r}} + b_2\ \eta_{c\text{-}nm\text{-}i}\right) \tag{3.18}$$

$$a_2 = 0.5(1 + \text{sign}(M_{nm}^{-1}V_n - V_m)) \tag{3.19}$$

$$b_2 = 0.5(1 - \text{sign}(M_{nm}^{-1}V_n - V_m)) \tag{3.20}$$

$$Q_{c\text{-}nm}^{\mathbf{(c)}} = P_{nm}^{\mathbf{(c)}}\ \tan\varphi_{c\text{-}nm} \tag{3.21}$$

For Case 3b, the power equation at the DC-bus side is expressed as follows:

$$P_{nm}^{(\mathbf{d})} = G_{nm}^{dc}(V_n^2 - V_n M_{mn}^{-1} V_m) \tag{3.22}$$

3.2.3.3 Connection between Two DC Buses

Case 4 represents a connection between two DC buses via a DC line, as depicted in Figure 3.3(e). In this case, the DC power equation is given by

$$P_{nm}^{(\mathbf{e})} = G_{nm}^{dc}(V_n^2 - V_n V_m) \tag{3.23}$$

3.3 Formulation of the Unified LF Model

Implementation of the LF model in any generic hybrid DS requires that the system configuration and parameters be described in a matrix format. The following matrices have been defined and are used as input for the LF model.

1. Configuration matrices: The following three binary matrices are defined based on the given hybrid DS configuration:
   (a) Bus-type vector W ($N_b \times 1$): This vector describes the type (AC or DC) of each bus in the hybrid DS:
      i. $W_n = 0$, if bus n is AC.
      ii. $W_n = 1$, if bus n is DC.
   (b) Connection matrix U ($N_b \times N_b$): This matrix describes the connection of the hybrid distribution network:
      i. $U_{nm} = 0$, if no line connects buses n and m.
      ii. $U_{nm} = 1$, if a line connects buses n and m.
   (c) Line-type matrix D ($N_b \times N_b$): This matrix describes the type (AC or DC) of each line in the hybrid DS:
      i. $D_{nm} = 0$, if the line connecting buses n and m is AC.
      ii. $D_{nm} = 1$, if the line connecting buses n and m is DC.

2. AC admittance matrix Y ($N_b \times N_b$): The element Y_{nm} in this matrix is the admittance of the AC line connecting bus n to bus m, and can be expressed as follows:

$$Y_{nm}(\omega) = G_{nm}(\omega) + j\, B_{nm}(\omega) = \frac{1}{R_{nm} + j\, \omega\, L_{nm}} \tag{3.24}$$

   where ($\omega = \omega^* = 2\pi \times 60\,\text{Hz}$) for grid-connected systems.

3. DC conductance matrix G^{dc} ($N_b \times N_b$): The element G^{dc}_{nm} in this matrix is the conductance of the DC line connecting bus n to bus m.

3.3.1 Power Balance Equations

The unified active and reactive power balance equations for the AC-DC hybrid system are given by

$$P_n^{inj} = P_n^{cal} \quad , \qquad \forall\ n = 1, 2, ..., N_b \tag{3.25}$$

$$Q_n^{inj} = Q_n^{cal} \quad , \qquad \forall\ n = 1, 2, ..., N_b \tag{3.26}$$

The equations for P_n^{inj}, P_n^{cal}, Q_n^{inj}, and Q_n^{cal} are expressed as (3.27)-(3.30), respectively. P_n^{inj} and Q_n^{inj} represent the net active and reactive power injected into bus n and are dependent on the loads and DGs connected at that bus. The respective equations for P_n^{inj} and Q_n^{inj}, expressed as (3.27) and (3.29), are derived based on the AC and DC buses classified as indicated in Figure 3.1. P_n^{cal} and Q_n^{cal} represent the calculated active and reactive power transmitted through the lines connected to bus n. The respective equations for P_n^{cal} and Q_n^{cal}, given as (3.28) and (3.30), are derived based on 1) the hybrid configuration cases classified according to Section 3.2.3, and 2) the configuration matrices (W, U, and D). For a given set of elements for the matrices (W, U, and D), only one configuration is activated at a time in the equations (3.27)-(3.30).

$$\begin{aligned} P_n^{inj} = \overline{W_n}\Big(P_{Gn}^{ac} - P_{Ln}^{ac} + \eta_{c\text{-}n\text{-}i}\, P_{Gn}^{dc} - \eta_{c\text{-}n\text{-}r}^{-1}\, P_{Ln}^{dc}\Big) \\ + W_n\Big(P_{Gn}^{dc} - P_{Ln}^{dc} + \eta_{c\text{-}n\text{-}r}\, P_{Gn}^{ac} - \eta_{c\text{-}n\text{-}i}^{-1}\, P_{Ln}^{ac}\Big)\ , \quad \forall\ n \in N_b \end{aligned} \tag{3.27}$$

$$
\begin{aligned}
P_n^{cal} = \sum_{\substack{m=1 \\ m \neq n}}^{N_b} U_{nm} \Big[& \overline{W_n}\ \overline{W_m}\ \overline{D_{nm}}\ \left(V_n^2\, G_{nm}(\omega) - V_n\, V_m\, (G_{nm}(\omega)\, \cos\theta_{nm} + B_{nm}(\omega)\, \sin\theta_{nm})\right) \\
& + \overline{W_n}\ \overline{W_m}\ D_{nm}\ \left(G_{nm}^{dc}\, (M_{nm}^{-2}\, V_n^2 - M_{nm}^{-1}\, V_n\, M_{mn}^{-1}\, V_m)\right) \left(a_1\ \eta_{c\text{-}nm\text{-}r}^{-1} + b_1\ \eta_{c\text{-}nm\text{-}i}\right) \\
& + \overline{W_n}\ W_m\ D_{nm}\ \left(G_{nm}^{dc}\, (M_{nm}^{-2}\, V_n^2 - M_{nm}^{-1}\, V_n\, V_m)\right) \left(a_2\ \eta_{c\text{-}nm\text{-}r}^{-1} + b_2\ \eta_{c\text{-}nm\text{-}i}\right) \\
& + W_n\ \overline{W_m}\ D_{nm}\ \left(G_{nm}^{dc}\, (V_n^2 - V_n\, M_{mn}^{-1}\, V_m)\right) \\
& + W_n\ W_m\ D_{nm}\ \left(G_{nm}^{dc}\, (V_n^2 - V_n\, V_m)\right) \Big]\ ,\ \forall\ n \in N_b
\end{aligned} \tag{3.28}
$$

$$
Q_n^{inj} = \overline{W_n}\Big(Q_{Gn}^{ac} - Q_{Ln}^{ac} + Q_{Gn\text{-}c}^{dc} - Q_{Ln\text{-}c}^{dc}\Big)\ ,\quad \forall\ n \in N_b \tag{3.29}
$$

$$
\begin{aligned}
Q_n^{cal} = \sum_{\substack{m=1 \\ m \neq n}}^{N_b} U_{nm} \Big[& \overline{W_n}\ \overline{W_m}\ \overline{D_{nm}}\ \left(-V_n^2\, B_{nm}(\omega) - V_n\, V_m\, (G_{nm}(\omega)\, \sin\theta_{nm} - B_{nm}(\omega)\, \cos\theta_{nm})\right) \\
& + \overline{W_n}\ \overline{W_m}\ D_{nm}\ P_{nm}\ \tan\varphi_{c\text{-}nm} \\
& + \overline{W_n}\ W_m\ D_{nm}\ P_{nm}\ \tan\varphi_{c\text{-}nm} \Big]\ ,\quad \forall\ n \in N_b
\end{aligned} \tag{3.30}
$$

For isolated AC-DC hybrid DSs, the droop-based control can be used to achieve proportional power sharing for AC and DC DGs [77]. In this case, the AC droop equations (3.31)-(3.32) as well as the DC droop equation (3.33) are then combined with (3.27)-(3.30).

$$
P_G^{ac} = (\omega_0\ -\ \omega)\ /\ \psi_p^{ac} \tag{3.31}
$$

$$
Q_G^{ac} = (V_0^{ac}\ -\ V^{ac})\ /\ \psi_q^{ac} \tag{3.32}
$$

$$
P_G^{dc} = (V_0^{dc}\ -\ V^{dc})\ /\ \psi_p^{dc} \tag{3.33}
$$

where

$$
\psi_p^{ac} = (\omega^{max}\ -\ \omega^{min})\ /\ P_G^{ac,max} \tag{3.34}
$$

$$
\psi_q^{ac} = (V^{ac,max}\ -\ V^{ac,min})\ /\ Q_G^{ac,max} \tag{3.35}
$$

$$
\psi_p^{dc} = (V^{dc,max}\ -\ V^{dc,min})\ /\ P_G^{dc,max} \tag{3.36}
$$

3.3.2 Parameters and Variables for AC and DC Buses

Table 3.1 summarizes the known parameters and unknown variables for all types of system buses. The known parameters at each bus are considered to be equality constraints, while the unknown variables constitute the output of the LF model.

Table 3.1: Parameters and Variables for AC and DC Buses

Bus (n) Type			$\boldsymbol{V_n}$	$\boldsymbol{\theta_n}$	$\boldsymbol{P_n^{inj}}$	$\boldsymbol{Q_n^{inj}}$
AC	Slack Bus*		Known	0.0°	Variable	Variable
	Load (P-Q) Bus		Variable	Variable	Known	Known
	(P-V) Bus	$Q_G^{min} \leq Q_G \leq Q_G^{max}$	Known	Variable	Known	Variable
		$Q_G > Q_G^{max}$	Variable	Variable	Known	Q_G=Q_G^{max}
		$Q_G < Q_G^{min}$	Variable	Variable	Known	Q_G=Q_G^{min}
	Droop-based DG Bus**		Variable	Variable	Variable	Variable
DC	Load (or P^{dc}) Bus		Variable	–	Known	–
	(V^{dc}) Bus	$P_G^{min} \leq P_G \leq P_G^{max}$	Known	–	Variable	–
		$P_G > P_G^{max}$	Variable	–	P_G=P_G^{max}	–
		$P_G < P_G^{min}$	Variable	–	P_G=P_G^{min}	–
	Droop-based DG Bus**		Variable	–	Variable	–

* Connected to a stiff AC source (e.g., the distribution substation).

** Used in isolated systems (e.g., AC-DC hybrid microgrids).

3.3.3 Solution Procedures

The hybrid LF problem is defined by a system of equations that are solved simultaneously. In order to find the LF solution in this study, a generalized reduced gradient (GRG) method [79, 80] is used for solving the optimization problem described below.

$$\min \ \|F(x)\|_2 \quad , \quad x \in \mathbb{R}^{n_v} \tag{3.37}$$

where

$$F(x) = \begin{cases} P_i^{inj} - P_i^{cal} & , \forall\ i \in N_b \\ Q_i^{inj} - Q_i^{cal} & , \forall\ i \in N_b \\ P_{G_i}^{ac} - \frac{1}{\psi_{p,i}^{ac}} \left(\omega_0 - \omega\right) & , \forall\ i \in N_{G\text{-}dr}^{ac} \\ Q_{G_i}^{ac} - \frac{1}{\psi_{q,i}^{ac}} \left(V_{i,0}^{ac} - V_i^{ac}\right) & , \forall\ i \in N_{G\text{-}dr}^{ac} \\ P_{G_i}^{dc} - \frac{1}{\psi_{p,i}^{dc}} \left(V_{i,0}^{dc} - V_i^{dc}\right) & , \forall\ i \in N_{G\text{-}dr}^{dc} \\ \widehat{V}_i^{dc} - \widehat{\omega} & , \forall\ i \in N_{c\text{-}iso} \\ Q_{c\text{-}i} - \frac{1}{\psi_{q,c\text{-}i}^{ac}} \left(V_{c\text{-}i,0}^{ac} - V_{c\text{-}i}^{ac}\right) & , \forall\ i \in N_{c\text{-}iso} \end{cases} \tag{3.38}$$

$F(x)$ is the set of the system equations that include the power balance equations, the droop equations, and the VSC equations; ($N_{G\text{-}dr}^{ac}$ and $N_{G\text{-}dr}^{dc}$) are the number of the droop-based AC and DC DGs, respectively; $N_{c\text{-}iso}$ is the number of VSCs in an isolated DS; and n_{v} is the number of the system unknown variables x.

The first step in the solution procedures is to define the type, the given parameters, and the unknown variables for each bus in the hybrid DS, as presented in Table 3.1. In the second step, the configuration matrices (W, U, and D) as well as the AC admittance matrix Y and the DC conductance matrix G^{dc} are constructed. In the third step, the system parameters are converted to per-unit values, and a flat start ($V^{(0)} = 1.0\,\mathrm{p.u.}$ and $\theta^{(0)} = 0.0^{\circ}$) is assumed for the unknown system voltages. Finally, the data prepared in the previous steps are then used as input to the LF model described by (3.25)-(3.38).

3.4 Case Studies

This section presents the case studies that were used for evaluating the effectiveness and accuracy of the proposed LF model. In the case studies, the proposed LF model was implemented in a general algebraic modeling system (GAMS) and executed on a desktop computer with the following specifications: Intel Core i7 2600 @ 3.4 GHz, 64 bit, and 8 GB

RAM. In the first case study, the accuracy of the proposed model was verified against the steady-state solution produced by PSCAD/EMTDC. The PSCAD/EMTDC is a time-domain software that can accurately model power system components using differential equations, and thus can be used for validating LF algorithms [40, 45, 81]. Such software takes a huge amount of computational time compared to the algebraic LF methods that can perform steady-state analyses in very short time.

3.4.1 Thirteen-Bus Test System

As shown in Figure 3.4, the hybrid DS used for the first case study was a 13-bus network. The data related to the loads and generators at each bus are presented in Figure 3.4. Table 3.2 summarizes the impedances of the network under study. The base values for the per-unit conversion in this system are S_{base}= 10 MVA, V^{ac}_{base}= 4.16 kV, and V^{dc}_{base}= 6.8 kV. The efficiency and the power factor of the VSCs are given as 98 % and 95 %, respectively. Regarding the bus classifications, bus 1 represents a slack bus, buses (3 and 8) are P-V buses, bus 5 is a V^{dc} bus, and the remaining buses are considered as load buses. The results obtained from the proposed LF model and the steady-state solution provided by the PSCAD software are listed in Tables 3.3 and 3.4. The LF model converged with a system total power mismatch of 6.9×10^{-10} p.u., which is equal to $\big(\|P^{inj}_n - P^{cal}_n\|_2 + \|Q^{inj}_n - Q^{cal}_n\|_2\,,\ \forall\, n \in N_b\big)$, and the computational time was found to be 124 ms.

Table 3.2: Impedances of the 13-Bus Test System

From Bus	To Bus	Resistance (Ω)	Reactance (Ω)	From Bus	To Bus	Resistance (Ω)	Reactance (Ω)
1	2	0.2218	0.3630	5	6	0.2208*	–
1	9	0.2218	0.3630	6	13	0.4415*	–
2	3	0.8870	1.4520	7	8	0.4435	0.7260
3	10	0.0500	0.7540	7	12	0.0500	0.7540
3	11	0.0500	0.7540	7	13	0.0500	0.7540
4	5	0.2208*	–	8	9	0.4435	0.7260
4	11	0.4415*	–	10	12	0.8830*	–

* DC resistances.

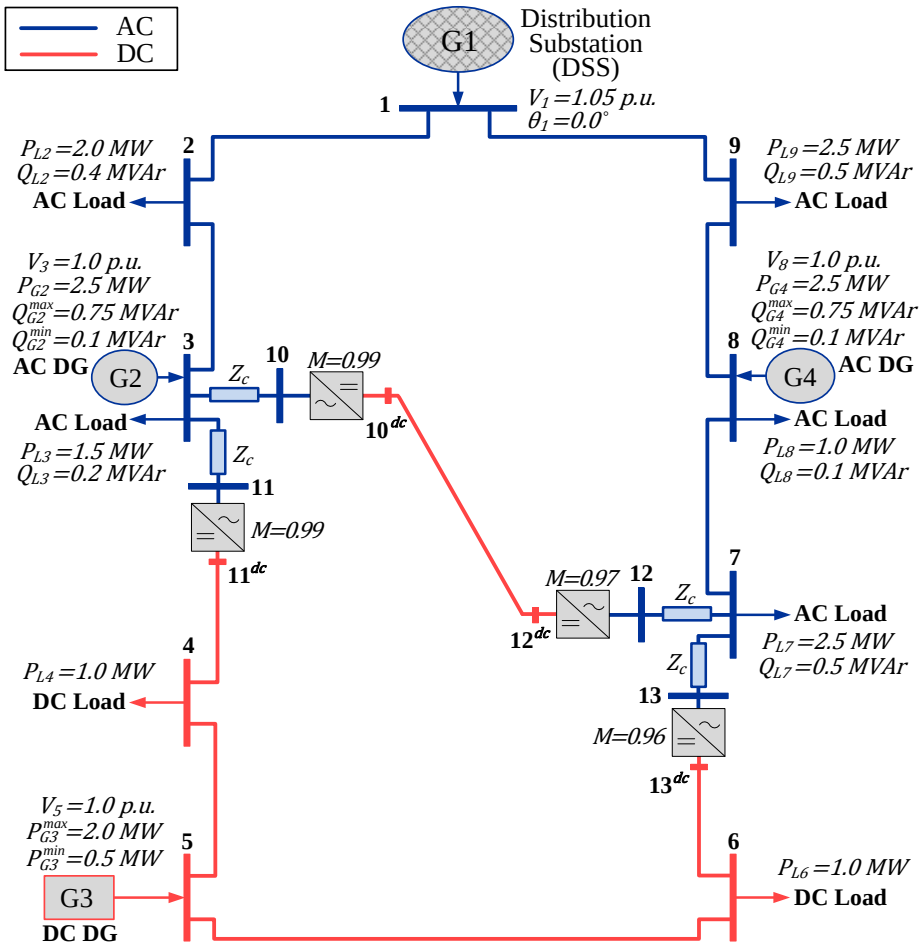

Figure 3.4: Thirteen-bus test system.

To evaluate the accuracy of the proposed LF model, the percentage errors between the PSCAD solution and the LF model solution were calculated for the system variables. As can be seen in Table 3.3, the maximum error for the voltage magnitudes at the system buses is as low as 0.04 %, while the maximum errors for the generated active and reactive powers are no greater than 0.03 % and 0.028 %, respectively. Using the data in Table 3.4, the percentage errors were also calculated for the line flows. The maximum errors for the active and reactive line flows are only 0.032 % and 0.033 %, respectively. The comparison of the results obtained from the proposed LF model and those produced by the PSCAD software therefore demonstrates the effectiveness and accuracy of the proposed model.

Table 3.3: LF Solution and PSCAD Results for the 13-Bus Test System: Bus Voltages and Generators' Data

		LF Model Results		**PSCAD Results**	
Bus No. (n)	Bus Type	V_n (p.u.)	θ_n (deg.)	V_n (p.u.)	θ_n (deg.)
1	AC, Slack Bus	1.0500	0.0000	1.05000	0.00000
2	AC, Load Bus	1.0130	-2.0627	1.01300	-2.0772
3	AC, P-V Bus	1.0000	-2.4637	1.00000	-2.4637
4	DC, Load Bus	0.9970	–	0.99738	–
5	DC, V^{dc} Bus	1.0000	–	1.00000	–
6	DC, Load Bus	0.9940	–	0.99380	–
7	AC, Load Bus	0.9460	-6.6463	0.94560	-6.6396
8	AC, P-V Bus	1.0000	-2.9794	1.00000	-2.9794
9	AC, Load Bus	1.0040	-2.6356	1.00400	-2.6560
10	AC, Load Bus	0.9880	-4.0680	0.98780	-4.1068
11	AC, Load Bus	0.9920	-3.6096	0.99188	-3.6274
12	AC, Load Bus	0.9560	-4.9847	0.95610	-4.9876
13	AC, Load Bus	0.9510	-5.7869	0.95080	-5.8398
Bus No. (n)	Bus Type	P_{Gn} (MW)	Q_{Gn} (MVAr)	P_{Gn} (MW)	Q_{Gn} (MVAr)
1	AC, Slack Bus	4.9210	1.2399	4.9240	1.2390
3	AC, P-V Bus	2.5000	0.5300	2.5000	0.5305
5	DC, V^{dc} Bus	1.8701	–	1.8726	–
8	AC, P-V Bus	2.5000	0.4238	2.5000	0.4266

3.4.2 Modified IEEE 33-Bus Test System

The modified IEEE 33-bus DS was used for the second case study, as shown in Figure 3.5. The original IEEE 33-bus DS presented in [82] has been modified to include DC buses and lines. The DC buses were selected where the majority of loads and DGs are DC. The network impedances and the load data are listed in Table 3.5 and Table 3.6, respectively. The base values used for this test system are S_{base}= 10 MVA, V^{ac}_{base}= 12.66 kV, ω^*= $2\pi\times60$ Hz, and V^{dc}_{base}= 20.67 kV. The efficiency of all AC-DC converters used in this case study is given as 95 %, and the power factor of the VSCs installed in the network lines is given as 95 %.

Table 3.4: LF Solution and PSCAD Results for the 13-Bus Test System: Line Flows

From	To	**LF Model Results**		**PSCAD Results**	
Bus	Bus	P (MW)	Q (MVAr)	P (MW)	Q (MVAr)
1	2	2.183000	0.573300	2.186000	0.571600
1	9	2.738000	0.666600	2.737000	0.667000
2	1	-2.123800	-0.476400	-2.127000	-0.474400
2	3	0.123800	0.076400	0.126900	0.074420
3	2	-0.122700	-0.074600	-0.125800	-0.072650
3	10	0.656400	0.236500	0.657200	0.238000
3	11	0.466300	0.163700	0.467600	0.165100
4	5	-0.545700	–	-0.547900	–
4	11^{dc}	-0.454300	–	-0.452100	–
5	4	0.547100	–	0.549341	–
5	6	1.323000	–	1.323260	–
6	5	-1.314700	–	-1.314900	–
6	13^{dc}	0.314700	–	0.314900	–
7	8	-1.572900	-0.220100	-1.575000	-0.223000
7	12	-0.620000	-0.183800	-0.619200	-0.182600
7	13	-0.307100	-0.096000	-0.306100	-0.094400
8	7	1.645200	0.338500	1.647000	0.341700
8	9	-0.145200	-0.014700	-0.144300	-0.015090
9	1	-2.645700	-0.515600	-2.645000	-0.516000
9	8	0.145700	0.015600	0.144900	0.015974
10	3	-0.655000	-0.215300	-0.652000	-0.212000
10^{dc}	12^{dc}	0.641900	–	0.641950	–
11	3	-0.465600	-0.153000	-0.463000	-0.150300
11^{dc}	4	0.456288	–	0.454060	–
12	7	0.621300	0.204200	0.623600	0.207500
12^{dc}	10^{dc}	-0.633980	–	-0.634100	–
13^{dc}	6	-0.313670	–	-0.314000	–
13	7	0.307400	0.101100	0.310600	0.104000

Regarding the bus classifications, bus 1 represents a slack bus, buses (5, 24, and 29) are P-V buses, and the remaining buses are considered as load buses. The results obtained from the proposed LF model are listed in Tables 3.7, 3.8, and 3.9. The LF model converged with a system total power mismatch of 1.2×10^{-10} p.u., and the computational time was found to be 207 ms.

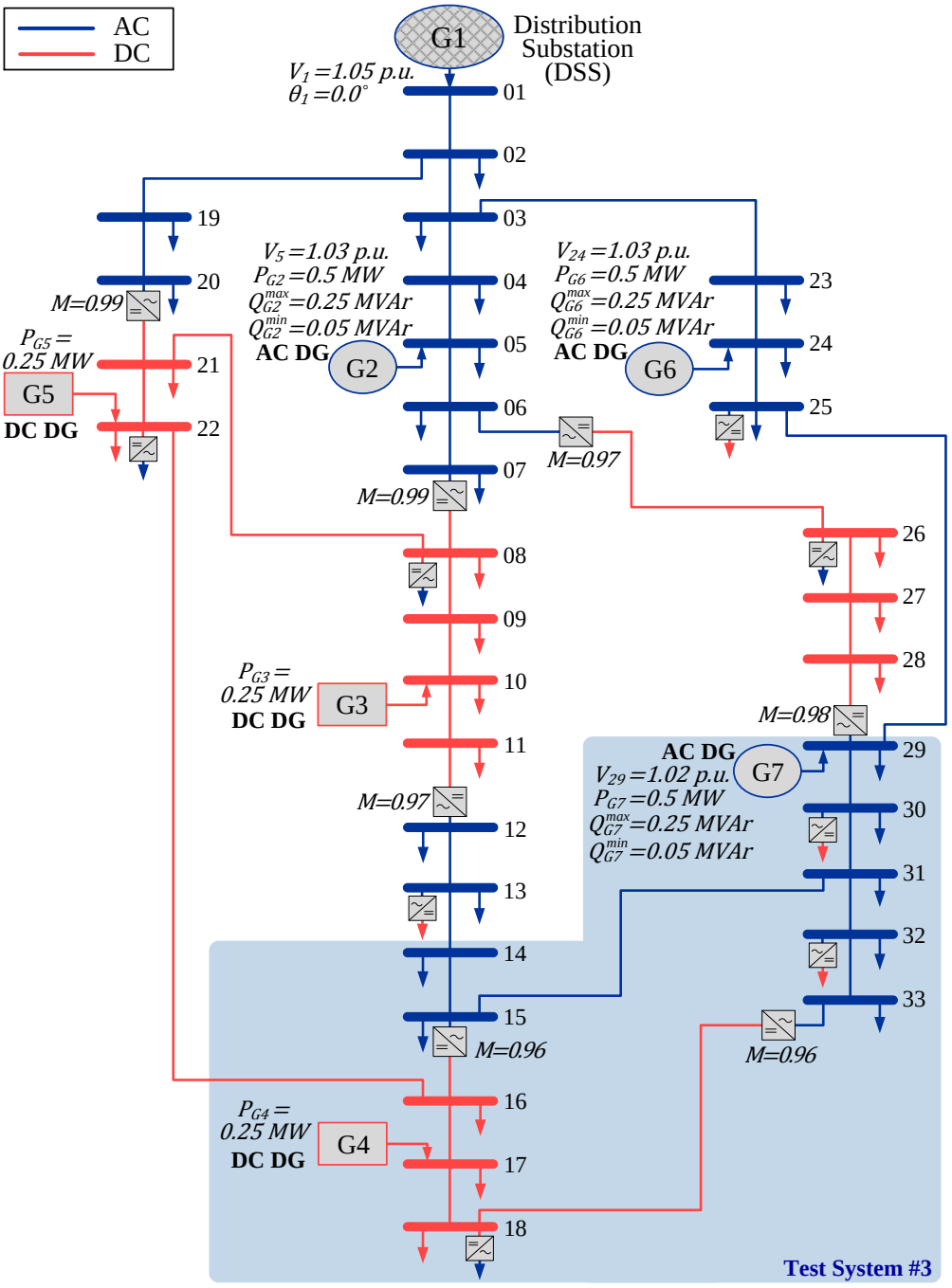

Figure 3.5: 33-bus hybrid distribution system.

Table 3.5: Impedances of the 33-Bus Test System, ($\omega = 1.0$ p.u.)

From Bus	To Bus	Resistance (Ω)	Reactance (Ω)	From Bus	To Bus	Resistance (Ω)	Reactance (Ω)
1	2	0.0922	0.0470	15	31	2.0000	2.0000
2	3	0.4930	0.2511	16	17	2.5780*	–
2	19	0.1640	0.1565	16	22	4.0000*	–
3	4	0.3660	0.1864	17	18	1.4640*	–
3	23	0.4512	0.3083	18	33	1.0000*	–
4	5	0.3811	0.1941	19	20	1.5042	1.3554
5	6	0.8190	0.7070	20	21	0.8190*	–
6	7	0.1872	0.6188	21	22	1.4178*	–
6	26	0.4060*	–	23	24	0.8980	0.7091
7	8	1.4228*	–	24	25	0.8960	0.7011
8	9	2.0600*	–	25	29	0.5000	0.5000
8	21	4.0000*	–	26	27	0.5684*	–
9	10	2.0880*	–	27	28	2.1180*	–
10	11	0.3932*	–	28	29	1.6084*	–
11	12	0.7488*	–	29	30	0.5075	0.2585
12	13	1.4680	1.1550	30	31	0.9744	0.9630
13	14	0.5416	0.7129	31	32	0.3105	0.3619
14	15	0.5910	0.5260	32	33	0.3410	0.5302
15	16	1.4926*	–				

* DC resistances.

3.4.3 Isolated AC-DC Hybrid Test System

For the third case study, it is assumed that the shaded area (Test System # 3) in Figure 3.5 has been islanded. Two more DGs were added to this isolated system: 1) AC DG at bus 31, and 2) DC DG at bus 16. The two AC DGs as well as the two DC DGs are operated as droop-controlled DGs. Because the system frequency is considered as an additional variable, the voltage angle of one of the system AC buses (e.g., bus 31) is taken as a reference (i.e., $\theta_{31} = 0.0°$) in order to equalize the number of variables and the number of system equations. Taking the limits of the frequency and the AC/DC voltages as $\pm 1\%$ and $\pm 5\%$ [83], respectively, the droop gains for the AC and DC DGs can then

Table 3.6: Load Data of the 33-Bus Test System

Bus No.	P_L^{ac} (kW)	Q_L^{ac} (kVAr)	P_L^{dc} (kW)	Bus No.	P_L^{ac} (kW)	Q_L^{ac} (kVAr)	P_L^{dc} (kW)	Bus No.	P_L^{ac} (kW)	Q_L^{ac} (kVAr)	P_L^{dc} (kW)
1	–	–	–	12	120	70	–	23	180	100	–
2	200	120	–	13	60	15	60	24	115	60	–
3	180	80	–	14	400	200	–	25	300	100	300
4	240	160	–	15	260	105	–	26	60	35	60
5	125	60	–	16	–	–	60	27	–	–	200
6	200	100	–	17	–	–	60	28	–	–	120
7	200	100	–	18	45	20	45	29	85	35	–
8	120	70	120	19	180	80	–	30	100	60	100
9	–	–	120	20	180	80	–	31	170	50	–
10	–	–	120	21	–	–	300	32	145	70	145
11	–	–	300	22	90	45	90	33	240	160	–

Table 3.7: LF Solution for the 33-Bus Test System: Voltage Magnitudes and Angles

Bus No.	V_n (p.u.)	θ_n (deg.)	Bus No.	V_n (p.u.)	θ_n (deg.)	Bus No.	V_n (p.u.)	θ_n (deg.)
1	1.05000	0.00000	12	0.99317	-0.62317	23	1.03477	-0.05338
2	1.04709	-0.00972	13	0.99215	-0.66568	24	1.03000	-0.11852
3	1.03776	-0.02781	14	0.99225	-0.66363	25	1.02238	-0.21870
4	1.03360	-0.03683	15	0.99449	-0.62944	26	1.04951	–
5	1.03000	-0.05114	16	1.03692	–	27	1.04808	–
6	1.01912	-0.27694	17	1.03884	–	28	1.04371	–
7	1.01869	-0.29890	18	1.03930	–	29	1.02000	-0.22492
8	1.02923	–	19	1.04503	-0.05930	30	1.01404	-0.24914
9	1.02674	–	20	1.02871	-0.43950	31	1.00228	-0.50558
10	1.02479	–	21	1.03702	–	32	1.00006	-0.57217
11	1.02430	–	22	1.03715	–	33	0.99823	-0.63485

Table 3.8: LF Solution for the 33-Bus Test System: Generators' Data

	G1	G2	G3	G4	G5	G6	G7
P_G (MW)	4.3435	0.5000	0.2500	0.2500	0.2500	0.5000	0.5000
Q_G (MVAr)	1.8900	0.1400	–	–	–	0.2435	0.0819

Table 3.9: LF Solution for the 33-Bus Test System: Line Flows

Bus n	Bus m	P_{nm} (kW)	Q_{nm} (kVAr)	Bus n	Bus m	P_{nm} (kW)	Q_{nm} (kVAr)
1	2	4343.5	1890.0	16	22	-25.421*	–
2	3	2566.4	1195.6	17	18	-140.03*	–
2	19	1565.4	568.38	18	33	-232.46*	–
3	4	1533.3	706.90	19	20	1382.8	485.91
3	23	830.65	397.28	20	21	1184.3	389.28
4	5	1287.2	543.82	21	8	862.72*	–
5	6	1657.9	621.60	21	20	-1122.9*	–
6	7	125.96	75.735	21	22	-39.831*	–
6	26	1316.8	432.82	22	16	25.427*	–
7	8	-74.069	-24.345	23	24	648.43	295.77
8	7	77.986*	–	24	25	1030.8	477.22
8	9	531.93*	–	25	29	408.19	371.90
8	21	-856.24*	–	26	6	-1249.6*	–
9	10	410.65*	–	26	27	1126.5*	–
10	11	539.86*	–	27	28	924.95*	–
11	12	239.61*	–	28	29	801.09*	–
12	11	-227.54	-74.788	29	28	-758.93	-249.45
12	13	107.54	4.7880	29	30	1581.2	667.32
13	14	-15.728	-10.297	30	31	1367.0	602.75
14	15	-415.73	-210.30	31	15	399.33	226.67
15	16	-279.83	-91.975	31	32	784.45	313.04
15	31	-396.71	-224.05	32	33	485.44	241.44
16	15	294.84*	–	33	18	244.82	80.467
16	17	-329.42*	–				

* DC power.

be calculated using (3.34)-(3.36), as shown in Table 3.10. The active and reactive powers of the two converters ($VSC_{15\text{-}16}$ and $VSC_{33\text{-}18}$) are controlled autonomously using the last two equations in (3.38). The capacity and the maximum reactive power of each VSC are given as 400 kVA and 100 kVAr, respectively. The upper and lower limits of the modulation index are given as 1.0 and 0.77, respectively [83]. The results obtained from the proposed LF model are listed in Tables 3.10 and 3.11, and the modulation indices of the VSCs were found to be $M_{15\text{-}16} = 0.991$ and $M_{33\text{-}18} = 0.996$. The LF model converged with a system total power mismatch of 0.9×10^{-10} p.u., and the computational time was found to be 167 ms.

Table 3.10: Test System # 3: Input Data and LF Solution for the System DGs

		Input Data		**Droop Gains**			**LF Solution**	
Bus No.	DG No.	P_G^{max} (MW)	Q_G^{max} (MVAr)	ψ_p^{ac} (p.u.)	ψ_q^{ac} (p.u.)	ψ_p^{dc} (p.u.)	P_G (MW)	Q_G (MVAr)
29	G7	0.50	0.25	0.40	4.0	–	0.3473	0.1740
31	G8	1.25	0.50	0.16	2.0	–	0.8683	0.3576
17	G4*	0.25	–	–	–	4.000	0.1715	–
16	G9*	0.75	–	–	–	1.333	0.5109	–

* DC DGs.

Table 3.11: LF Solution for the Test System # 3: Voltage Magnitudes, Voltage Angles, and Line Flows. ($\omega = 0.9961$ p.u.)

Bus Voltages			**Active and Reactive Power Flows**							
Bus (n)	V_n (p.u.)	θ_n (deg.)	Bus (n)	Bus (m)	P_{nm} (kW)	Q_{nm} (kVAr)	Bus (n)	Bus (m)	P_{nm} (kW)	Q_{nm} (kVAr)
14	0.9695	-0.0916	14	15	-400.00	-200.00	29	30	262.31	139.05
15	0.9717	-0.0569	15	14	400.79	200.70	30	29	-262.02	-138.90
16	0.9819	–	15	16	-356.56	-78.345	30	31	56.757	78.901
17	0.9814	–	15	31	-304.23	-227.35	31	15	306.13	229.25
18	0.9808	–	16	15	375.84*	–	31	30	-56.697	-78.842
29	0.9804	-0.0095	16	17	75.102*	–	31	32	448.84	157.24
30	0.9793	-0.0084	17	16	-75.067*	–	32	31	-448.38	-156.71
31	0.9785	0.0000	17	18	186.53*	–	32	33	150.75	86.705
32	0.9772	-0.0422	18	17	-186.41*	–	33	18	-89.318	-73.399
33	0.9766	-0.0610	18	33	94.040*	–	33	32	-150.68	-86.601

* DC power.

3.4.4 Discussion on Scalability

To assess the effect of the system size on the execution time and accuracy of the proposed LF model, the LF problem of a 132-bus AC-DC hybrid system was solved using the pro-

posed model. The 132-bus hybrid DS shown in Figure 3.6 includes one main distribution substation (DSS) and four subsystems, each representing a 33-bus network identical to the network in Figure 3.5. The proposed LF model successfully converged with a system total power mismatch of 3.84×10^{-13} p.u., and the computational time was found to be 936 ms. These results demonstrate that the proposed model can be efficiently applied to large hybrid DSs.

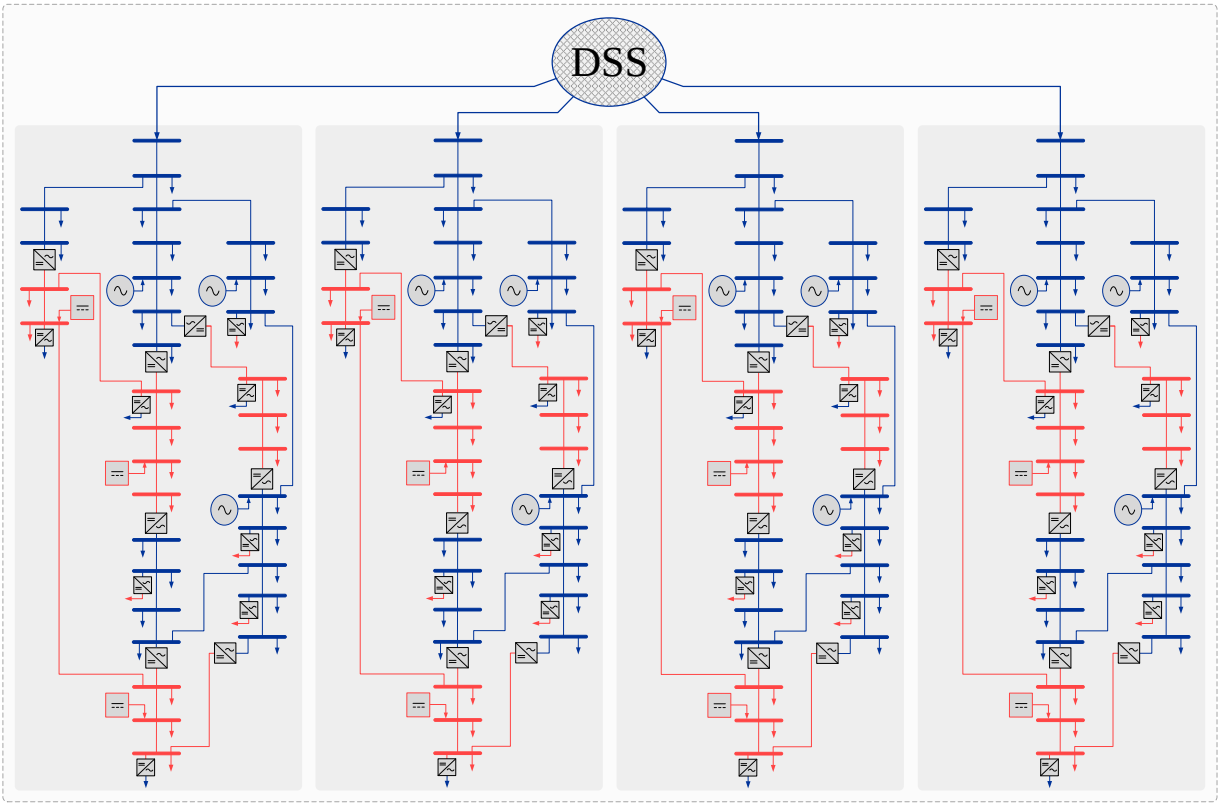

Figure 3.6: 132-bus hybrid distribution system.

For each case study, the proposed model successfully reached convergence, and the LF solution was found without the need to divide the main hybrid network into several AC and DC subgrids. In addition, the obtained results reflect the computational efficiency of the proposed model, where the model has provided accurate LF solutions in a time frame suitable for real-time applications. Based on the update rate of the smart grid meters, the

execution time of the LF algorithms used for real-time operation should be in the range of several seconds to a few minutes [84]. The proposed LF model can therefore be used for the online applications in future smart DSs.

3.5 Conclusion

This chapter proposes a novel AC-DC LF model for hybrid DSs. The detailed analysis presented includes consideration of the possible AC-DC hybrid DS configurations. In the proposed LF model, VSCs are employed for AC-DC power conversions. The proposed model can solve the LF problem for the AC and DC portions of the hybrid DS simultaneously based on the integration of the AC and DC power equations into one unified model. Employing three binary matrices in the unified power equations allows any configuration of AC-DC hybrid DSs to be described, which introduces a high degree of flexibility into the proposed LF model. The proposed model was applied for solving the LF problem of grid-connected and isolated hybrid DSs that included a variety of types of loads, DGs, buses, and lines. The effectiveness and accuracy of the proposed model was verified against the steady-state solution produced by PSCAD/EMTDC software. The results demonstrate that the proposed LF model can provide an accurate solution while also offering the flexibility and speed required for online smart-grid applications. The proposed model is generic and can be integrated in a variety of applications in power systems. Therefore, based on the mathematical formulation of this LF model, new techniques for the planning, operation, and reconfiguration of AC-DC hybrid DSs are presented in the following chapters.

Chapter 4

An Energy Management Scheme for AC-DC Hybrid DSs Considering the Network-Reconfiguration Capability

4.1 Introduction

This chapter presents an EMS for AC-DC hybrid DSs. The proposed EMS includes two stages: 1) the day-ahead stage, in which a proposed reconfiguration technique is employed to determine the most efficient configuration for each hour of the following day, and 2) the real-time stage, in which a proposed OPF-based LCM technique (OPF-LCM) is used for guaranteeing a reliable and optimal operating schedule for a hybrid DS. The proposed two-stage EMS was successfully tested on a case study of a hybrid DS that included different types of loads and DGs, such as PV panels, wind DGs, and EV charging stations (EVSs). The benefits provided by the proposed EMS were verified through a comparison of the EMS solution and the base-case solution.

This chapter is organized as follows: Section 4.2 describes the structure of AC-DC hybrid DSs and introduces the concept of the proposed two-stage EMS. Section 4.3 presents the formulation and procedures of the proposed reconfiguration algorithm. The formulation of the proposed OPF-LCM technique is explained in Section 4.4. The case study used for

evaluating the benefits provided by the proposed two-stage EMS is described in Section 4.5. The final section summarizes the conclusions of this chapter.

4.2 Description of the AC-DC Hybrid DSs and the Proposed Two-Stage EMS

As discussed earlier in Chapter 1, future smart DSs will include different types of AC and DC loads and DGs. For the optimal accommodation of these loads and DGs, the current belief is that DS networks should be AC-DC hybrid systems [5–8] that include AC/DC buses, AC/DC lines, and AC-DC converters, as illustrated in Figure 4.1. In this study, VSCs are installed in the network lines for AC-DC power conversions. Figure 4.1 also shows the possible types of hybrid DS buses and lines, as well as the connection of the system loads and DGs to the AC and DC buses [83].

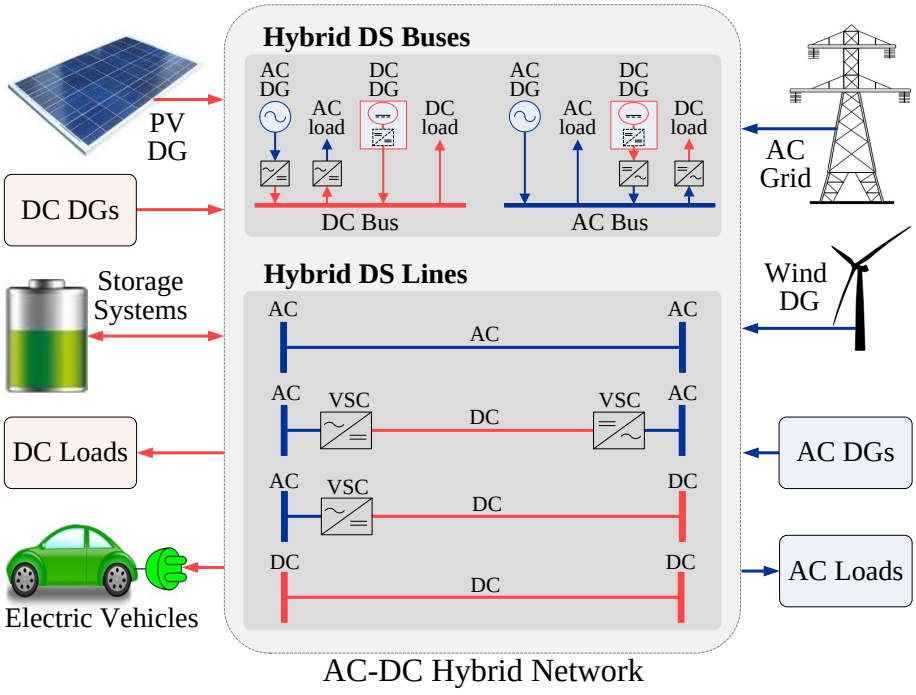

Figure 4.1: Structure and components of AC-DC hybrid DSs.

Achieving reliable and optimal operation of future hybrid DSs will require efficient energy management techniques. This study proposes an EMS that includes two stages. In Stage 1, the day-ahead stage, a network reconfiguration technique proposed for AC-DC hybrid DSs determines the most efficient network topologies for the next 24 hours. The objective of the proposed technique is to minimize day-ahead energy losses. Day-ahead forecasted data related to load demands and renewable-based DGs are assumed to be available and are used as input to the Stage-1 reconfiguration technique.

In Stage 2, the real-time stage, an OPF-LCM technique is employed as a means of guaranteeing the reliable and optimal operation of the hybrid DS. In this stage, the optimal online operation of the hybrid DS is achieved through the minimization of DS operation costs. An LCM is also applied in order to maintain system reliability and the continuity of the supply in the case of abnormal conditions [85]. According to the reliability standards provided by the North American Electric Reliability Corporation (NERC), the LCM is considered as one of the contingency reserve services [85]. Customers in LCM programs sign contracts with the utility operator, agreeing to reduce their demands when requested in order to guarantee system reliability and the continuity of supply. Each customer participating in a program benefits from the incentives specified in the contract as well as from reduced energy consumption bills [86].

For reliable and optimal real-time operation, the update rate of a DS operational schedule should be in the range of several seconds to a few minutes. This rate is dependent on the speed of the available forecasting and metering systems that can provide highly accurate data to the utility operator. In this study, the proposed OPF-LCM is assumed to be executed every 5 min under normal operating conditions [84]. However, the proposed OPF-LCM can also be executed in a very short time in the case of abnormal operating scenarios, as set out in Section 4.5.4.

4.3 Stage 1: The Reconfiguration Algorithm

The primary goal of the proposed reconfiguration algorithm is to determine the optimal day-ahead reconfiguration schedule that minimizes DS energy losses. The network configuration is described by the connection matrix $U(N_b \times N_b)$. The elements of U represent the binary decision variables of the reconfiguration algorithm. The element U_{nm} is equal to 0

if the line connecting buses n and m is open, and equal to 1 if the line connecting buses n and m is closed. The AC-DC hybrid reconfiguration problem presented in this study is a mixed-integer nonlinear programming problem with discontinuous derivatives, and it has been divided into two nested optimization problems: a master problem and a subproblem. The formulation of the reconfiguration algorithm is explained in the following subsections.

4.3.1 Formulation of the Master Problem

The master problem is a mixed-integer optimization problem that is formulated using a genetic algorithm (GA) [87]. The master problem constraints apply only to independent integer variables, whose values are used as input to the subproblem. The following are the objective function and the constraints of the master problem.

4.3.1.1 Objective Function

The objective function is to minimize the day-ahead energy losses, as follows:

$$\min \ \mathcal{F}_{master} = \sum_{t=1}^{T} \left(\mathcal{P}_{loss,t} \ \Delta t \right) \tag{4.1}$$

4.3.1.2 Network Topology Constraints

The network topology constraints are divided into 1) the integer constraint (4.2) for the binary variables of the connection matrix U and 2) the radiality constraints (4.3)-(4.4) for maintaining the radial operation of the DS.

$$\begin{cases} U_{nm,t} \in \{0\,,1\} & \text{if } \ U_{nm} \in \mathbb{S} \\ U_{nm,,t} = 1 & \text{if } \ U_{nm} \in \mathbb{S}_c \\ U_{nm,t} = 0 & \text{otherwise} \end{cases} \quad , \ \forall \ n, m \in N_b \ , \ t \in T \tag{4.2}$$

$$\sum_{n=1}^{N_b} \sum_{\substack{m=1 \\ m>n}}^{N_b} U_{nm,t} = N_b - 1 \ \ , \ \forall \ t \in T \tag{4.3}$$

$$\sum_{m=1}^{N_b} U_{nm,t} \geq 1 \quad , \quad \forall\ n \in N_b\,,\, t \in T \tag{4.4}$$

4.3.1.3 Switching Constraints

The switching constraints (4.5)-(4.6) are used for guaranteeing that the number of switching actions will not violate the maximum allowable limits. The constraint expressed in (4.5) limits the number of daily switching actions for each controlled switch, while the constraint defined in (4.6) limits the number of switching actions per hour.

$$\sum_{t=1}^{T} \mid U_{nm,t} - U_{nm,t-1} \mid \ \leq \ N_{SW,s}^{max} \ , \ \forall\ U_{nm} \in \mathbb{S} \tag{4.5}$$

$$\sum_{n=1}^{N_b} \sum_{\substack{m=1 \\ m>n}}^{N_b} \mid U_{nm,t} - U_{nm,t-1} \mid \ \leq \ N_{SW,t}^{max} \ , \ \forall\ t \in T \tag{4.6}$$

4.3.2 Formulation of the Subproblem

The subproblem is designed to solve the OPF problem for each GA chromosome at each hour t. The problem is implemented in GAMS as a nonlinear programming problem with discontinuous derivatives (DNLP) and is solved using a GRG method [80]. The constraints of the subproblem are on dependent variables, whose values are determined based on the values selected for the independent variables in the master problem. The following are the objective function and the constraints of the subproblem.

4.3.2.1 Objective Function

The objective function is to minimize the power losses for each GA chromosome at each hour t, as follows:

$$\min\ \mathcal{F}_{sub} = \mathcal{P}_{loss} = \left[\, P_{TG} - P_{TD} \,\right] \tag{4.7}$$

where

$$P_{TG} = \sum_{j=1}^{\mathfrak{B}_G^{ac}} P_{G_j}^{ac} + \sum_{l=1}^{\mathfrak{B}_G^{dc}} P_{G_l}^{dc} \tag{4.8}$$

$$P_{TD} = \sum_{n=1}^{N_b} \left(P_{Ln}^{ac} + P_{Ln}^{dc} \right) \tag{4.9}$$

4.3.2.2 Power Balance Constraints

The active and reactive power balance constraints at each bus are given by

$$P_n^{inj} = P_n^{cal} \quad , \ \forall\ n \in N_b \tag{4.10}$$

$$Q_n^{inj} = Q_n^{cal} \quad , \ \forall\ n \in N_b \tag{4.11}$$

The equations for P_n^{inj}, P_n^{cal}, Q_n^{inj}, and Q_n^{cal} are as expressed in (4.12)-(4.15), respectively. The values of a_1, b_1, a_2, and b_2 are dependent on the direction of the power flow and are defined as (3.15), (3.16), (3.19), and (3.20), respectively. In the reconfiguration algorithm, the LCM technique is not activated; i.e., the terms related to the curtailed active and reactive powers in equations (4.12) and (4.14) are zeros. The LCM variables (ΔP_{Ln}^{ac}, ΔP_{Ln}^{dc}, and ΔQ_{Ln}^{ac}) are used only in the OPF-LCM algorithm.

$$\begin{aligned} P_n^{inj} = {} & \overline{W_n} \left(P_{Gn}^{ac} - (P_{Ln}^{ac} - \Delta P_{Ln}^{ac}) + \eta_{c\text{-}n\text{-}i}\, P_{Gn}^{dc} - \eta_{c\text{-}n\text{-}r}^{-1} (P_{Ln}^{dc} - \Delta P_{Ln}^{dc}) \right) \\ & + W_n \left(P_{Gn}^{dc} - (P_{Ln}^{dc} - \Delta P_{Ln}^{dc}) + \eta_{c\text{-}n\text{-}r}\, P_{Gn}^{ac} - \eta_{c\text{-}n\text{-}i}^{-1} (P_{Ln}^{ac} - \Delta P_{Ln}^{ac}) \right) , \ \forall\ n \in N_b \end{aligned} \tag{4.12}$$

$$\begin{aligned} P_n^{cal} = \sum_{\substack{m=1 \\ m \neq n}}^{N_b} U_{nm} \Big[& \overline{W_n}\ \overline{W_m}\ \overline{D_{nm}}\ \left(V_n^2\, G_{nm} - V_n\, V_m\, (G_{nm}\, \cos\theta_{nm} + B_{nm}\, \sin\theta_{nm}) \right) \\ & + \overline{W_n}\ \overline{W_m}\ D_{nm}\ \left(G_{nm}^{dc}\, (M_{nm}^{-2}\, V_n^2 - M_{nm}^{-1}\, V_n\, M_{mn}^{-1}\, V_m) \right) \left(a_1\ \eta_{c\text{-}nm\text{-}r}^{-1} + b_1\ \eta_{c\text{-}nm\text{-}i} \right) \\ & + \overline{W_n}\ W_m\ D_{nm}\ \left(G_{nm}^{dc}\, (M_{nm}^{-2}\, V_n^2 - M_{nm}^{-1}\, V_n\, V_m) \right) \left(a_2\ \eta_{c\text{-}nm\text{-}r}^{-1} + b_2\ \eta_{c\text{-}nm\text{-}i} \right) \\ & + W_n\ \overline{W_m}\ D_{nm}\ \left(G_{nm}^{dc}\, (V_n^2 - V_n\, M_{mn}^{-1}\, V_m) \right) \\ & + W_n\ W_m\ D_{nm}\ \left(G_{nm}^{dc}\, (V_n^2 - V_n\, V_m) \right) \Big] , \ \forall\ n \in N_b \end{aligned} \tag{4.13}$$

$$Q_n^{inj} = \overline{W_n}\left(Q_{Gn}^{ac} - (Q_{Ln}^{ac} - \Delta Q_{Ln}^{ac}) + Q_{Gn\text{-}c}^{dc} - Q_{Ln\text{-}c}^{dc} \right), \quad \forall\, n \in N_b \tag{4.14}$$

$$Q_n^{cal} = \sum_{\substack{m=1 \\ m\neq n}}^{N_b} U_{nm}\Big[\overline{W_n}\ \overline{W_m}\ \overline{D_{nm}}\ \left(- V_n^2\, B_{nm} - V_n\, V_m\, (G_{nm}\, \sin\theta_{nm} - B_{nm}\, \cos\theta_{nm})\right) + \overline{W_n}\ \overline{W_m}\ D_{nm}\ Q_{c\text{-}nm} + \overline{W_n}\ W_m\ D_{nm}\ Q_{c\text{-}nm}\Big], \quad \forall\, n \in N_b \tag{4.15}$$

4.3.2.3 Network Security Constraints

The network security constraints given by (4.16)-(4.18) include the limits for voltage magnitudes, voltage angles, and line capacities.

$$V_n^{min} \leq V_n \leq V_n^{max} \quad , \quad \forall\, n \in N_b \tag{4.16}$$

$$\theta_n^{min} \leq \theta_n \leq \theta_n^{max} \quad , \quad \forall\, n \in N_b \tag{4.17}$$

$$\sqrt{P_{nm}^2 + Q_{nm}^2} \ \leq \ S_{nm}^{max} \quad , \quad \forall\, n, m \in N_b \tag{4.18}$$

4.3.2.4 Converter Constraints

The converter constraints include the capacity limits and modulation index limits for each converter in the system. These constraints are expressed as follows:

$$\sqrt{P_c^2 + Q_c^2} \ \leq \ S_c^{max} \quad , \quad \forall\, c \in N_c \tag{4.19}$$

$$M_{nm}^{min} \leq M_{nm} \leq M_{nm}^{max} \quad , \quad \forall\, n, m \in N_b \tag{4.20}$$

4.3.2.5 Generator Constraints

The active and reactive power limits for the system generators are expressed as follows:

$$P_{G_j}^{ac-min} \leq P_{G_j}^{ac} \leq P_{G_j}^{ac-max} \ , \ \forall\, j \in \mathfrak{B}_G^{ac} \tag{4.21}$$

$$P_{G_l}^{dc-min} \leq P_{G_l}^{dc} \leq P_{G_l}^{dc-max} \ , \ \forall\, l \in \mathfrak{B}_G^{dc} \tag{4.22}$$

$$Q_{G_j}^{ac-min} \leq Q_{G_j}^{ac} \leq Q_{G_j}^{ac-max} \ , \ \forall\, j \in \mathfrak{B}_G^{ac} \tag{4.23}$$

4.3.3 The Methodology of the Reconfiguration Algorithm

The reconfiguration algorithm is aimed at finding the optimal network configuration described by the binary connection matrix U at each hour during the next day. Accordingly, the output of the reconfiguration algorithm at each hour t is represented by the optimal GA chromosome that consists of the elements of U. The procedures that comprise the proposed reconfiguration algorithm are illustrated in Figure 4.2.

4.4 Stage 2: The OPF-LCM Algorithm

The main goal of the OPF-LCM algorithm is to minimize DS operation costs, including load-curtailment costs, as indicated in (4.24). The optimization constraints include the OPF constraints (4.10)-(4.23) as well as the LCM constraints (4.25)-(4.27). It is worth mentioning that the power factor for each AC load participating in the LCM program is assumed to be kept constant. Therefore, any curtailed active power from any AC load will be associated with curtailed reactive power. According to the NERC reliability standards [85], an LCM technique represents a contingency reserve service that can be used in the case of abnormal operating conditions. In this study, the LCM algorithm is accordingly used mainly to guarantee the reliable and optimal satisfaction of DS operational constraints. The load-curtailment cost is selected to be higher than the marginal costs at all system buses for two reasons: 1) to encourage customers to participate in LCM programs, and 2) to ensure that loads will not be curtailed under normal operating conditions. This feature guarantees that the financial profitability of the utility operator will be unaffected. The proposed OPF-LCM algorithm is implemented in GAMS as a DNLP problem and is then solved using a GRG method [80]. The formulation of the OPF-LCM algorithm is as follows:

$$\min\ C_{OPF} = \Bigg[\sum_{j=1}^{\mathfrak{B}_G^{ac}} C_{G_j}^{ac}\, P_{G_j}^{ac} + \sum_{l=1}^{\mathfrak{B}_G^{dc}} C_{G_l}^{dc}\, P_{G_l}^{dc} + \sum_{i=1}^{\mathcal{N}_{LCM}^{ac}} \lambda_{L_{i,ac}}\, \Delta P_{L_i}^{ac} + \sum_{k=1}^{\mathcal{N}_{LCM}^{dc}} \lambda_{L_{k,dc}}\, \Delta P_{L_k}^{dc} \Bigg] \tag{4.24}$$

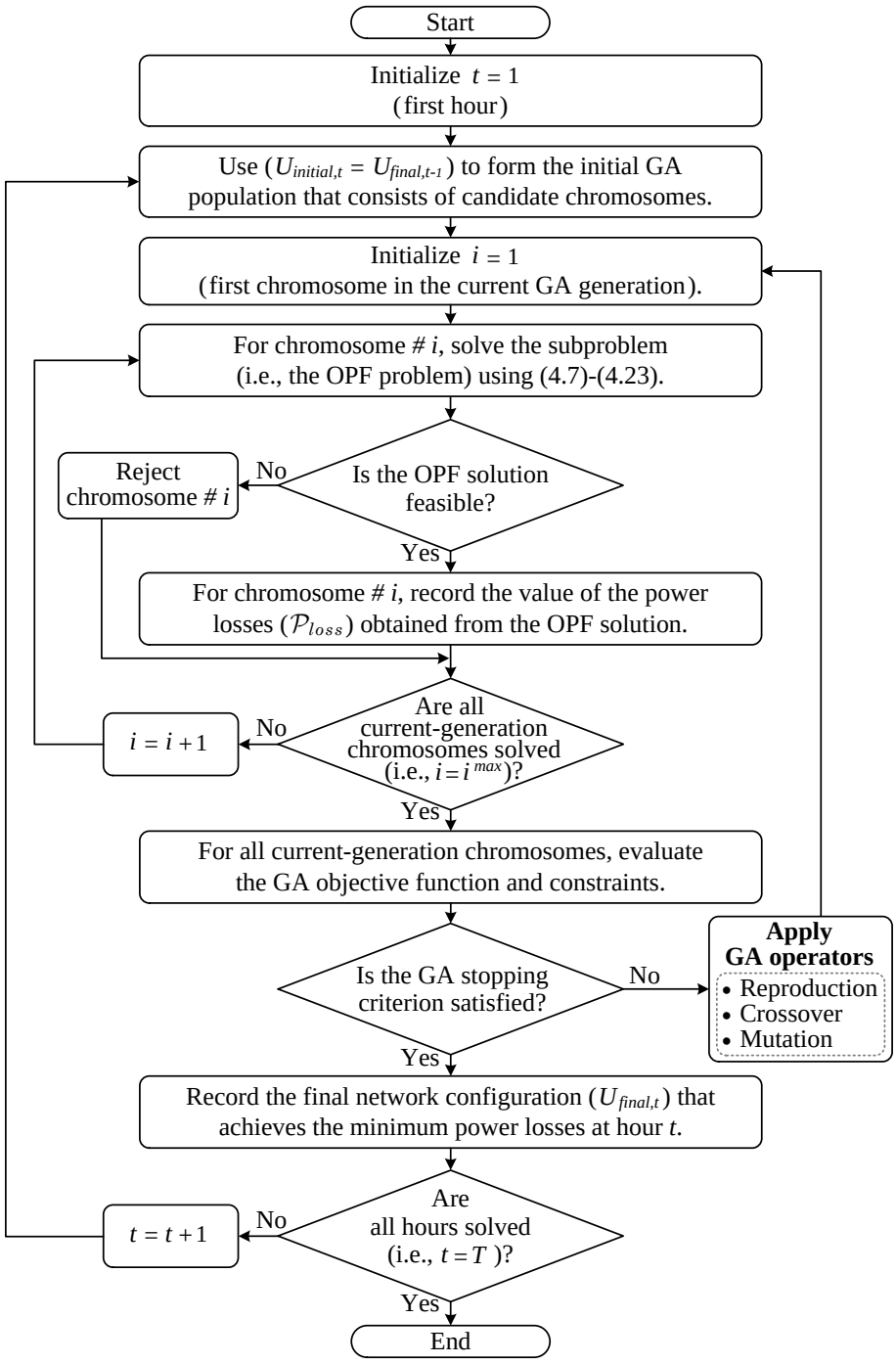

Figure 4.2: Flowchart for the proposed reconfiguration algorithm.

Subject to:

$$(4.10) - (4.23)$$

$$0.0 \leq \Delta P^{ac}_{L_i} \leq \alpha_{L_{i,ac}} P^{ac}_{L_i} \quad , \quad \forall\, i \in \mathcal{N}^{ac}_{LCM} \tag{4.25}$$

$$0.0 \leq \Delta P^{dc}_{L_k} \leq \alpha_{L_{k,dc}} P^{dc}_{L_k} \quad , \quad \forall\, k \in \mathcal{N}^{dc}_{LCM} \tag{4.26}$$

$$\Delta Q^{ac}_{L_i} = \Delta P^{ac}_{L_i} \tan\left(\cos^{-1}(PF_{L_{i,ac}})\right), \forall\, i \in \mathcal{N}^{ac}_{LCM} \tag{4.27}$$

4.5 Case Study

This section presents the case study that was used for evaluating the effectiveness of the proposed two-stage EMS. The proposed EMS was executed on a PC with the following specifications: Intel Core i7 2600 @ 3.4 GHz, 64 bit, and 8 GB RAM. The system description and the simulation results are provided in the following subsections.

4.5.1 Description of the Case-Study System

The modified IEEE 33-bus DS shown in Figure 4.3 was used for the case study. The basic IEEE 33-bus DS presented in [82] has been modified to include DC sections. These DC sections were selected so that the majority of loads and DGs would be DC. The network impedances are shown in Table 4.1. The data given for the energy resources and load demands are listed in Tables 4.2 and 4.3, respectively. The base values used for this test system are S_{base}= 10 MVA, V^{ac}_{base}= 12.66 kV, and V^{dc}_{base}= 20.67 kV. The upper and lower limits for the voltage magnitudes and angles are given as $V^{max}_n = 1.05$ p.u., $V^{min}_n = 0.95$ p.u., $\theta^{max}_n = \pi/4$ rad, and $\theta^{min}_n = -\pi/4$ rad, respectively. The efficiency of the AC-DC converters is given as 95 %. The upper and lower modulation-index limits for the VSCs are given as 1.0 and 0.77, respectively [83]. The hybrid DS under study includes 37 sections; each can be open or closed. The line capacities are given as 5.0 MVA for section S1, 3.5 MVA for sections S2 and S18, and 2.5 MVA for the remaining sections in the network. Each section is equipped with two controlled switches (i.e., one switch at each section-end). These permit the isolation of the section in the case of a contingency, maintenance, or network reconfiguration. For the purposes of network reconfiguration, the maximum switching limits are given as $N^{max}_{SW,t} = 6$ and $N^{max}_{SW,s} = 4$ [48].

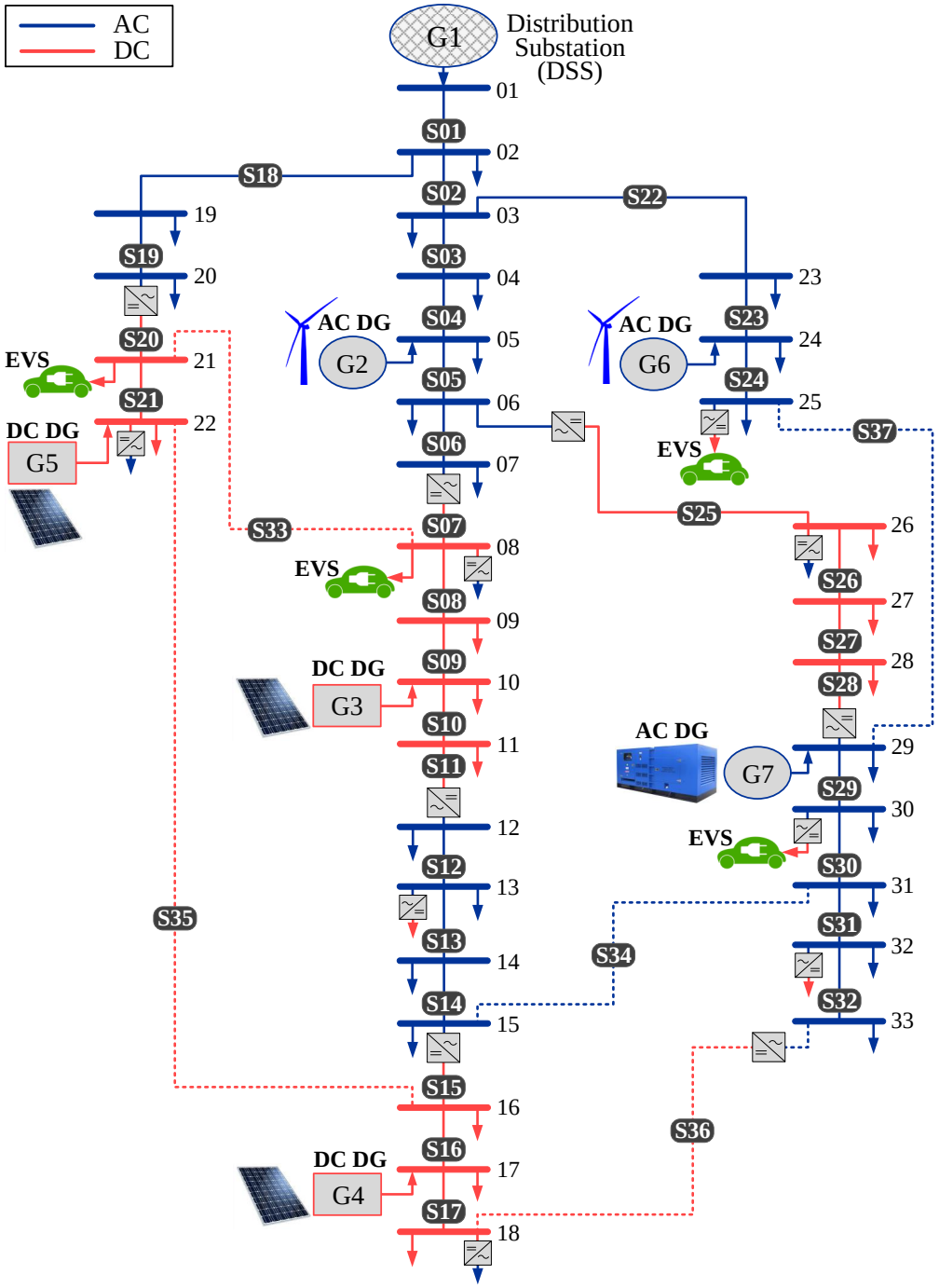

Figure 4.3: 33-bus AC-DC hybrid distribution system.

Table 4.1: Impedances of the 33-Bus Hybrid Distribution System

Line No.	From Bus	To Bus	Resistance (Ω)	Reactance (Ω)	Line No.	From Bus	To Bus	Resistance (Ω)	Reactance (Ω)
S01	1	2	0.0922	0.0470	S20*	20	21	0.8190	–
S02	2	3	0.4930	0.2511	S21*	21	22	1.4178	–
S03	3	4	0.3660	0.1864	S22	3	23	0.4512	0.3083
S04	4	5	0.3811	0.1941	S23	23	24	0.8980	0.7091
S05	5	6	0.8190	0.7070	S24	24	25	0.8960	0.7011
S06	6	7	0.1872	0.6188	S25*	6	26	0.4060	–
S07*	7	8	1.4228	–	S26*	26	27	0.5684	–
S08*	8	9	2.0600	–	S27*	27	28	2.1180	–
S09*	9	10	2.0880	–	S28*	28	29	1.6084	–
S10*	10	11	0.3932	–	S29	29	30	0.5075	0.2585
S11*	11	12	0.7488	–	S30	30	31	0.9744	0.9630
S12	12	13	1.4680	1.1550	S31	31	32	0.3105	0.3619
S13	13	14	0.5416	0.7129	S32	32	33	0.3410	0.5302
S14	14	15	0.5910	0.5260	S33[1,*]	8	21	4.0000	–
S15*	15	16	1.4926	–	S34[1]	15	31	2.0000	2.0000
S16*	16	17	2.5780	–	S35[1,*]	16	22	4.0000	–
S17*	17	18	1.4640	–	S36[1,*]	18	33	1.0000	–
S18	2	19	0.1640	0.1565	S37[1]	25	29	0.5000	0.5000
S19	19	20	1.5042	1.3554					

[1] Tie lines (i.e., normally open sections).
* DC lines.

Table 4.2: Data for the Energy Resources in the Case-Study System

Resource No.	Resource Type	P_G^{max} (MW)	P_G^{min} (MW)	Q_G^{max} (MVAr)	Q_G^{min} (MVAr)
G1	DSS, (AC power)	10.0	0.80	5.00	0.50
G2	Wind DG, (AC power)	0.50	–	–	–
G3	Solar PV, (DC power)	0.25	–	–	–
G4	Solar PV, (DC power)	0.25	–	–	–
G5	Solar PV, (DC power)	0.25	–	–	–
G6	Wind DG, (AC power)	0.50	–	–	–
G7	Diesel DG, (AC power)	0.50	0.05	0.25	0.05

Table 4.3: Load Data for the 33-Bus Hybrid Distribution System

Bus No.	P_L^{ac} (kW)	Q_L^{ac} (kVAr)	P_L^{dc} (kW)	Bus No.	P_L^{ac} (kW)	Q_L^{ac} (kVAr)	P_L^{dc} (kW)	Bus No.	P_L^{ac} (kW)	Q_L^{ac} (kVAr)	P_L^{dc} (kW)
1	–	–	–	12	60	35	–	23	90	50	–
2	100	60	–	13	60	35	60	24	420	200	–
3	90	40	–	14	120	80	–	25	420	200	200
4	120	80	–	15	60	10	–	26	60	25	60
5	60	30	–	16	–	–	60	27	–	–	60
6	60	20	–	17	–	–	60	28	–	–	60
7	200	100	–	18	90	40	90	29	120	70	–
8	200	100	200	19	90	40	–	30	200	600	200
9	–	–	60	20	90	40	–	31	150	70	–
10	–	–	60	21	–	–	200	32	210	100	210
11	–	–	45	22	90	40	80	33	60	40	–

4.5.2 Day-Ahead Forecasted Data for the Stochastic Variables

Figure 4.4 shows the day-ahead forecasted values for the stochastic variables: Load demands, PV DGs, Wind DGs, and EVS demands [8]. The forecasted data are given as percentages of the maximum value of each stochastic variable.

4.5.3 Results from the Day-Ahead Reconfiguration Algorithm

Table 4.4 shows a comparison of the results obtained from the proposed reconfiguration algorithm and those obtained from the base-case system. The base-case system has five normally open sections: S33, S34, S35, S36, and S37. The value of the day-ahead energy losses was found to be 6203.389 kWh for the base-case system. This amount was reduced to 4188.960 kWh when the proposed reconfiguration algorithm was employed. The comparison therefore revealed that, for the DS under study, the proposed algorithm successfully achieved a significant reduction of 2014.429 kWh (i.e., 32.47 %) in day-ahead energy losses. It is also important to mention that the execution time of the proposed reconfiguration algorithm was found to be 3.59 h, which is suitable for day-ahead studies.

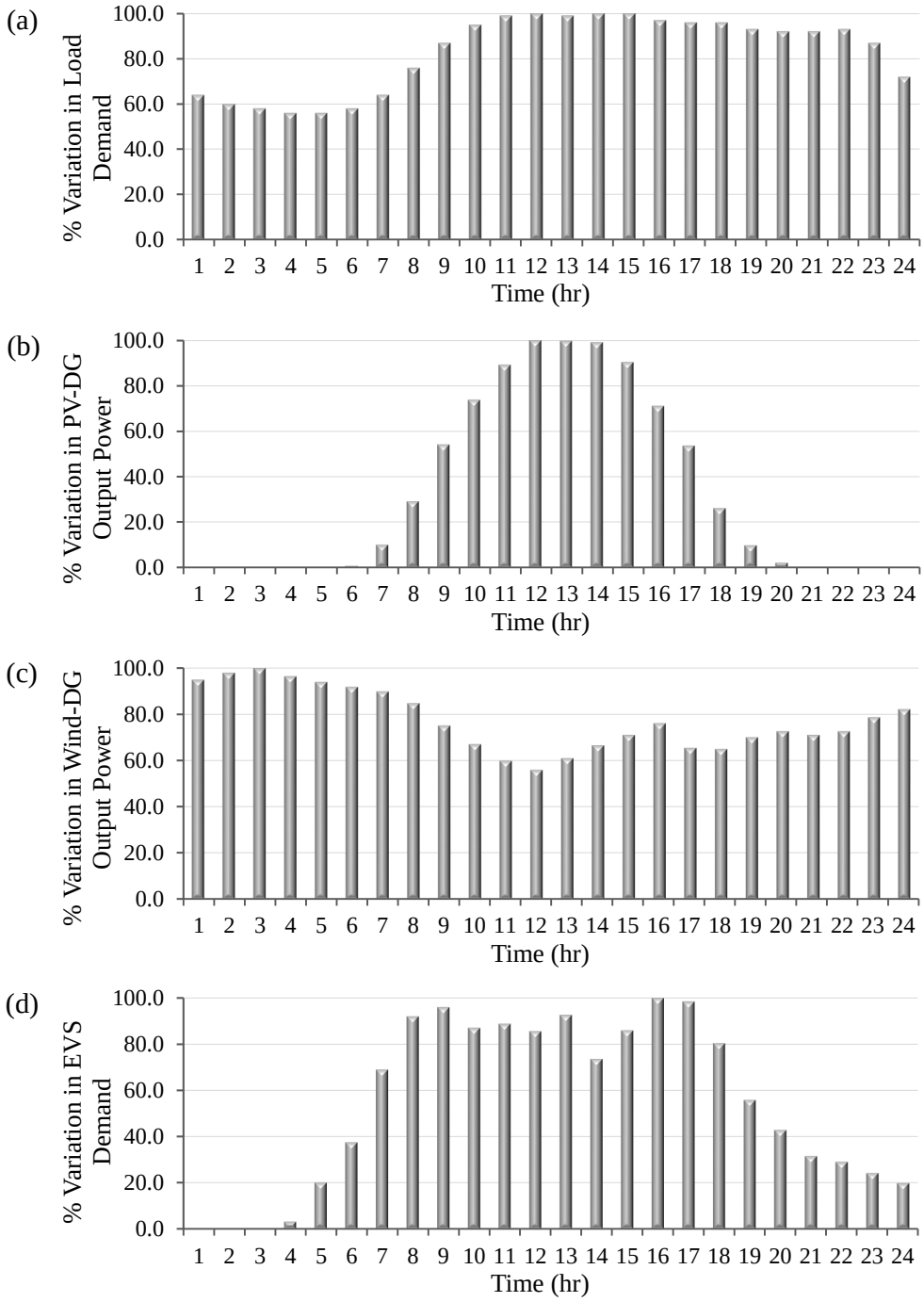

Figure 4.4: Day-ahead forecasted data for (a) load demand, (b) PV-DG output power, (c) wind-DG output power, and (d) EVS demand.

Table 4.4: Results from the Reconfiguration Algorithm

Hour	**Base Case**	**Proposed Algorithm**	
	Power Losses (kW)	Opened Sections	Power Losses (kW)
1	148.5933	12, 33, 34, 36, 37	116.3084
2	132.4126	12, 33, 34, 36, 37	103.5316
3	124.5572	12, 27, 33, 34, 36	93.8902
4	119.8076	12, 15, 27, 33, 36	75.2494
5	133.4649	12, 15, 27, 33, 36	84.6155
6	155.1893	12, 15, 27, 33, 36	98.6335
7	198.9151	12, 15, 27, 33, 36	127.9448
8	256.9839	11, 15, 27, 33, 36	167.6322
9	291.4380	11, 15, 27, 33, 36	197.9775
10	304.5958	09, 15, 27, 33, 36	199.9063
11	313.0286	12, 15, 27, 33, 36	225.3547
12	304.0452	12, 15, 26, 33, 36	225.3549
13	304.7966	12, 15, 16, 26, 33	221.6607
14	288.6735	12, 15, 27, 33, 36	208.6887
15	310.2004	12, 15, 27, 33, 36	222.1661
16	329.4775	12, 15, 27, 33, 36	230.7330
17	346.9587	09, 15, 27, 33, 36	225.7921
18	361.2525	09, 15, 27, 33, 36	243.5978
19	336.1397	11, 15, 27, 33, 36	216.0136
20	325.4578	11, 15, 27, 33, 36	205.4842
21	316.4762	11, 15, 27, 32, 33	199.3346
22	318.8711	11, 15, 27, 32, 33	200.6130
23	279.9771	11, 15, 27, 32, 33	173.9948
24	202.0767	11, 15, 27, 32, 33	124.4827
Total Losses	**6203.389 kWh**		**4188.960 kWh**

4.5.4 Results from the OPF-LCM Algorithm

The DS network, including the distribution substation, is owned by the utility. The renewable DGs are assumed to be owned by customers and are operated according to the FIT program [14]. The FIT program was introduced to promote the application of renewable

DGs, including PV panels and wind DGs. The cost of the electric energy supplied from the DSS and G7 is given as 92.2 \$/MWh [88]. Under the FIT program, the tariff costs paid to the owners of the PV and wind DGs are given as 209 \$/MWh and 128 \$/MWh, respectively [89]. The maximum allowable curtailment ratios for the AC and DC system loads are given as $\alpha_{L_{ac}} = 15\,\%$ and $\alpha_{L_{dc}} = 15\,\%$, respectively. The load-curtailment cost was selected to be 115 \$/MWh [48]. Table 4.5 shows the results for a number of abnormal operating scenarios, including 1) forecast errors in the forecasted data for load demands and renewable DGs, 2) unavailability of one or more of the system DGs, and 3) combinations of 1 and 2. For the system's stochastic variables (load demands and renewable DGs), the forecast error is represented by the percentage difference between the actual value and the forecasted value, as follows:

$$\%\,\mathrm{FE} = \frac{AV - FV}{FV} \times 100 \tag{4.28}$$

where FE is the percentage forecast error, AV is the actual value of a stochastic variable, and FV is the day-ahead forecasted value of a stochastic variable.

The results listed in Table 4.5 demonstrate that the proposed OPF-LCM successfully guaranteed reliable and optimal operation under a variety of abnormal operating scenarios. For scenarios ($\mathcal{S}6 - \mathcal{S}13$), the OPF algorithm failed to find the feasible solutions that can satisfy the operational and security constraints (4.10)-(4.23). However, employing the OPF-LCM algorithm successfully achieved optimal and feasible solutions and guaranteed reliable operation of the system. In this study, the reliable operation means that the system operational and security constraints are satisfied under abnormal operating conditions. For the other abnormal scenarios ($\mathcal{S}1 - \mathcal{S}5$, $\mathcal{S}14$, and $\mathcal{S}15$), the OPF-LCM algorithm was capable of finding optimal solutions without the need to curtail any load demand (i.e., the curtailed load is equal to zero). These results prove that the proposed OPF-LCM algorithm will not curtail the system loads unless the system security constraints are violated. It is also important to mention that the execution time of the OPF-LCM algorithm was found to be 358 ms, which is suitable for real-time applications.

Table 4.5: Simulation Results from the OPF-LCM Algorithm for Different Abnormal Scenarios

Abnormal Scenarios				**Without LCM**	**With LCM**	
Scenario No. ($\mathcal{S}$)	at hour No. (t)	Description of Scenario $\mathcal{S}$	Open Sections at hour t	OPF Solution C_{OPF} (\$)	OPF Solution C_{OPF} (\$)	Curtailed Load (kW)
1	3	+10 % forecast error (FE*) in all forecasted data	$12, 27, 33, 34, 36$	291.8128	291.8128	00.00
2	4	+10 % FE* in load demands, and -10 % FE* in wind-DG powers	$12, 15, 27, 33, 36$	275.8031	275.8031	00.00
3	8	+20 % FE* in EVS demands	$11, 15, 27, 33, 36$	443.1791	443.1791	00.00
4	9	PV DGs (G3, G4, and G5) out of service	$11, 15, 27, 33, 36$	449.8362	449.8362	00.00
5	10	Wind DGs (G2 and G6) out of service	$09, 15, 27, 33, 36$	511.0928	511.0928	00.00
6	11	Wind DGs (G2 and G6) out of service	$12, 15, 27, 33, 36$	INFES**	544.2359	149.8438
7	12	Wind DGs out of service, and +10 % FE* in EVS demands	$12, 15, 26, 33, 36$	INFES**	562.2994	191.7169
8	13	PV DGs (G3, G4, and G5) out of service	$12, 15, 16, 26, 33$	INFES**	495.4526	93.98690
9	14	PV DGs out of service, and +10 % FE* in load demands	$12, 15, 27, 33, 36$	INFES**	525.7824	109.3226
10	15	Diesel DG (G7) out of service	$12, 15, 27, 33, 36$	INFES**	576.0538	260.4285
11	16	Diesel DG (G7) out of service	$12, 15, 27, 33, 36$	INFES**	560.2626	208.4188
12	17	Diesel DG (G7) out of service, and +10 % FE* in load demands	$09, 15, 27, 33, 36$	INFES**	577.7203	370.0701
13	18	+10 % FE* in both load demands and EVS demands	$09, 15, 27, 33, 36$	INFES**	540.1266	31.68000
14	19	-10 % FE* in output power of wind DGs (G2 and G6)	$11, 15, 27, 33, 36$	446.1025	446.1025	00.00
15	21	-10 % FE* in wind-DG powers, and +10 % FE* in EVS demands	$11, 15, 27, 32, 33$	417.0847	417.0847	00.00

* The forecast error (FE) is the percentage difference between the actual value and the forecasted value, as expressed in (4.28).

** Infeasible OPF solution due to the violation of one or more of the operational and security constraints (4.10) - (4.23).

4.6 Conclusion

In this chapter, a two-stage EMS is proposed to achieve reliable and optimal operation for AC-DC hybrid DSs. In Stage 1, a proposed network reconfiguration algorithm determines the optimal day-ahead reconfiguration schedule for the hybrid DS. The objective of the proposed reconfiguration algorithm is to minimize DS energy losses based on consideration of the day-ahead forecasted data for load demands and renewable DGs. The reconfiguration algorithm takes into account the maximum number of daily switching actions for each controlled switch, as well as the maximum number of switching actions at each hour during the next day. In Stage 2, a proposed real-time OPF-LCM algorithm minimizes the operation costs of the hybrid DS and guarantees reliable DS operation in the case of abnormal conditions. The proposed two-stage EMS was successfully applied to a hybrid DS with different types of loads and DGs. With respect to the day-ahead stage, the reconfiguration algorithm successfully produced an optimal 24 h reconfiguration schedule for the DS under study. The effectiveness of the proposed reconfiguration algorithm was verified through a comparison of the results obtained from the reconfiguration algorithm and those obtained from the base-case system. The comparison demonstrated that the proposed algorithm successfully achieved a significant reduction in DS energy losses. In the real-time stage, the proposed OPF-LCM algorithm effectively achieved reliable and optimal DS operation under different abnormal operating conditions.

Chapter 5

A Planning Approach for the Network Configuration of AC-DC Hybrid DSs

5.1 Introduction

This chapter presents a novel planning model that can be used for determining an optimal network configuration for future hybrid DSs. The proposed planning model takes into account the stochastic behavior of load demands and renewable-based DGs. The stochastic variations are addressed in the model using an MCS technique. The three binary matrices that are used for describing the AC-DC configuration of a hybrid DS are employed as the decision variables of the planning model. All bus and line selections are interchangeable and can be either AC or DC as needed for the minimization of DS investment and operation costs. The proposed model was tested on a case study of a hybrid DS that included PV panels, wind DGs, and EV charging stations. The solution derived by the model was then compared with the solution obtained using a traditional AC planning technique in order to evaluate the effectiveness of the proposed model. This chapter is organized as follows: Section 5.2 describes the hybrid planning problem. Section 5.3 explains the problem formulation and provides a detailed analysis of the optimization models used for solving the hybrid planning problem. The planning procedures are outlined in Section 5.4. Section 5.5 discusses the stochastic models of load demands and renewable DGs. Section 5.6 describes the case study that was employed for evaluating the effectiveness of the proposed planning model. The final section presents the conclusions of this chapter.

5.2 Problem Description

Figure 5.1 shows a multi-zone DS that includes different types of AC and DC loads and generators. The objective is to plan an AC-DC hybrid system that optimally accommodates all system resources: loads and generators. The optimal solution for the hybrid planning problem is determined based on three main decisions: 1) the type (AC or DC) of system buses, 2) the specific connections between system buses (i.e., the network connections), and 3) the type (AC or DC) of network lines. Each bus in the hybrid DS can be either AC or DC, as shown in Figure 3.1. In addition, the possible cases for the connection between AC/DC buses via AC/DC lines and VSCs are illustrated in Figure 3.3. The network configuration is described by the three binary matrices (W, U, and D). These matrices, which are defined in Section 3.3, represent the binary decision variables in the proposed planning model.

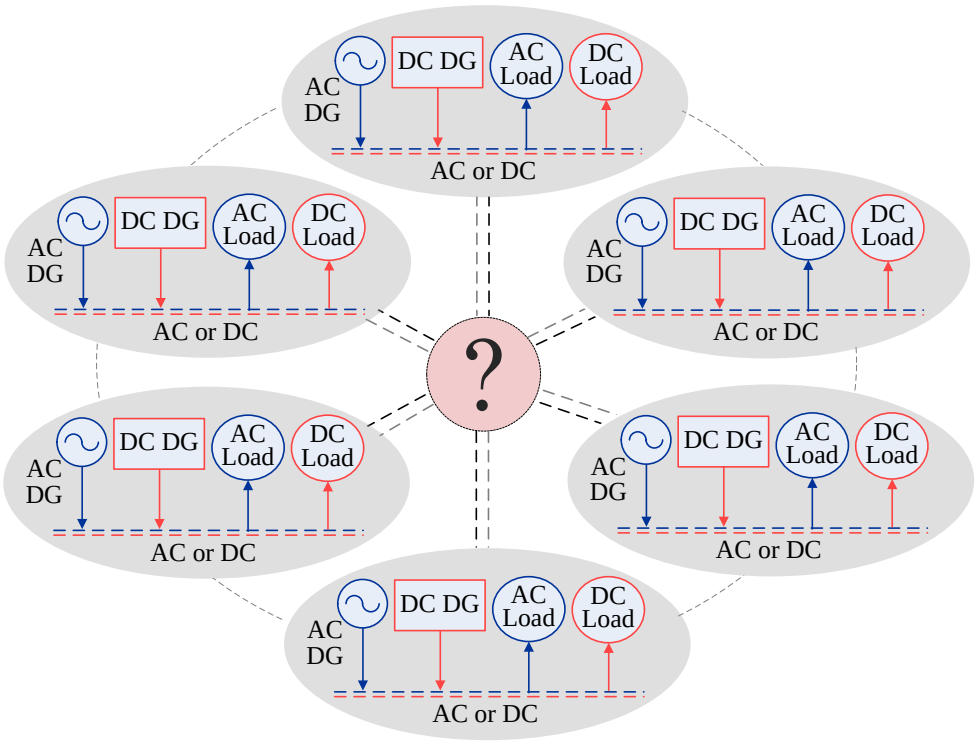

Figure 5.1: Planning problem.

5.3 Formulation of the Planning Model

The planning goal is to find the optimal system configuration that achieves the minimum planning costs, which include the DS investment and operation costs. In its entirety, the planning problem comprises mixed-integer nonlinear programming with discontinuous derivatives and so cannot be formulated in one optimization model. In this study, two optimization models are therefore integrated in order to achieve the planning objective. The first solves the master problem, and the second solves the subproblem. The two problems are described below.

5.3.1 The Master Problem

The master problem is formulated using a GA and is solved as a mixed-integer programming problem. The master problem constraints are only on the independent variables (W, U, and D), whose values are used as input to the subproblem. The objective function and the optimization constraints are as specified in the following explanations.

5.3.1.1 Objective Function

The objective function is to minimize the total present cost value (C_{NPV}), which includes the DS investment and operation costs, as follows:

$$\min Z_{master} = C_{NPV} \tag{5.1}$$

where

$$C_{NPV} = IC + RC \tag{5.2}$$

$$RC = \sum_{t=1}^{T_P} \frac{C_{AOM,t}}{(1+d)^t} \tag{5.3}$$

$$C_{AOM,t} = 8760 \times \mathbb{E}(C_{OPF,s,t}) + \beta_m \times IC \ , \ \forall \ t \in T_P \tag{5.4}$$

5.3.1.2 Integer Constraints

The integer constraints for the binary variables of the configuration matrices are expressed as follows:

$$W_n \in \{0,1\} \quad , \quad \forall\ n \in N_b \tag{5.5}$$

$$U_{nm} \in \{0,1\} \quad , \quad \forall\ n,m \in N_b \tag{5.6}$$

$$D_{nm} \in \{0,1\} \quad , \quad \forall\ n,m \in N_b \tag{5.7}$$

5.3.1.3 Bus Connectivity Constraints

These constraints are employed as a means of avoiding isolation and/or over-connectivity for each bus in the system, as follows:

$$\sum_{m=1}^{N_b} U_{nm} \geq N_{l,n}^{min}, \quad 1 \leq N_{l,n}^{min} \leq N_{l,n}^{max} \quad , \quad \forall\ n \in N_b \tag{5.8}$$

$$\sum_{m=1}^{N_b} U_{nm} \leq N_{l,n}^{max},\ N_{l,n}^{min} \leq N_{l,n}^{max} \leq N_b{-}1\ ,\ \forall\ n \in N_b \tag{5.9}$$

where $N_{l,n}^{min}$ and $N_{l,n}^{max}$ represent the respective minimum and maximum number of lines that can be connected to each bus in the DS network. The selection of $N_{l,n}^{min}$ and $N_{l,n}^{max}$ is dependent on the type of system configuration and level of network reliability required. If a radial DS is needed, the value of $N_{l,n}^{min}$ is set to be 1 for all $n \in N_b$, and the constraint (5.10) is added to the formulation of the master problem.

$$\sum_{n=1}^{N_b} \sum_{\substack{m=1 \\ m>n}}^{N_b} U_{nm} = N_b - 1 \tag{5.10}$$

5.3.2 The Subproblem

The subproblem is employed to determine the optimal operation cost for each individual scenario of the network configuration. The problem is formulated in GAMS as a DNLP problem and is solved using a GRG method [80]. The objective function (5.11) is to minimize the summation of the AC and DC generation costs. The constraints can be classified into four groups: 1) the active and reactive power balance constraints (5.12)-(5.13), 2) the network constraints (5.14)-(5.16), 3) the AC-DC converter constraints (5.17)-(5.18), and 4) the generator constraints (5.19)-(5.21). The constraints of the subproblem are on dependent variables, whose values are determined based on the values selected for the independent variables in the master problem. The formulation of the subproblem is as follows:

$$\min \; Z_{sub} = \sum_{j=1}^{\mathfrak{B}_G^{ac}} C_{G_j}^{ac} \; P_{G_j}^{ac} + \sum_{l=1}^{\mathfrak{B}_G^{dc}} C_{G_l}^{dc} \; P_{G_l}^{dc} \tag{5.11}$$

Subject to:

$$P_n^{inj} = P_n^{cal} \quad , \quad \forall \; n \in N_b \tag{5.12}$$

$$Q_n^{inj} = Q_n^{cal} \quad , \quad \forall \; n \in N_b \tag{5.13}$$

$$V_n^{min} \leq V_n \leq V_n^{max} \quad , \quad \forall \; n \in N_b \tag{5.14}$$

$$\theta_n^{min} \leq \theta_n \leq \theta_n^{max} \quad , \quad \forall \; n \in N_b \tag{5.15}$$

$$\sqrt{P_{nm}^2 + Q_{nm}^2} \; \leq \; S_{nm}^{max} \quad , \quad \forall \; n, m \in N_b \tag{5.16}$$

$$\sqrt{P_c^2 + Q_c^2} \; \leq \; S_c^{max} \quad , \quad \forall \; c \in N_c \tag{5.17}$$

$$M_{nm}^{min} \leq M_{nm} \leq M_{nm}^{max} \quad , \quad \forall \; n, m \in N_b \tag{5.18}$$

$$P_{G_j}^{ac-min} \leq P_{G_j}^{ac} \leq P_{G_j}^{ac-max} \quad , \quad \forall \; j \in \mathfrak{B}_G^{ac} \tag{5.19}$$

$$P_{G_l}^{dc-min} \leq P_{G_l}^{dc} \leq P_{G_l}^{dc-max} \quad , \quad \forall \; l \in \mathfrak{B}_G^{dc} \tag{5.20}$$

$$Q_{G_j}^{ac-min} \leq Q_{G_j}^{ac} \leq Q_{G_j}^{ac-max} \quad , \quad \forall \; j \in \mathfrak{B}_G^{ac} \tag{5.21}$$

The equations for P_n^{inj}, P_n^{cal}, Q_n^{inj}, and Q_n^{cal} are as expressed in (5.22)-(5.25), respectively. The values of a_1, b_1, a_2, and b_2 are dependent on the direction of the power flow and are given in (3.15), (3.16), (3.19), and (3.20), respectively.

$$P_n^{inj} = \overline{W_n}\left(P_{Gn}^{ac} - P_{Ln}^{ac} + \eta_{c\text{-}n\text{-}i}\, P_{Gn}^{dc} - \eta_{c\text{-}n\text{-}r}^{-1}\, P_{Ln}^{dc} \right) + W_n\left(P_{Gn}^{dc} - P_{Ln}^{dc} + \eta_{c\text{-}n\text{-}r}\, P_{Gn}^{ac} - \eta_{c\text{-}n\text{-}i}^{-1}\, P_{Ln}^{ac} \right), \quad \forall\, n \in N_b \tag{5.22}$$

$$\begin{aligned} P_n^{cal} = \sum_{\substack{m=1 \\ m\neq n}}^{N_b} U_{nm} \Big[& \overline{W_n}\ \overline{W_m}\ \overline{D_{nm}}\ \left(V_n^2\, G_{nm} - V_n\, V_m\, (G_{nm}\, \cos\theta_{nm} + B_{nm}\, \sin\theta_{nm})\right) \\ & + \overline{W_n}\ \overline{W_m}\ D_{nm}\ \left(G_{nm}^{dc}\, (M_{nm}^{-2}\, V_n^2 - M_{nm}^{-1}\, V_n\, M_{mn}^{-1}\, V_m)\right) \left(a_1\ \eta_{c\text{-}nm\text{-}r}^{-1} + b_1\ \eta_{c\text{-}nm\text{-}i}\right) \\ & + \overline{W_n}\ W_m\ D_{nm}\ \left(G_{nm}^{dc}\, (M_{nm}^{-2}\, V_n^2 - M_{nm}^{-1}\, V_n\, V_m)\right) \left(a_2\ \eta_{c\text{-}nm\text{-}r}^{-1} + b_2\ \eta_{c\text{-}nm\text{-}i}\right) \\ & + W_n\ \overline{W_m}\ D_{nm}\ \left(G_{nm}^{dc}\, (V_n^2 - V_n\, M_{mn}^{-1}\, V_m)\right) \\ & + W_n\ W_m\ D_{nm}\ \left(G_{nm}^{dc}\, (V_n^2 - V_n\, V_m)\right) \Big], \ \forall\, n \in N_b \end{aligned} \tag{5.23}$$

$$Q_n^{inj} = \overline{W_n}\left(Q_{Gn}^{ac} - Q_{Ln}^{ac} + Q_{Gn\text{-}c}^{dc} - Q_{Ln\text{-}c}^{dc} \right), \quad \forall\, n \in N_b \tag{5.24}$$

$$\begin{aligned} Q_n^{cal} = \sum_{\substack{m=1 \\ m\neq n}}^{N_b} U_{nm} \Big[& \overline{W_n}\ \overline{W_m}\ \overline{D_{nm}}\ \left(- V_n^2\, B_{nm} - V_n\, V_m\, (G_{nm}\, \sin\theta_{nm} - B_{nm}\, \cos\theta_{nm})\right) \\ & + \overline{W_n}\ \overline{W_m}\ D_{nm}\ Q_{c\text{-}nm} + \overline{W_n}\ W_m\ D_{nm}\ Q_{c\text{-}nm} \Big], \quad \forall\, n \in N_b \end{aligned} \tag{5.25}$$

5.4 Planning Methodology

The primary planning objective is to minimize the total system costs, including investment and operation costs. The planning model input includes stochastic models for the AC/DC loads and DGs in the system. The planning model output comprises the binary configuration matrices (W, U, and D), which provide decisions about the optimal hybrid configuration. Each bus in the hybrid DS is flexible and can be either AC or DC as needed for optimizing the planning objective. Accordingly, the proposed planning strategy facil-

itates the connection of renewable DGs to AC or DC buses based on equal opportunities for the DG owners. The use of the MCS technique enables consideration of the stochastic variations associated with renewable DGs and load demands.

5.4.1 Planning Model Procedures

The flowchart of the proposed planning model is presented in Figure 5.2. The procedures can be described as follows:

1. Initialize a GA population that consists of GA chromosomes, each representing one combination of the possible AC-DC configurations. Steps 2 to 6 are performed for each chromosome in the current GA generation.

2. Generate an MCS scenario that includes random values for the stochastic variables: load demands and renewable DGs.

3. Solve the subproblem (i.e., the OPF problem) using (5.11)-(5.25) to find the optimal operation cost of the MCS scenario selected.

4. Examine the MCS stopping criterion. The OPF solution for different MCS scenarios is represented by a stochastic variable $C_{OPF,s}$. The MCS process can be terminated using either a fixed number of iterations [90] or the stopping criterion described in (5.26) [91]. Steps 2 to 4 are repeated until the MCS stopping criterion is satisfied.

$$\frac{\sigma(C_{OPF,s})}{\mathbb{E}(C_{OPF,s})} \leq \varepsilon \tag{5.26}$$

5. The minimum permissible number of feasible OPF solutions as a percentage of the total number of solutions for different MCS scenarios is defined as α_f^{min}. To maintain an acceptable stochastic risk level, the value of α_f^{min} is chosen to be 95 %. The higher the value of α_f^{min}, the lower the stochastic risk level. For any configuration, if α_f^{min} is achieved, the operation cost of this configuration is then represented by $\mathbb{E}(C_{OPF,s})$; otherwise, this configuration is discarded.

6. For the current configuration, calculate the investment cost (IC) of the network lines and converters, and then calculate the running cost (RC) using (5.3) and (5.4).

7. For all chromosomes in the current GA generation, calculate the cost function using (5.2), and then evaluate the GA objective function and constraints.

8. Check the GA stopping criterion; if it is not satisfied, update the GA generation by applying the GA operations (reproduction, crossover, and mutation). Then repeat Steps 2 to 8 until the GA stopping criterion is satisfied.

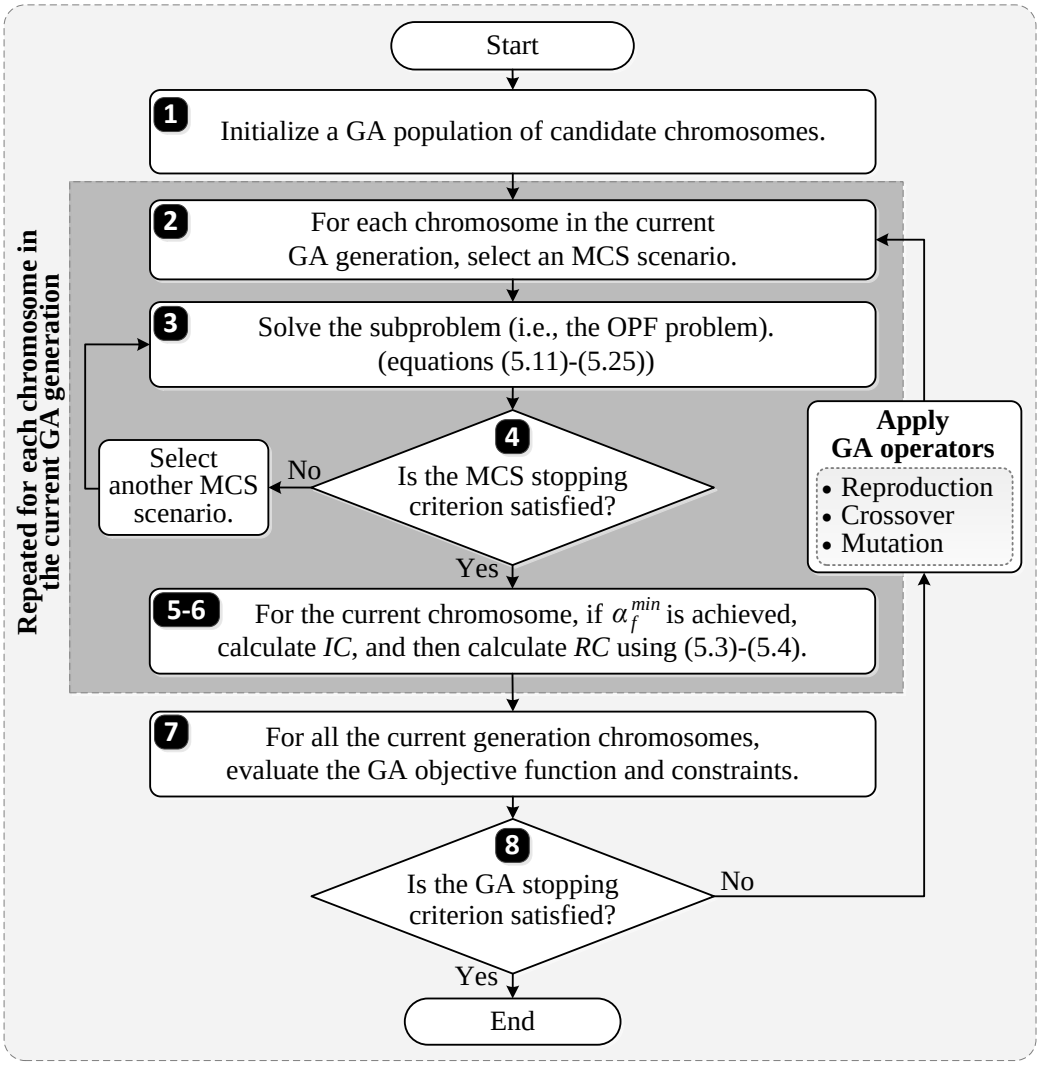

Figure 5.2: Flowchart for the proposed stochastic planning model.

5.4.2 Optimization Techniques

The proposed planning strategy uses two optimization platforms: GA and GAMS. In the first, the GA generates all possible AC-DC configurations. GA can find an optimal solution of any objective function, even if this function is discrete or if its derivatives are not defined. GA is a population-based algorithm that depends on iterative process and uses probabilistic transition rules. Initially, the population is randomly generated, and each individual in the population represents a candidate solution, which is ranked by means of a fitness function to measure its goodness with respect to the given problem [92]. The search procedure in GAs is based on three main operators: reproduction, crossover, and mutation. These operators are used to search for the best solution among a number of candidate solutions. In the proposed planning model, the GA chromosome describes the system configuration based on the previously mentioned binary matrices (W, U, and D), as shown in Figure 5.3. GAMS is used for solving the OPF problem for each configuration generated by the GA. The OPF problem is solved by a CONOPT solver, which applies a generalized reduced gradient (GRG) method [80].

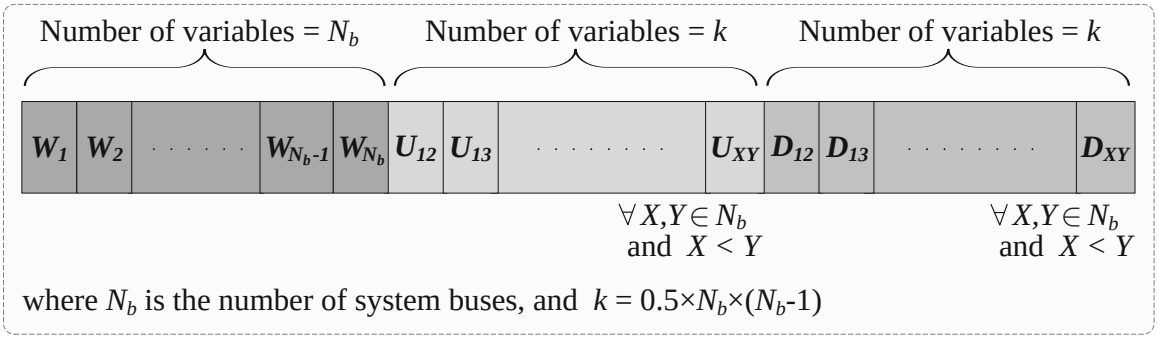

Figure 5.3: Structure of the GA chromosome in the proposed planning model.

5.5 Stochastic Models

This section discusses the stochastic variables presented in hybrid DSs. These variables include: the power demand associated with the AC/DC loads, the output power of wind DGs, the output power of PV DGs, and the power demand of EV charging stations.

5.5.1 AC and DC Load Demands

The annual variation in demand can be incorporated by dividing the year into four seasons, and then representing each season by a typical day. The load profile of a representative day for each season is shown in Figure 5.4(a), based on the data provided in [93]. The hourly demand of each representative is given as a percentage of the annual peak demand. These four load profiles are then used for deriving the cumulative distribution functions (CDFs) presented in Figure 5.4(b).

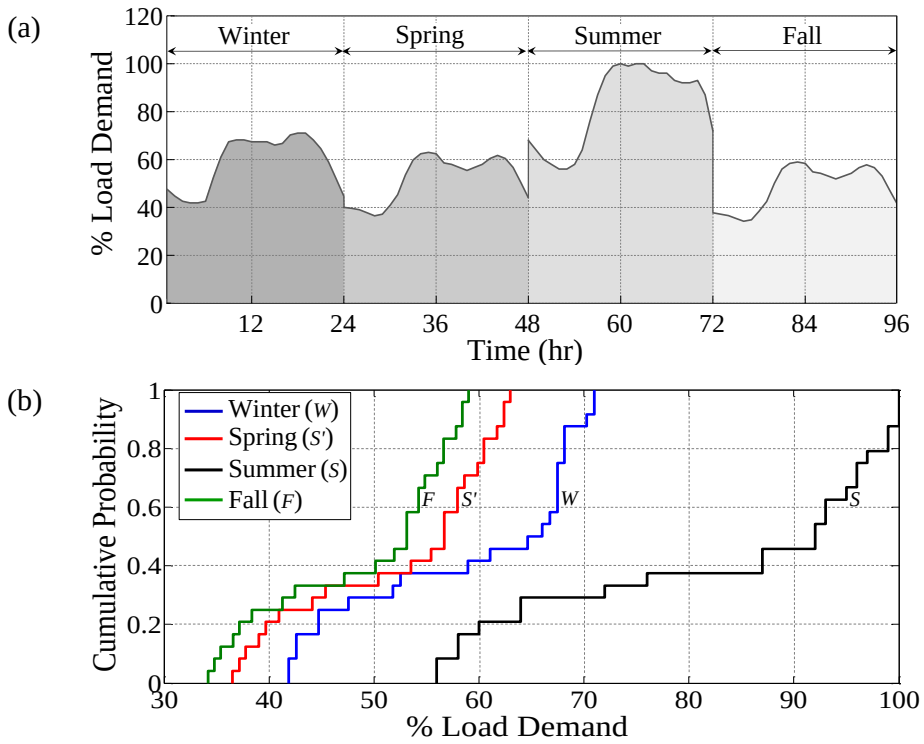

Figure 5.4: Variations in the AC and DC loads: (a) demand for a typical day in each season; (b) CDF for each typical day.

5.5.2 Wind DG Output Power

The seasonal data provided in [93] were used for modeling the electrical output power from the wind DG, as shown in Figure 5.5(a). The hourly power generated during a typical day

for each of the four seasons is given as a percentage of the annual maximum output power of the wind DG. These four daily profiles were then used for deriving the CDFs presented in Figure 5.5(b).

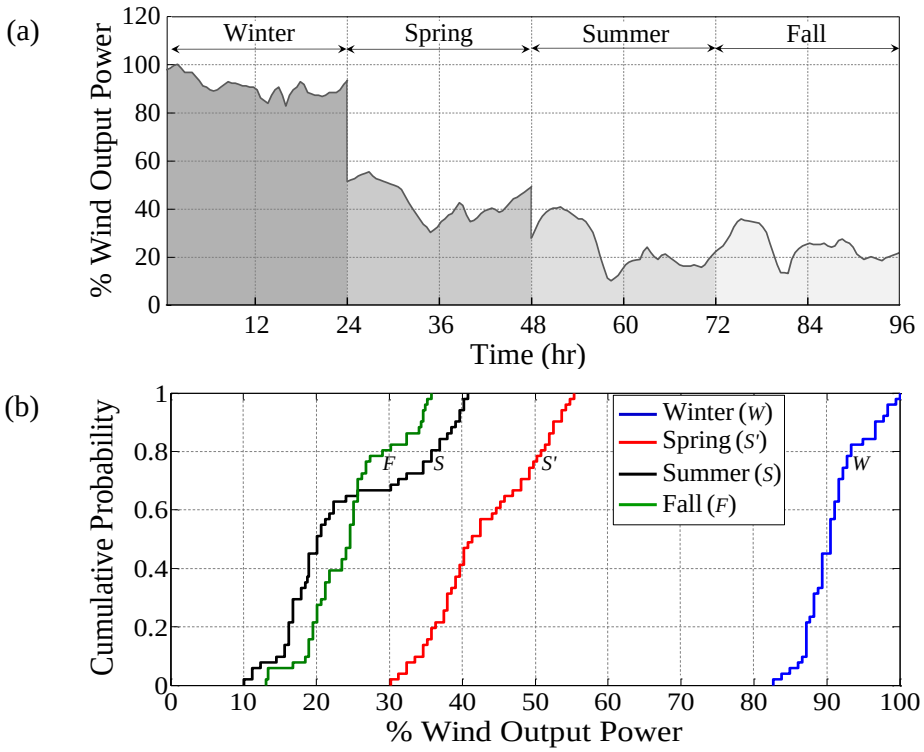

Figure 5.5: Variations in the wind DG output power: (a) power generated during a typical day in each season; (b) CDF for each typical day.

5.5.3 PV DG Output Power

Figure 5.6(a) shows the seasonal hourly variations in the PV output power, based on the historical data for three successive years provided in [94]. The hourly PV power generated during a typical day for each season is given as a percentage of the annual maximum output power. These four daily profiles were then used for deriving the CDFs presented in Figure 5.6(b).

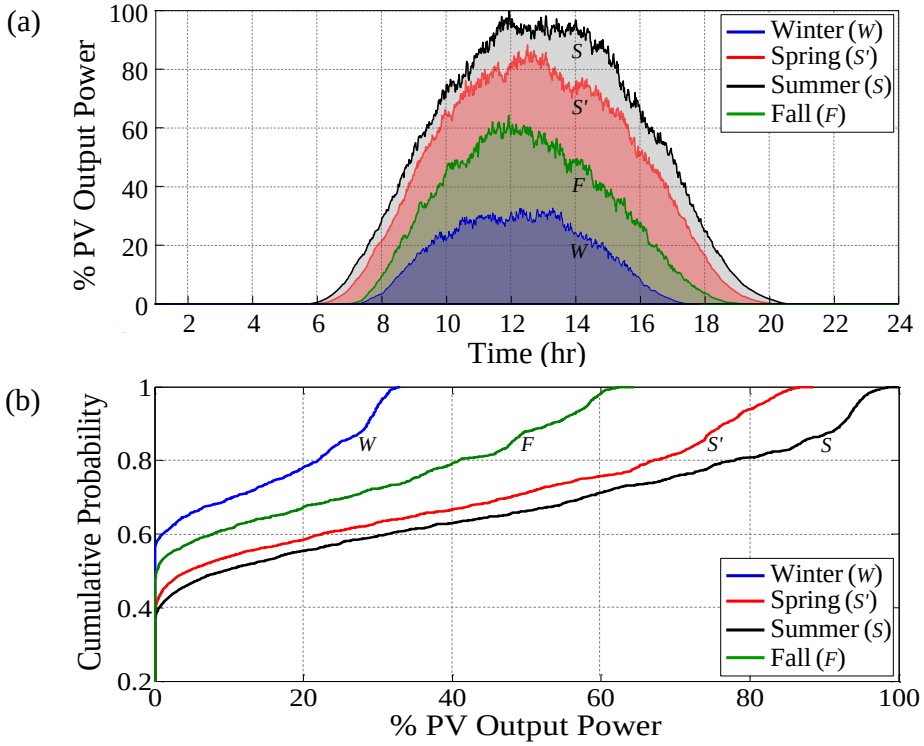

Figure 5.6: Variations in the PV output power: (a) power generated during a typical day in each season; (b) CDF for each typical day.

5.5.4 EV Charging Station Demand

The hourly load variation for an EV charging station for a typical day is illustrated in Figure 5.7(a), based on the 15-pole station model described in [95]. The hourly load demand of this typical day is given as a percentage of the peak demand of the station. This load profile was then used for deriving the CDF presented in Figure 5.7(b).

5.5.5 Best Fitting Distributions for the Stochastic Models

The aforementioned stochastic models are analyzed in order to generate the best fitting distributions. Table 5.1 shows the parameters of the best fitting distributions for the stochastic variables associated with load demands and renewable DGs. The Johnson SB distribution,

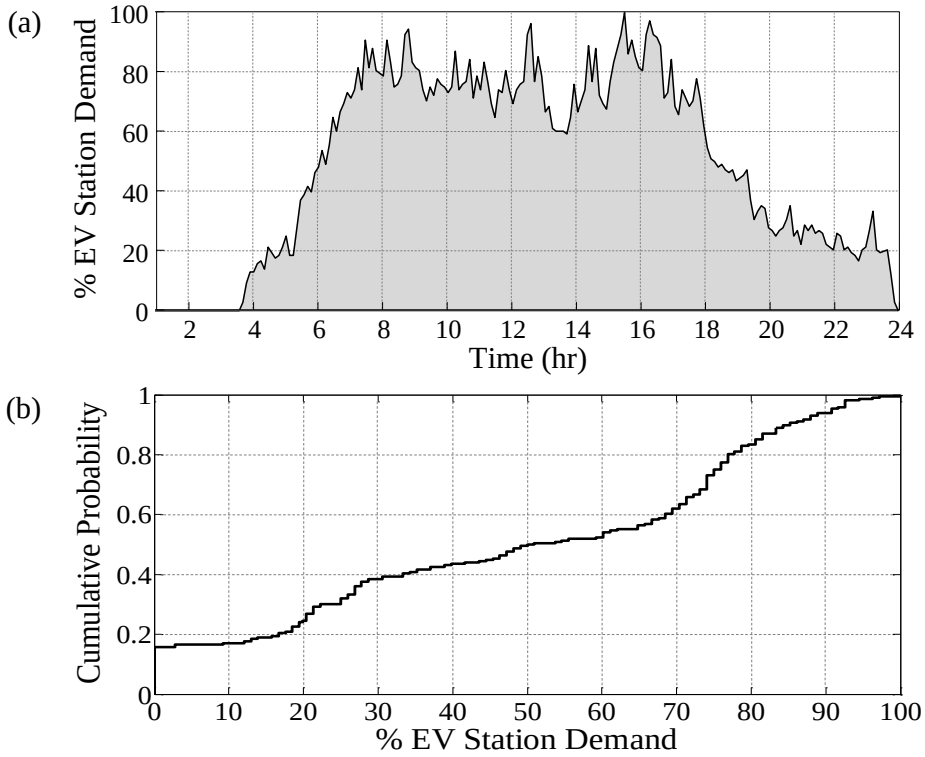

Figure 5.7: Variations in the EV charging station demand: (a) demand for a typical day; (b) CDF for the typical day.

expressed as (5.27) [96], was found to be the best fit for representing the stochastic models of PV-DG output power, wind-DG output power, and EV station demand.

$$F_1(x) = \Phi\left(\gamma + \delta \ln\left(\frac{z}{1-z}\right)\right) \tag{5.27}$$

where $F_1(x)$ is the CDF of the Johnson SB distribution; $z = \frac{x-\zeta}{\lambda}$; δ, γ are shape parameters; ζ is a location parameter; λ is a scale parameter; and $\Phi(\blacklozenge)$ is the Laplace integral (i.e., the CDF of the standard normal distribution), which is given by

$$\Phi(x) = \frac{1}{\sqrt{2\pi}} \int_0^x e^{-0.5\,t^2}\, dt \tag{5.28}$$

The generalized Pareto distribution, expressed as (5.29) [96], was found to be the best fit for representing the stochastic models of load demands.

$$F_2(x) = 1 - \left(1 + k\frac{(x-\mu)}{\sigma}\right)^{-\frac{1}{k}} \quad , \quad k \neq 0 \tag{5.29}$$

where $F_2(x)$ is the CDF of the generalized Pareto distribution, k is a shape parameter, μ is a location parameter, and σ is a scale parameter. The CDF parameters for the stochastic variables are shown in Table 5.1. For each stochastic variable, the parameters listed in Table 5.1 provide the stochastic variations of the variable as a percentage of its annual maximum value.

Table 5.1: CDF Parameters for the Stochastic Variables

Stochastic Variables	Seasons	CDF Parameters
PV-DG Power	Winter	γ= 0.6561, δ= 0.1853, λ= 30.5430, ζ= -0.4102
	Spring	γ= 0.4549, δ= 0.2182, λ= 81.8414, ζ= -1.3103
	Summer	γ= 0.4199, δ= 0.2332, λ= 96.1342, ζ= -1.6687
	Fall	γ= 0.6052, δ= 0.2301, λ= 59.0836, ζ= -1.0902
Wind-DG Power	Winter	γ= 1.4584, δ= 1.6624, λ= 32.9295, ζ= 80.6751
	Spring	γ= 0.1402, δ= 0.6340, λ= 25.9017, ζ= 30.9977
	Summer	γ= 0.3993, δ= 0.3682, λ= 28.1423, ζ= 13.8442
	Fall	γ= 0.7441, δ= 1.6674, λ= 43.7649, ζ= 7.0870
EV Station	All	γ= -0.1555, δ= 0.4199, λ= 94.1582, ζ= -4.1414
Load Demand	Winter	k= -2.0498, σ= 76.5706, μ= 33.8229
	Spring	k= -2.0299, σ= 64.7435, μ= 30.9216
	Summer	k= -2.1535, σ= 123.2435, μ= 43.8349
	Fall	k= -2.0299, σ= 60.6328, μ= 28.9583

5.6 Case Study

The system examined in the case study includes 13 zones, each including generally different types of elements: AC and/or DC loads and/or DGs. The zones are clustered according to the geographical location of each element in the system. Each zone can be represented by a bus, which has the flexibility to become either AC or DC, as shown in Figure 5.8.

The distribution substation (DSS) of the utility grid is connected at bus (1). The goal is to determine a suitable DS that can optimally accommodate all of the loads and DGs represented in the case study.

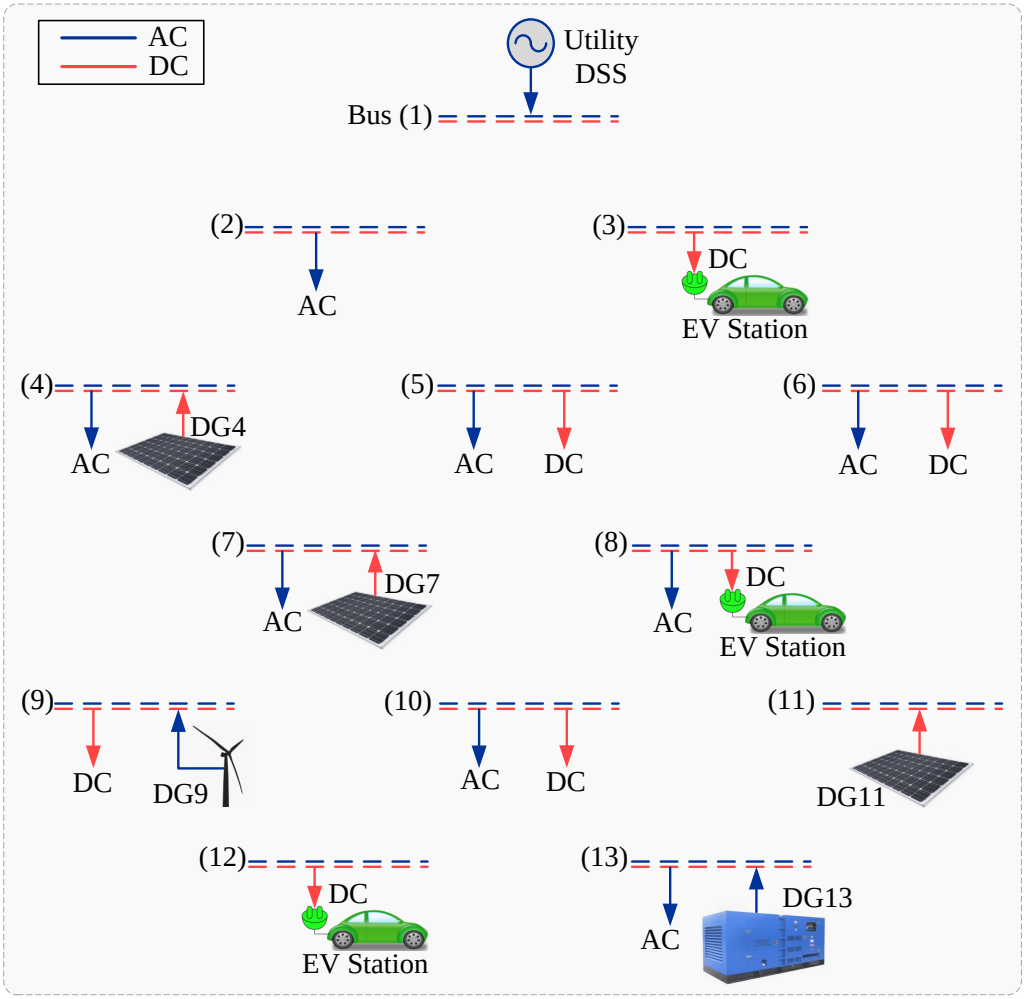

Figure 5.8: Thirteen-bus case study system.

5.6.1 System Parameters

Different types of loads and generators are represented in the system under study. Table 5.2 lists the generator data, including the active power limits, the reactive power limits, and

the energy costs for electric power in Ontario, Canada [88, 89]. It is assumed that all renewable-based DGs are owned by private customers and are operated according to the FIT program [89]. The operation costs of these renewable DGs represent the tariff paid by the utility to the DG owners.

Table 5.2: Data for the System Generators

DG No.	DG Type	P_G^{max} (MW)	P_G^{min} (MW)	Q_G^{max} (MVAr)	Q_G^{min} (MVAr)	Energy Cost ($/MWh)
G1	DSS, AC	10.0	1.0	4.80	0.80	92.20
DG4	Solar PV, DC	1.50	–	–	–	209.0
DG7	Solar PV, DC	1.50	–	–	–	209.0
DG9	Wind DG, AC	1.00	–	–	–	128.0
DG11	Solar PV, DC	1.50	–	–	–	209.0
DG13	Diesel DG, AC	2.00	0.2	0.96	0.10	92.20

The peak demands of the AC and DC loads at each bus are given in Table 5.3. The demand data are for the planning horizon year (year #15). A 0.7 % annual rate of growth in Canadian energy demand [97] was used for this case study.

Table 5.3: Load Demands at System Buses

	AC Loads		DC Loads
Bus No.	P_L^{ac} (MW)	Q_L^{ac} (MVAR)	P_L^{dc} (MW)
1	–	–	–
2	1.00	0.45	–
3	–	–	1.25
4	0.50	0.25	–
5	0.50	0.25	0.50
6	0.75	0.35	0.75
7	0.50	0.25	–
8	0.50	0.25	1.25
9	–	–	0.85
10	0.50	0.25	0.50
11	–	–	–
12	–	–	1.25
13	0.75	0.35	–

The determination of the geographical distances between each network bus and its neighbors is a key design feature. The following matrix (X) indicates the distances (in miles) between system buses and was used as input to the planning model.

$$X = \begin{bmatrix}
0.0 & 1.0 & 1.0 & 2.0 & 1.4 & 2.0 & 2.4 & 2.4 & 3.4 & 2.8 & 3.4 & 3.8 & 3.8 \\
1.0 & 0.0 & 1.4 & 1.0 & 1.0 & 2.4 & 1.4 & 2.0 & 2.4 & 2.4 & 3.0 & 2.8 & 3.4 \\
1.0 & 1.4 & 0.0 & 2.4 & 1.0 & 1.0 & 2.0 & 1.4 & 3.0 & 2.4 & 2.4 & 3.4 & 2.8 \\
2.0 & 1.0 & 2.4 & 0.0 & 1.4 & 2.8 & 1.0 & 2.8 & 1.4 & 2.0 & 3.4 & 2.4 & 3.0 \\
1.4 & 1.0 & 1.0 & 1.4 & 0.0 & 1.4 & 1.0 & 1.0 & 2.0 & 1.4 & 2.0 & 2.4 & 2.4 \\
2.0 & 2.4 & 1.0 & 2.8 & 1.4 & 0.0 & 2.4 & 1.0 & 3.4 & 2.0 & 1.4 & 3.0 & 2.4 \\
2.4 & 1.4 & 2.0 & 1.0 & 1.0 & 2.4 & 0.0 & 1.4 & 1.0 & 1.0 & 2.4 & 1.4 & 2.0 \\
2.4 & 2.0 & 1.4 & 2.4 & 1.0 & 1.0 & 1.4 & 0.0 & 2.4 & 1.0 & 1.0 & 2.0 & 1.4 \\
3.4 & 2.4 & 3.0 & 1.4 & 2.0 & 3.4 & 1.0 & 2.4 & 0.0 & 1.4 & 2.8 & 1.0 & 2.4 \\
2.8 & 2.4 & 2.4 & 2.0 & 1.4 & 2.0 & 1.0 & 1.0 & 1.4 & 0.0 & 1.4 & 1.0 & 1.0 \\
3.4 & 3.0 & 2.4 & 3.4 & 2.0 & 1.4 & 2.4 & 1.0 & 2.8 & 1.4 & 0.0 & 2.4 & 1.0 \\
3.8 & 2.8 & 3.4 & 2.4 & 2.4 & 3.0 & 1.4 & 2.0 & 1.0 & 1.0 & 2.4 & 0.0 & 1.4 \\
3.8 & 3.4 & 2.8 & 3.0 & 2.4 & 2.4 & 2.0 & 1.4 & 2.4 & 1.0 & 1.0 & 1.4 & 0.0
\end{bmatrix}$$

Table 5.4 indicates other input parameters employed in the case study. $AWG\#4/0$ aluminum conductor steel-reinforced (ACSR) cables were used for the AC and DC network lines. The DC resistance of this type of cable is (0.4415 Ω/mile), while the AC impedance is $(0.4435 + j0.726\ \Omega/\text{mile})$ [98]. Table 5.5 shows the candidate capacities for the AC-DC converters that can be used to connect the system loads and DGs to the network buses.

5.6.2 Simulation Results

To evaluate the effectiveness of the proposed planning strategy, the problem for the DS under study was solved using two planning models. The first employs traditional AC planning, with buses and lines assumed to be AC, so that all binary elements of the bus and line matrices (W and D) are zeros, while the binary elements of the connection matrix (U) are variables [103]. In the second method, the proposed hybrid planning model, all buses and lines can become either AC or DC, so that the binary elements of all configuration matrices (W, U, and D) are variables. The solutions provided by the AC and hybrid planning models are presented in Figure 5.9 and Figure 5.10, respectively.

Table 5.4: Input Parameters for the Planning Model

Base values $(S_{base}, V^{ac}_{base}, V^{dc}_{base})$	10 MVA, 4.16 kV, 6.8 kV, respectively.
Voltage magnitude limits, p.u.	$V^{min}_n = 0.95$, $V^{max}_n = 1.05$
Voltage angle limits, in rad	$\theta^{min}_n = -\pi/4$, $\theta^{max}_n = \pi/4$
Capacity of the lines, in MVA	$S^{max}_{nm} = 2.0$
Modulation index limits [99]	$M^{min}_{nm} = 0.77$, $M^{max}_{nm} = 1.0$
Efficiency of the AC-DC converters	95 %
Bus connectivity constraints	$N^{min}_{l,n} = 1$, $N^{max}_{l,n} = 4$
Number of MCS scenarios	10,000 [90]
Type of the DC system	Unipolar
Cost of lines, in k$/mile	28.0 per single conductor [100]
Cost of converters, in $/kVA	170 [101]
Annual maintenance cost (β_m)	5 % of the investment cost (IC)
Planning period (T_P), in years	15
Discount rate (d)	7.5 % [102]

Table 5.5: Capacities of the Candidate AC-DC Converters Used for the Connection of the Loads and Generators at the System Buses (in MVA)

Bus No. (n)	DC Loads	DC DGs	AC Loads	AC DGs	If Bus (n) is AC		If Bus (n) is DC	
					Converters for DC loads	Converters for DC DGs	Converters for AC loads	Converters for AC DGs
1*	☐	☐	☐	☑	–	–	–	11.50
2	☐	☐	☑	☐	–	–	1.20	–
3	☑	☐	☐	☐	1.50	–	–	–
4	☐	☑	☑	☐	–	1.50	0.60	–
5	☑	☐	☑	☐	0.60	–	0.60	–
6	☑	☐	☑	☐	0.85	–	0.85	–
7	☐	☑	☑	☐	–	1.50	0.60	–
8	☑	☐	☑	☐	1.50	–	0.60	–
9	☑	☐	☐	☑	1.00	–	–	1.00
10	☑	☐	☑	☐	0.60	–	0.60	–
11	☐	☑	☐	☐	–	1.50	–	–
12	☑	☐	☐	☐	1.50	–	–	–
13	☐	☐	☑	☑	–	–	0.85	2.25

* The AC source at this bus is the DSS.

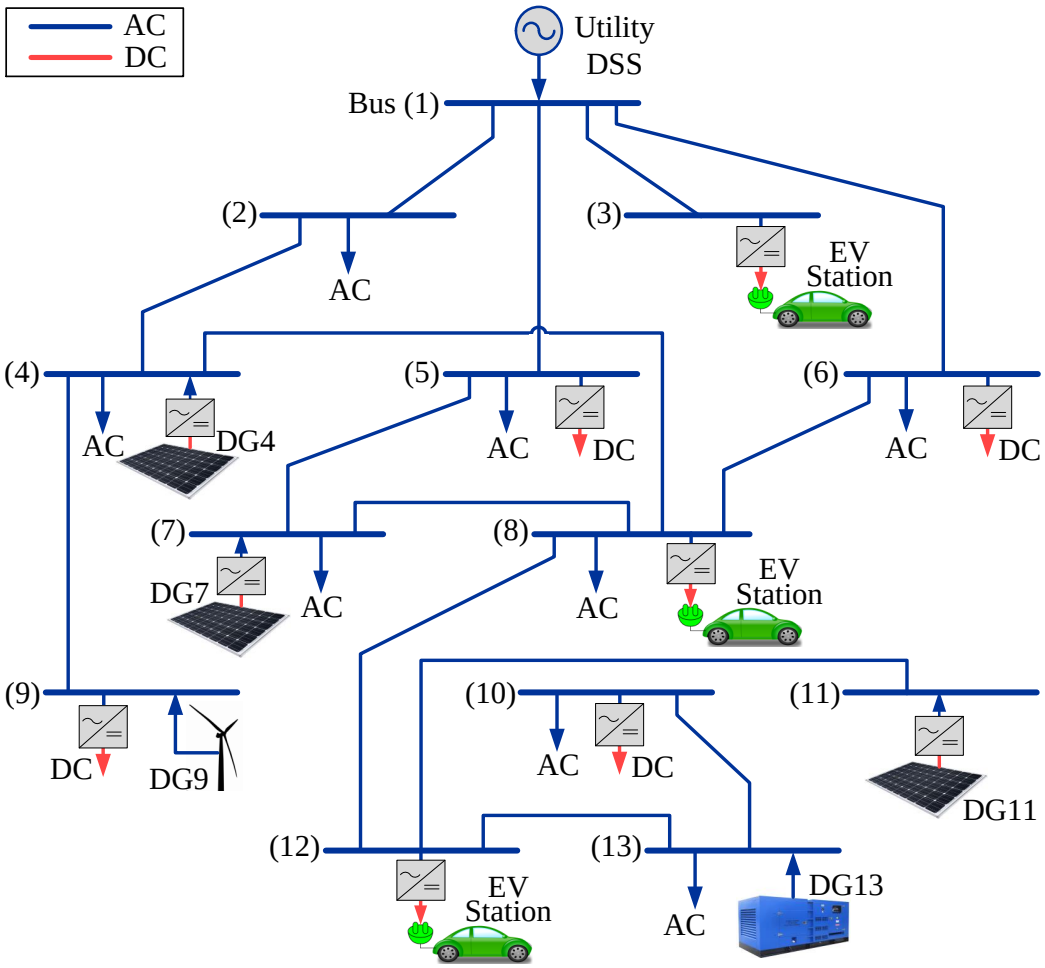

Figure 5.9: AC planning solution.

Table 5.6 summarizes the cost comparison between the AC solution and the hybrid solution. Figure 5.11 shows three cash flows: (a) the hybrid planning cash flow, in which the present cost value is 45.66 M$; (b) the AC planning cash flow, in which the present cost value is 47.36 M$; and (c) the differential cash flow, which represents the difference between (a) and (b). The present worth value of the cash flow in Figure 5.11(c) is calculated as 1.70 M$. For the DS under study, the hybrid planning method can thus clearly provide a cost saving of approximately 3.6 % of the total cost.

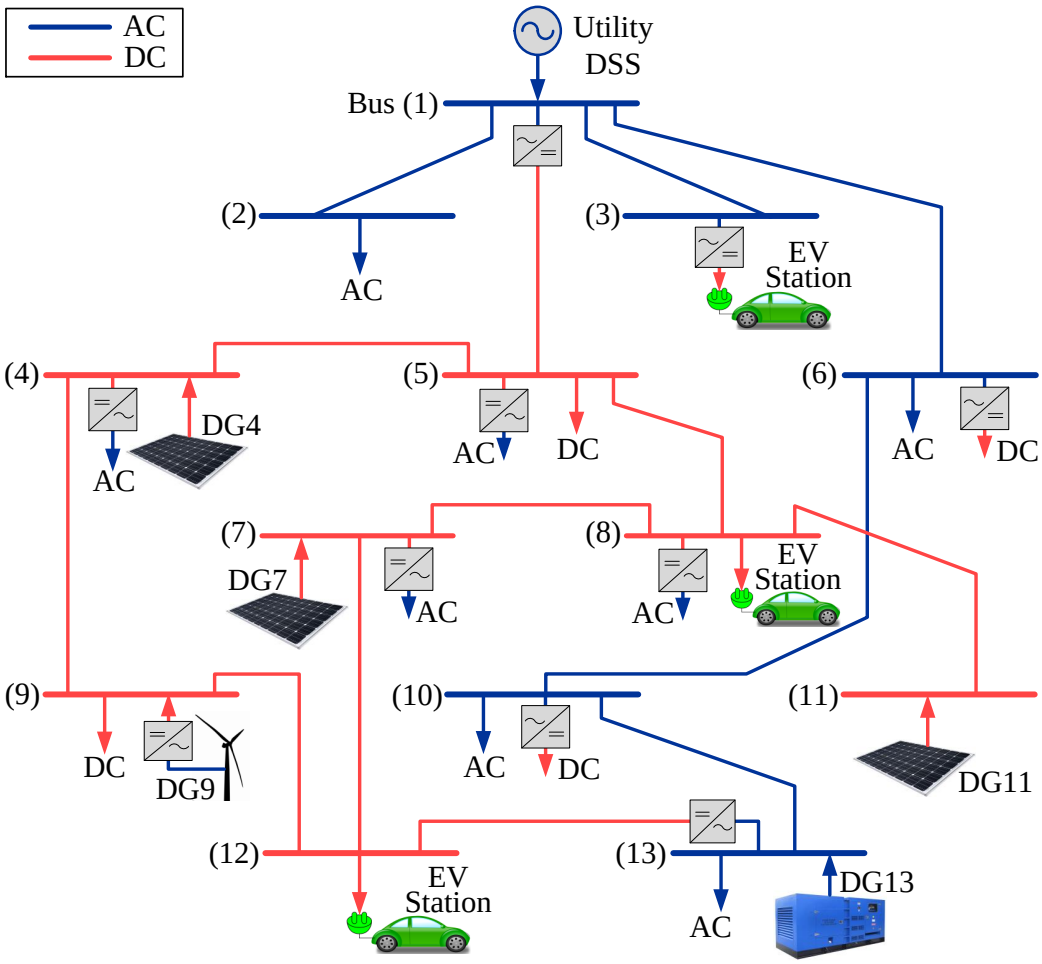

Figure 5.10: Hybrid planning solution.

Table 5.6: Comparison between the AC Solution and the Hybrid Solution

Costs	AC Solution	Hybrid Solution
Annual operation cost at year #15	5.0004 M$	4.9135 M$
Cost of network lines	1.7136 M$	1.2264 M$
Cost of system converters	2.0485 M$	1.7595 M$
Total investment cost	3.7621 M$	2.9859 M$
Total present cost value	47.360 M$	45.660 M$

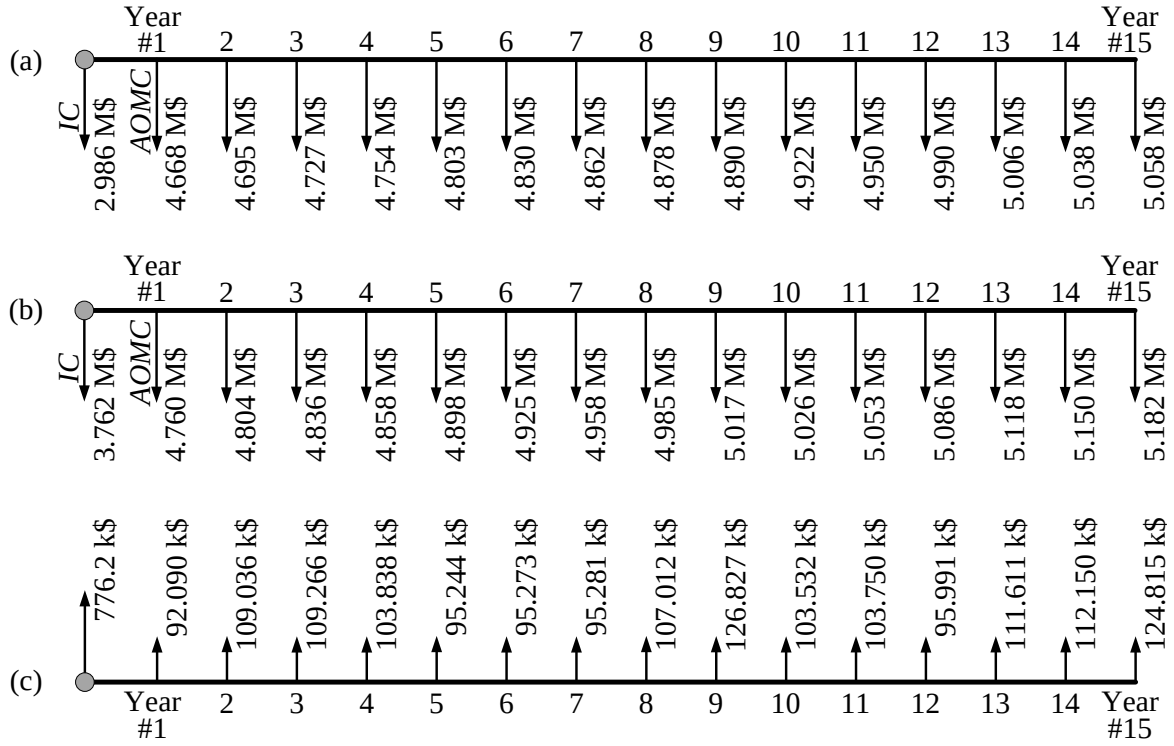

Figure 5.11: Cash flows: (a) cash flow for the hybrid solution; (b) cash flow for the AC solution; (c) differential cash flow (i.e., difference between (a) and (b)).

5.7 Conclusion

This chapter presents a novel stochastic planning model for AC-DC hybrid DSs. A connectivity profile has been introduced as a means of representing possible AC-DC hybrid bus and line configurations. Three binary matrices, proposed for describing the hybrid DS configuration, constitute the decision variables in the model. These matrices facilitate the flexibility to treat all buses and lines as either AC or DC in order to determine the optimal hybrid configuration that minimizes the DS investment and operation costs. The proposed model uses an MCS technique to enable consideration of the stochastic variations associated with the loads and renewable DGs. The hybrid planning problem presented in this chapter is formulated as two nested optimization problems: 1) the master problem is

formulated using a GA to search for the optimal hybrid configuration, and 2) the subproblem is used for determining the OPF solution for each configuration generated by the GA. The proposed planning model was tested on a 13-bus network that included different types of loads and DGs. The efficacy of the proposed model was verified through a comparison of its hybrid solution with the AC planning solution for the same case study. The proposed planning technique represents an efficient tool for the design of a truly AC-DC hybrid DS. The next chapter aims to incorporate the DS reliability as part of the formulation of the optimization problem, considering the failure rates of DS components.

Chapter 6

Reliability-Based Stochastic Planning for AC-DC Hybrid DSs

6.1 Introduction

This chapter completes the work presented in Chapter 5 through the development of a reliability-based stochastic planning model for the network configuration of AC-DC hybrid DSs. The new model presented in this chapter is formulated as a multi-objective optimization problem with two objectives: 1) minimize the investment and operation costs of the DS, and 2) maximize DS reliability, which can be achieved through minimization of the expected energy not supplied (EENS). The model input includes the failure rate data for hybrid DS components as well as the stochastic variations associated with load demands and renewable DGs. Consideration of these stochastic variations is included in the model through the use of an MCS technique. The model output comprises decisions about the optimal AC-DC network configuration that achieves the planning objectives. The model was applied for solving the DS planning problem of a case study. As a means of evaluating the effectiveness of the proposed model, the AC-DC hybrid solution provided by the model was compared with a purely AC solution for the same case study. For each of the two solutions, AC and hybrid, the relationship between system cost and reliability was explored through an examination of the Pareto front for the two objective functions.

This chapter is organized as follows: Section 6.2 describes the structure of the AC and DC buses and lines in hybrid DSs. Section 6.3 presents the formulation of the multi-objective optimization problem used for solving the hybrid planning problem. The planning procedures and methodology are introduced in Section 6.4. The case study used for evaluating the benefits provided by the proposed planning model is presented in Section 6.5, and the conclusions are summarized in Section 6.6.

6.2 Description of AC and DC Buses and Lines

As mentioned earlier in the previous chapters, hybrid DS buses and lines can be classified as shown in Figure 6.1 and Figure 6.2, respectively. Figure 6.1 shows the two possible types of buses (AC and DC) as well as the system load and DG connections to these buses. Figure 6.2 illustrates the possibilities for connecting AC/DC buses using AC/DC lines and VSCs. For the purposes of the study presented in this chapter, the primary goal of hybrid DS planning is to find the optimal network configuration that optimizes the DS costs and reliability. The network configuration is described by the binary matrices (W, U, and D), which are defined in Section 3.3. These matrices represent the planning decision variables.

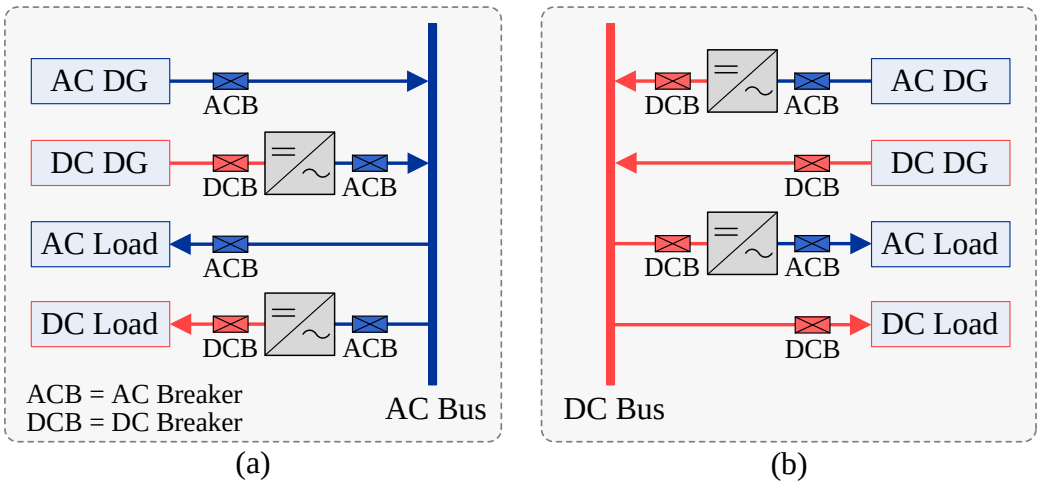

Figure 6.1: Hybrid DS buses: (a) AC bus; (b) DC bus.

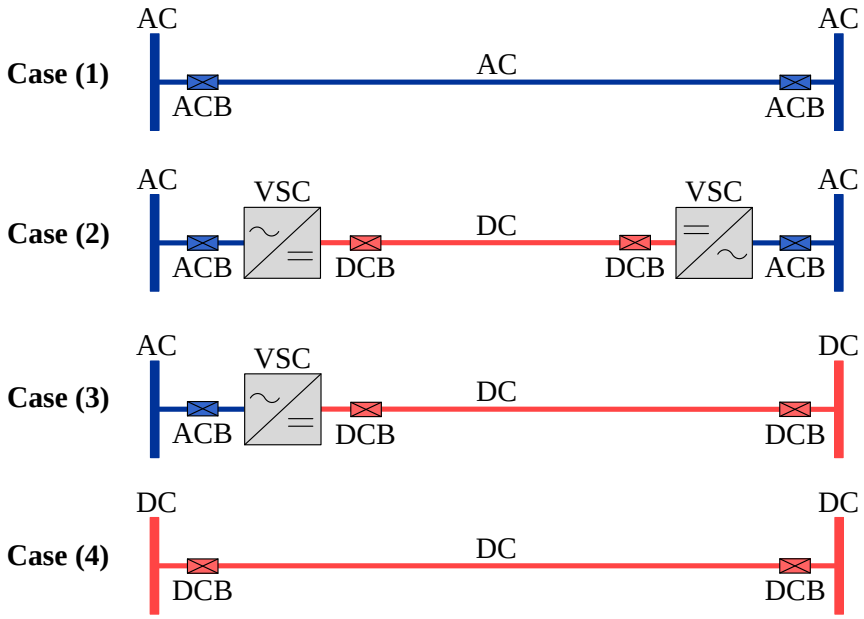

Figure 6.2: Possible AC-DC connections.

6.3 Modeling of the Hybrid Planning Problem

The planning model aims to simultaneously optimize the system costs and reliability in order to find the optimal AC-DC network configuration. The planning problem in this chapter is a multi-objective mixed-integer nonlinear programming problem with discontinuous derivatives, and it has been divided into two nested optimization problems: a master problem and a subproblem. The two problems are described in the following subsections.

6.3.1 Formulation of the Master Problem

The master problem is formulated using a multi-objective GA [87]. The first objective is to minimize the net present value of the system costs, while the second objective is to minimize the expected energy not supplied, as expressed in (6.1). The constraints can be classified into two groups: 1) integer constraints (5.5)-(5.7) for the binary variables of the configuration matrices, and 2) bus connectivity constraints (5.8)-(5.9), which are used for

identifying the minimum and maximum number of lines that can be connected to each bus in the DS network. The constraints of the master problem are on the independent variables (W, U, and D), whose values are used as input to the subproblem. The formulation of the master problem is as follows:

$$\min \; F_{master} = [\; C_{NPV} \quad EENS \;] \tag{6.1}$$

Subject to:

$$(5.5) - (5.9)$$

where

$$C_{NPV} = C_{INV} \; + \sum_{t=1}^{T_P} \frac{C_{AOM,t}}{(1+d)^t} \tag{6.2}$$

$$C_{AOM,t} = 8760 \; \mathbb{E}(C_{OPF,s,t}) + \beta_m \; C_{INV} \; , \; \forall \; t \in T_P \tag{6.3}$$

$$EENS = \sum_{t=1}^{T_P} \; \mathbb{E}(ENS_{s,t}) \tag{6.4}$$

The equations for C_{INV} and $ENS_{s,t}$ are as expressed in (6.5) and (6.6), respectively. As previously mentioned in Chapter 5, if a radial DS is needed, the value of $N_{l,n}^{min}$ in (5.8) is set to be 1 for all $n \in N_b$, and the constraint (5.10) is added to the formulation of the master problem.

$$\begin{aligned} C_{INV} = \sum_{n=1}^{N_b} \sum_{\substack{m=1 \\ m>n}}^{N_b} U_{nm} \Big[& \overline{W_n} \; \overline{W_m} \; D_{nm} \; (C_{dcl} \; X_{nm} + 2 \; C_{vsc\text{-}nm} + 2 \; C_{acb\text{-}nm} + 2 \; C_{dcb\text{-}nm}) \\ & + \overline{W_n} \; \overline{W_m} \; \overline{D_{nm}} \; (C_{acl} \; X_{nm} + 2 \; C_{acb\text{-}nm}) + W_n \; W_m \; D_{nm} \; (C_{dcl} \; X_{nm} + 2 \; C_{dcb\text{-}nm}) \\ & + (\overline{W_n} \; W_m \; D_{nm} + W_n \; \overline{W_m} \; D_{nm}) \, (C_{dcl} \; X_{nm} + C_{vsc\text{-}nm} + C_{acb\text{-}nm} + 2 \; C_{dcb\text{-}nm}) \Big] \\ + \sum_{n=1}^{N_b} \Big[& \overline{W_n} \left(C_{i\text{-}G_n^{dc}} + C_{acb\text{-}n\text{-}i} + C_{r\text{-}L_n^{dc}} + C_{acb\text{-}n\text{-}r} + C_{acb\text{-}G_n^{ac}} + C_{acb\text{-}L_n^{ac}} + C_{dcb\text{-}G_n^{dc}} + C_{dcb\text{-}L_n^{dc}} \right) \\ & + W_n \left(C_{r\text{-}G_n^{ac}} + C_{dcb\text{-}n\text{-}r} + C_{i\text{-}L_n^{ac}} + C_{dcb\text{-}n\text{-}i} + C_{acb\text{-}G_n^{ac}} + C_{acb\text{-}L_n^{ac}} + C_{dcb\text{-}G_n^{dc}} + C_{dcb\text{-}L_n^{dc}} \right) \Big] \end{aligned} \tag{6.5}$$

$$ENS_{s,t} = \sum_{n=1}^{N_b} \Bigg[\overline{W_n} \Big(P^{dc}_{Ln,s,t}(U_{f,bus\text{-}n} + U_{f,acb,L^{dc}_n} + U_{f,c\text{-}r,L^{dc}_n} + U_{f,dcb,L^{dc}_n}) + P^{ac}_{Ln,s,t}(U_{f,bus\text{-}n} + U_{f,acb,L^{ac}_n}) \Big) + W_n \Big(P^{ac}_{Ln,s,t}(U_{f,bus\text{-}n} + U_{f,dcb,L^{ac}_n} + U_{f,c\text{-}i,L^{ac}_n} + U_{f,acb,L^{ac}_n}) + P^{dc}_{Ln,s,t}(U_{f,bus\text{-}n} + U_{f,dcb,L^{dc}_n}) \Big) \Bigg], \quad \forall s \in \mathcal{N}_{MCS},\ t \in T_P \tag{6.6}$$

6.3.2 Formulation of the Subproblem

The subproblem is designed to solve the OPF problem for each MCS scenario for each GA chromosome. The subproblem constraints are on dependent variables, whose values are determined based on the values selected for the independent variables in the master problem. The objective function and the optimization constraints are identical to those of the subproblem in Chapter 5. The formulation of the subproblem can then be expressed as follows:

$$\min \left(\sum_{j=1}^{\mathfrak{B}^{ac}_G} C^{ac}_{G_j}\ P^{ac}_{G_j} + \sum_{l=1}^{\mathfrak{B}^{dc}_G} C^{dc}_{G_l}\ P^{dc}_{G_l} \right) \tag{6.7}$$

Subject to:

$$(5.12) - (5.25)$$

6.3.3 Calculations of the Probability of Failure at the System Buses

The probabilities of failure at the DS buses can be calculated based on the failure rate data for the distribution network components: AC/DC lines, AC/DC breakers, and AC-DC converters. For any DS component, the unavailability and the probability of failure can be calculated using (6.8) and (6.9), respectively.

$$U_f = \lambda_f\ \ t_f \tag{6.8}$$

$$Pr_f = U_f\ /\ 8760 \tag{6.9}$$

The probability of failure can be calculated for a number (K_s) of series components using (6.10), and can be calculated for a number (K_p) of parallel independent components using (6.11).

$$Pr_f = \sum_{k=1}^{K_s} Pr_{f,k} \tag{6.10}$$

$$Pr_f = \prod_{k=1}^{K_p} Pr_{f,k} \tag{6.11}$$

The six-bus network illustrated in Figure 6.3 provides an explanation of the way in which the unavailability $U_{f,bus\text{-}n}$ at the system buses can be calculated. Based on consideration of all possible paths from the source node to each load point, the unavailability at each bus can be calculated as shown in Table 6.1.

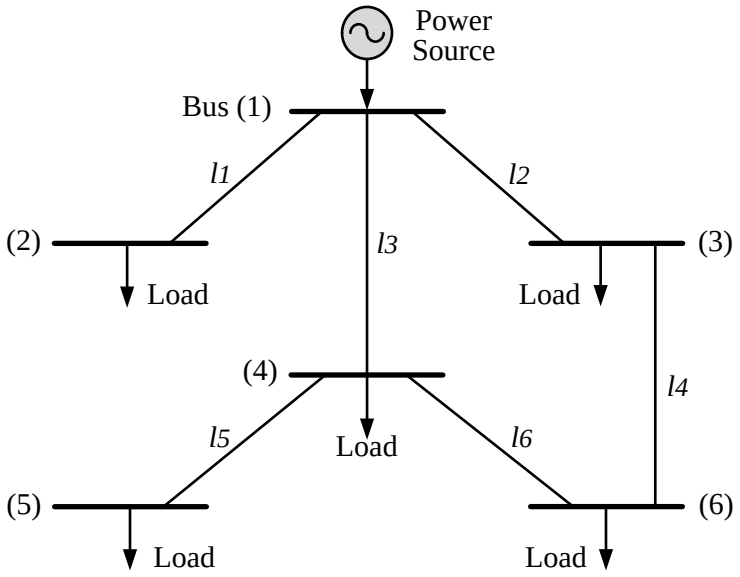

Figure 6.3: Example illustrating the calculation of unavailability at the system buses.

Each line in the hybrid DS network can be one of the four cases designated in Figure 6.2. For any line lx with a length L_{line}, the probability of failure can be calculated as shown in Table 6.2.

Table 6.1: Unavailability at the System Buses

Bus No. (n)	Unavailability ($U_{f,bus\text{-}n}$) (h/year)
2	$U_{f,bus\text{-}2} = 8760\,[Pr_{f,l1}]$
3	$U_{f,bus\text{-}3} = 8760\,[Pr_{f,l2}\,(Pr_{f,l3} + Pr_{f,l6} + Pr_{f,l4})]$
4	$U_{f,bus\text{-}4} = 8760\,[Pr_{f,l3}\,(Pr_{f,l2} + Pr_{f,l4} + Pr_{f,l6})]$
5	$U_{f,bus\text{-}5} = 8760\,[Pr_{f,l3}\,(Pr_{f,l2} + Pr_{f,l4} + Pr_{f,l6}) + Pr_{f,l5}]$
6	$U_{f,bus\text{-}6} = 8760\,[(Pr_{f,l2} + Pr_{f,l4})\,(Pr_{f,l3} + Pr_{f,l6})]$

Table 6.2: Probability of Failure for the Four Cases of AC-DC Connections

Case No.	Probability of Failure ($Pr_{f,lx}$)
(1)	$[\,2\,Pr_{f,acb} + Pr_{f,acl^1}\;L_{line}\,]$
(2)	$[\,2\,Pr_{f,dcb} + 2\,Pr_{f,acb} + 2\,Pr_{f,vsc} + Pr_{f,dcl^1}\;L_{line}\,]$
(3)	$[\,2\,Pr_{f,dcb} + Pr_{f,acb} + Pr_{f,vsc} + Pr_{f,dcl^1}\;L_{line}\,]$
(4)	$[\,2\,Pr_{f,dcb} + Pr_{f,dcl^1}\;L_{line}\,]$

[1] The failure rate data for the AC and DC lines are per circuit mile.

6.4 Planning Strategy and Procedures

The determination of the optimal AC-DC network configuration described by the matrices (W, U, and D) is the main goal of the proposed planning model. The planning model is formulated as a multi-objective optimization problem that has two objectives: 1) minimizing system costs, and 2) maximizing system reliability. The second objective is achieved through the minimization of the EENS in the system. The use of an MCS technique addresses the uncertainties related to the loads and renewable DGs. In this study, the Pareto optimality concept is used for the multi-objective optimization. A non-dominated sorting genetic algorithm (NSGA) is employed as a means of generating the optimal non-dominated Pareto front [104]. The solution sets for each GA generation are ranked based on an elitist genetic algorithm, which favors the individuals that have better fitness values and preserves diversity in the final Pareto front solutions [104]. The strategy underlying the

proposed planning model is shown in Figure 6.4, and the steps involved can be summarized as follows:

1. Select suitable GA chromosomes to form the initial GA population. Each chromosome represents a candidate AC-DC network configuration and consists of the binary elements of the configuration matrices (W, U, and D), as shown in Figure 5.3.

2. Perform Steps 3 to 7 for each chromosome in the current GA generation.

3. For the current chromosome, calculate the investment cost (C_{INV}) as well as the unavailability ($U_{f,bus\text{-}n}$) at each bus in the system.

4. Generate an MCS scenario that includes random values for the stochastic variables in the system. These stochastic variables include AC and DC load demands as well as renewable-based DGs.

5. Solve the subproblem to find the optimal operation cost of the current scenario. The OPF solution for different MCS scenarios is represented by the stochastic variable $C_{OPF,s}$.

6. Check the MCS stopping criterion, which can be determined by a) using a predefined number of MCS scenarios, or b) terminating the MCS process if the ratio between the standard deviation of $C_{OPF,s}$ and the mean of $C_{OPF,s}$ is less than a selected small tolerance ε [91]. If the MCS stopping criterion is satisfied, go to Step 7; otherwise, generate another MCS scenario and repeat Steps 5 and 6.

7. The minimum allowable number of feasible OPF solutions as a percentage of the total number of solutions for different MCS scenarios is defined as α_f^{min}. In this study, α_f^{min} is chosen to be 95 % in order to guarantee a lower level of stochastic risk. For any configuration, if α_f^{min} is achieved, the operation cost of this configuration is then represented by $\mathbb{E}(C_{OPF,s})$; otherwise, this configuration is rejected.

8. For all the current generation chromosomes, calculate C_{NPV} and $EENS$ using (6.2) and (6.4), respectively, and then evaluate the GA objective functions and constraints.

9. Examine the GA stopping criterion; if it is not satisfied, perform the GA operations (reproduction, crossover, and mutation) to update the GA generation.

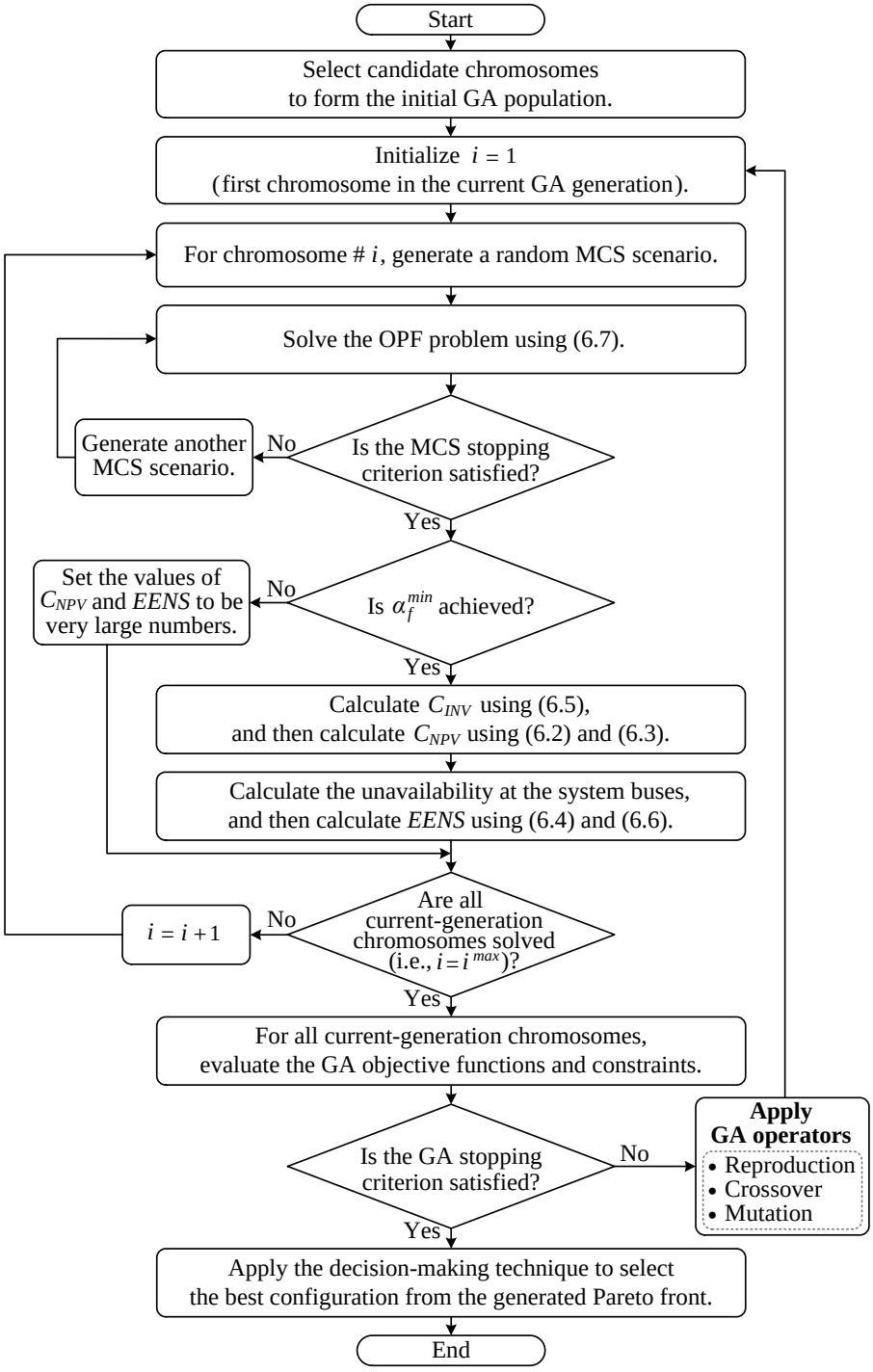

Figure 6.4: Flowchart for the reliability-based stochastic planning model.

10. Repeat Steps 2 to 9 until the GA stopping criterion is satisfied, following which, the non-dominated Pareto front is obtained.

11. Apply the decision-making technique expressed in (6.12) [91] to determine the best configuration from the generated Pareto front.

$$\min \; Z_p(x) = \left[\sum_{k=1}^{K} w_k^p \left| \frac{f_k(x) - f_k^0}{f_k^{max} - f_k^0} \right|^p \right]^{1/p} \tag{6.12}$$

where K is the total number of objectives ($K = 2$ in this study); f_k^0 is the value of objective k at the ideal point; $f_k(x)$ is the value of objective k at point $x \in X$; X is the total number of points in the Pareto front; f_k^{max} is the maximum value obtained for objective k; w_k is the weight assigned to objective k; and p defines the type of distance measure used.

The decision-making technique mentioned in Step 11 measures how close each solution in the Pareto front is to the ideal point. In a minimization problem, the ideal point is a fictitious point at which the value of each objective function is the minimum possible one. The DS planner can select the parameters (p, w_1, and w_2) according to his/her preferences. For example, in the case study presented in Section 6.5, the group dissatisfaction criterion was used (i.e., $p = 1$), which indicates that all deviations from the ideal point are directly proportional to their magnitude [91]. In addition, the two objectives were assumed to have equal priorities, so the weights were selected as ($w_1 = w_2 = 0.5$).

6.5 Case Study

This section presents the case study that was used for evaluating the effectiveness of the proposed planning model.

6.5.1 Description of the Case-Study System

Figure 6.5 shows a 14-zone case-study system that includes different types of AC and DC loads and DGs. Each zone in the system can be represented by a bus, which can be either AC or DC as needed for optimizing the planning objectives. The data given for the system loads and generators are listed in Table 6.3. The generator data include the active and

reactive power limits as well as the energy costs [88,89] for each generator. The costs of the renewable DGs represent the tariff paid to the DG owners [89]. The load data given in the table are the peak demands at the planning horizon year. The best-fitting distributions shown in Table 5.1 are used for representing the stochastic variables in the case-study system. These variables include: the demand associated with AC/DC loads, the output power of wind DGs, the output power of PV DGs, and the power demand of EV charging stations. The base values used in this case study are $S_{base} = 10\,\text{MVA}$, $V_{base}^{ac} = 4.16\,\text{kV}$, and $V_{base}^{dc} = 6.8\,\text{kV}$. Table 6.4 shows the failure data for hybrid DS components [105–107]. Other input parameters for the planning model are listed in Table 6.5.

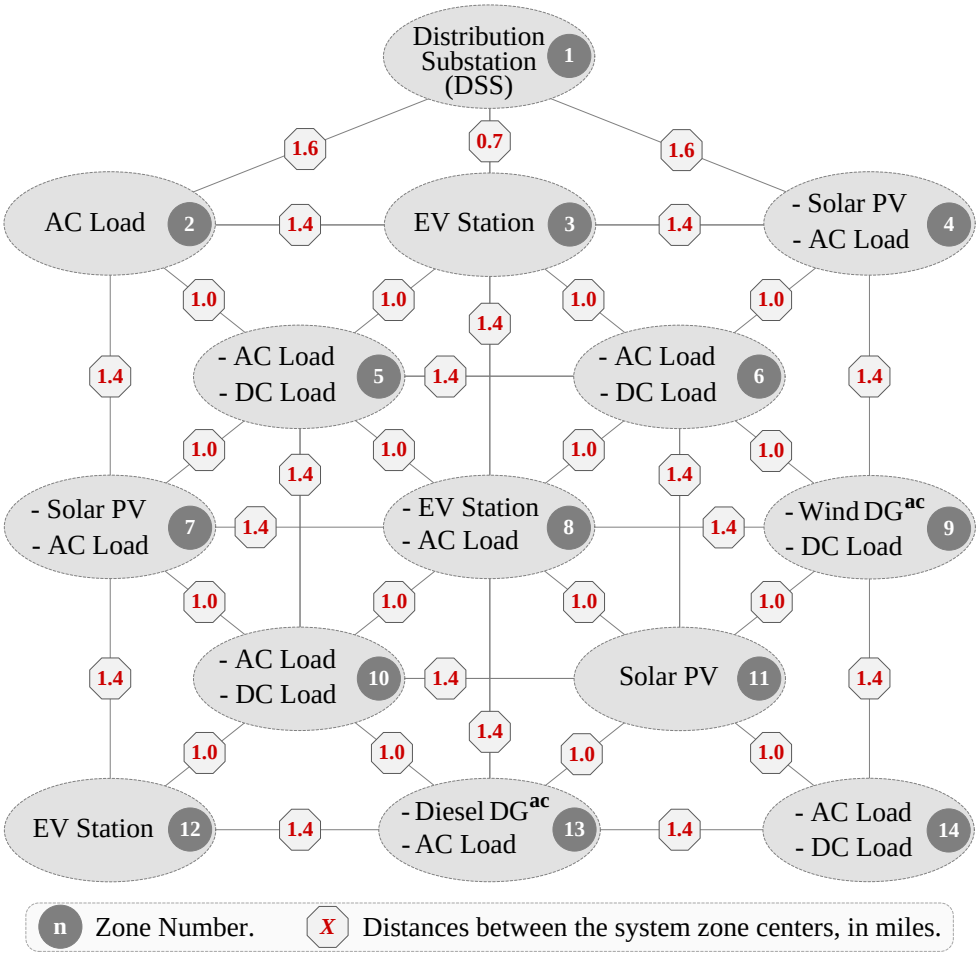

Figure 6.5: Fourteen-zone case-study system.

Table 6.3: Data for the System Loads and Generators

Zone No.	System Loads			System Generators				
	P_L^{ac} (MW)	Q_L^{ac} (MVAR)	P_L^{dc} (MW)	P_G^{max} (MW)	P_G^{min} (MW)	Q_G^{max} (MVAr)	Q_G^{min} (MVAr)	Energy Cost ($/MWh)
1*	–	–	–	10.0	1.00	4.80	0.80	92.20
2	1.00	0.45	–	–	–	–	–	–
3	–	–	1.25	–	–	–	–	–
4	0.50	0.25	–	1.75	–	–	–	209.0
5	0.50	0.25	0.50	–	–	–	–	–
6	0.75	0.35	0.75	–	–	–	–	–
7	0.50	0.25	–	1.75	–	–	–	209.0
8	0.50	0.25	1.25	–	–	–	–	–
9	–	–	0.85	1.00	–	–	–	128.0
10	0.50	0.25	0.50	–	–	–	–	–
11	–	–	–	1.75	–	–	–	209.0
12	–	–	1.25	–	–	–	–	–
13	0.75	0.35	–	2.25	0.20	1.00	0.10	92.20
14	0.50	0.25	0.50	–	–	–	–	–

* The energy source at this zone is the DSS.

Table 6.4: Failure Rates and Durations for Hybrid DS Components

Hybrid DS Components	Failure Rate λ_f (f/year)	Mean Down Time t_f (h/f)	Unavailability U_f (h/year)
AC Lines*	0.251330	4.000	$U_{f,acl} = 1.0053$
DC Lines*	0.335107	4.000	$U_{f,dcl} = 1.3404$
AC Breakers	0.018000	18.00	$U_{f,acb} = 0.3240$
DC Breakers	0.075000	3.000	$U_{f,dcb} = 0.2250$
Inverters	0.660515	5.321	$U_{f,c\text{-}i} = 3.5146$
Rectifiers	2.591962	3.471	$U_{f,c\text{-}r} = 8.9967$
VSCs	1.400000	4.100	$U_{f,vsc} = 5.7400$

* The failure rates for the AC and DC lines are per circuit mile.

Table 6.5: Input Parameters for the Planning Model

Voltage magnitude limits, p.u.	$V_n^{min} = 0.95$, $V_n^{max} = 1.05$
Voltage angle limits, in rad	$\theta_n^{min} = -\pi/4$, $\theta_n^{max} = \pi/4$
Capacity of the lines	$S_{nm}^{max} = 2.0$ MVA
Efficiency of AC-DC converters	95 %
Modulation index limits [99]	$M_{nm}^{min} = 0.77$, $M_{nm}^{max} = 1.0$
Bus connectivity constraints	$N_{l,1\text{-}14}^{min} = 1$, $N_{l,1}^{max} = 4$, $N_{l,2\text{-}14}^{max} = 3$
Type of DC system	Unipolar
Type of AC/DC network lines	AWG #4/0 ACSR
AC impedance of AWG #4/0 ACSR	$0.4435 + \mathrm{j}\,0.726$ Ω/mile [98]
DC resistance of AWG #4/0 ACSR	0.4415 Ω/mile [98]
Number of MCS scenarios ($\mathcal{N}_{MCS}$)	10,000 [90]
Planning period (T_P)	15 years
Annual rate of load growth	0.7 % [97]
Discount rate (d)	7.5 % [102]
Cost of lines	28.0 k$/mile per single conductor [100]
Cost of AC-DC converters	170.0 $/kVA [101]
Cost of 1200 A AC/DC breakers	24.0 k$/unit [108]
Cost of 2000 A AC/DC breakers	26.0 k$/unit [108]
Annual maintenance cost (β_m)	5 % of the investment cost (C_{INV})

6.5.2 Results and Discussion

In order to assess the benefits provided by the proposed planning model, the AC-DC hybrid solution obtained from the proposed model was compared with a purely AC solution for the same case study. The AC solution was obtained using traditional AC planning, in which all buses and lines are assumed to be AC (i.e., the elements of the binary matrices W and D are zeros). The resultant Pareto fronts for the AC and hybrid solutions are shown in Figure 6.6. The decision-making technique presented in equation (6.12) was applied with the following parameters ($p = 1$, $w_1 = 0.5$, and $w_2 = 0.5$) in order to find the best solutions (i.e., the best compromises) provided by the AC and the hybrid planning models from the generated Pareto fronts. The best AC and hybrid systems are presented in Figure 6.7 and

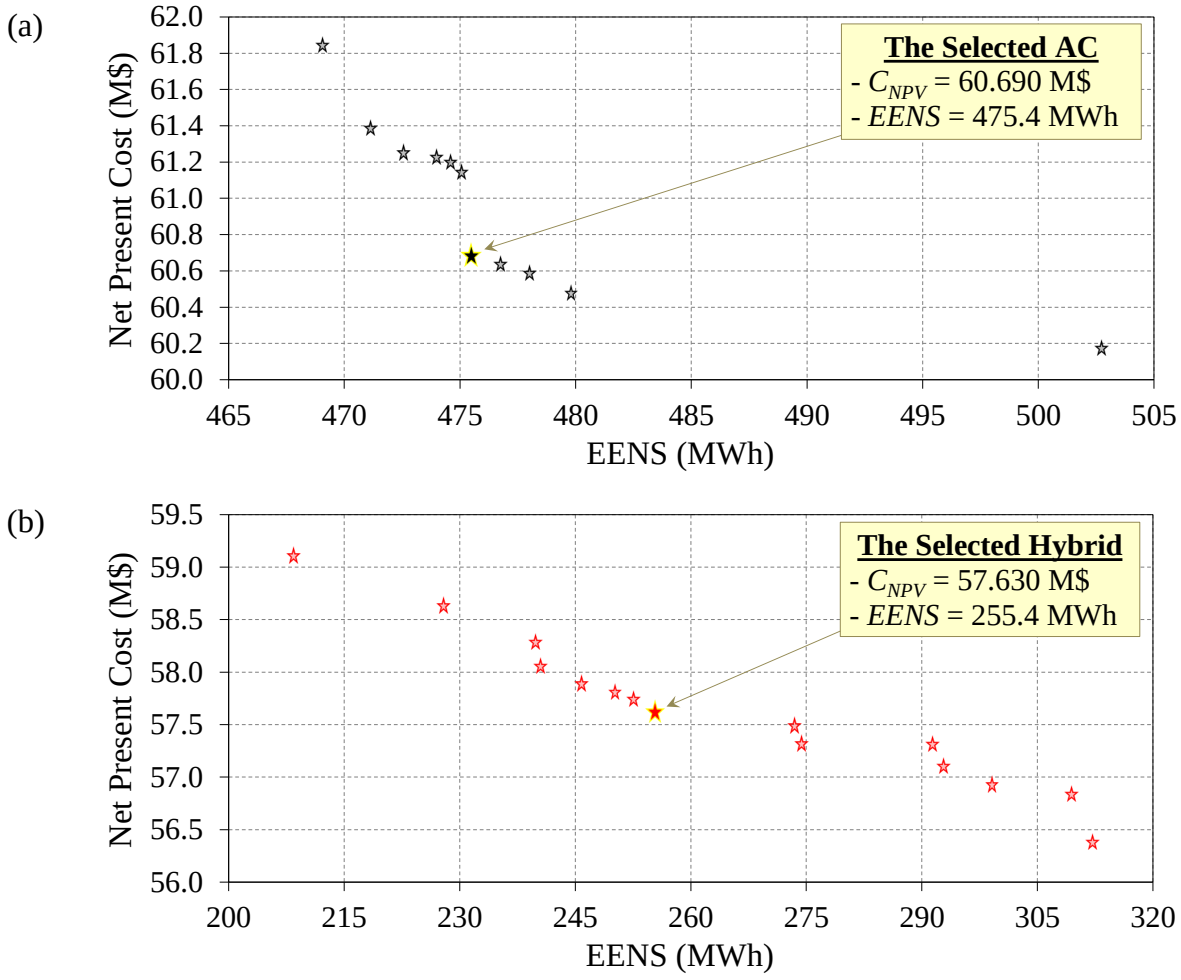

Figure 6.6: Pareto fronts for (a) the AC solution and (b) the hybrid solution.

Figure 6.8, respectively. The two objectives obtained for the AC system were found to be ($C_{NPV} = 60.69$ M$ and $EENS = 475.4$ MWh), while the two objectives obtained for the hybrid system were found to be ($C_{NPV} = 57.63$ M$ and $EENS = 255.4$ MWh). The results obtained demonstrate that, for the case under study, the proposed hybrid planning model has provided cost savings of 5.04 % as well as a significant 46.3 % reduction in the EENS. Additional comparisons presented in Table 6.6 further substantiate the superiority of the hybrid solution.

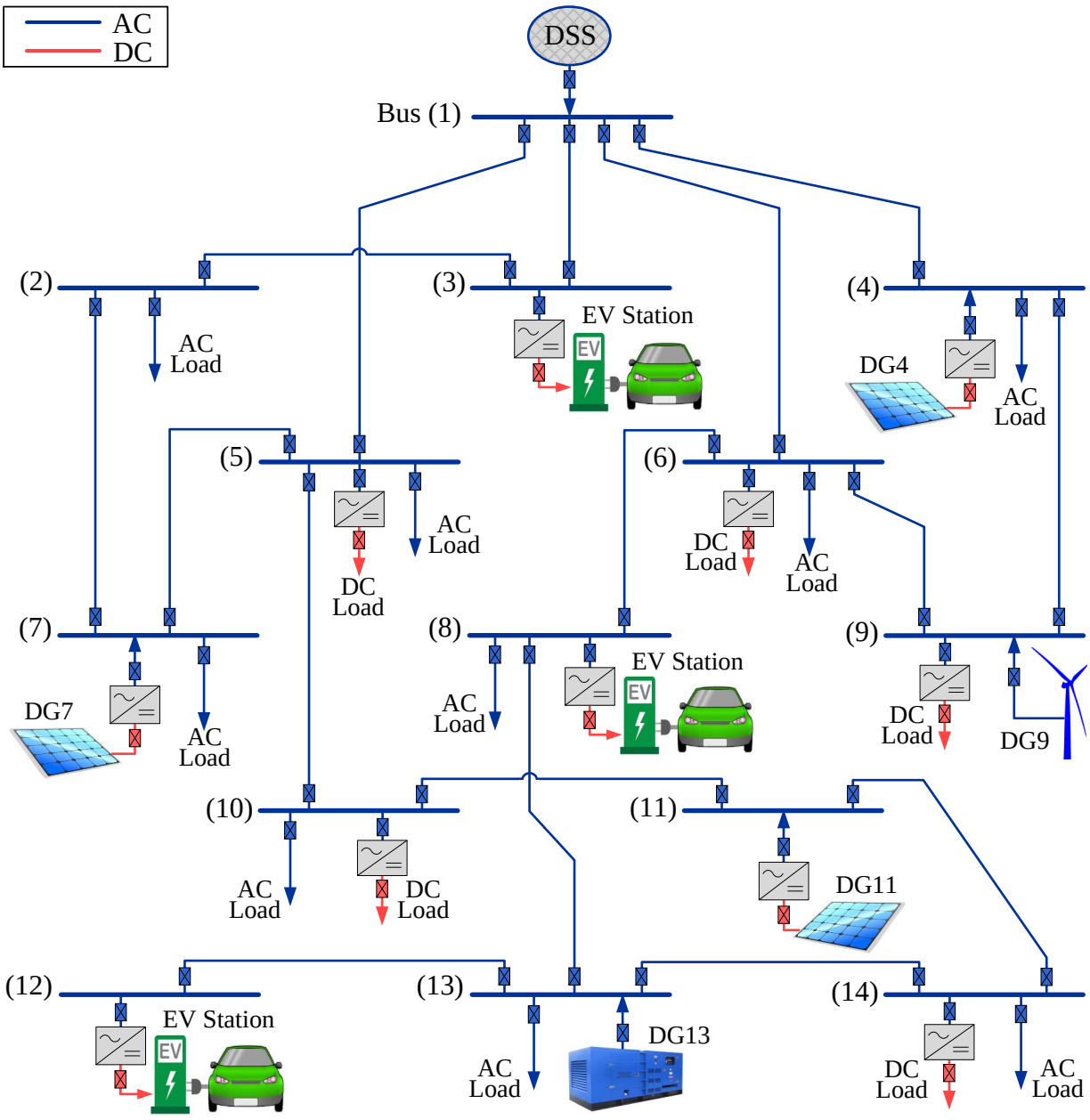

Figure 6.7: Best compromise solution obtained from the AC planning model.

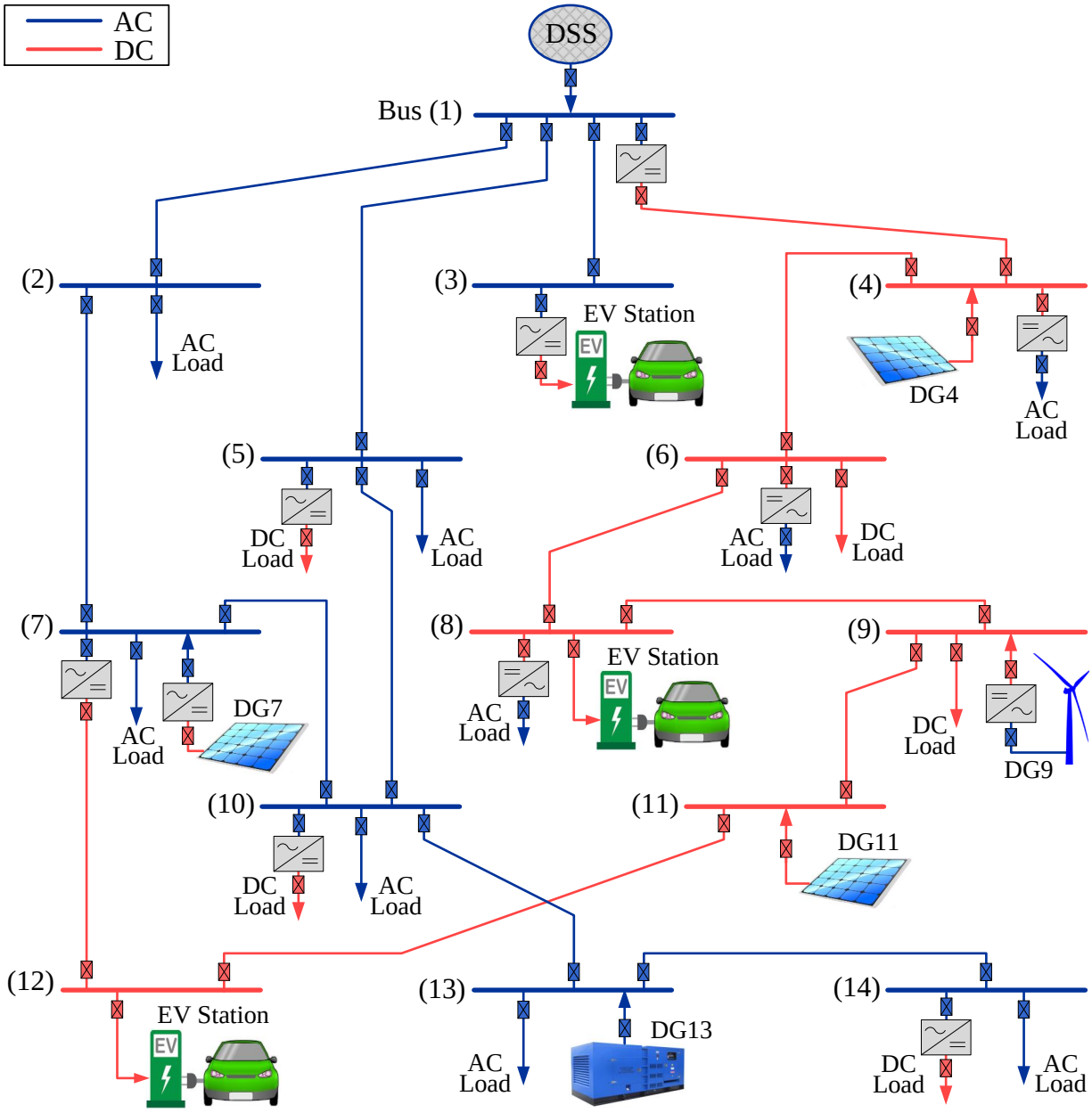

Figure 6.8: Best compromise solution obtained from the hybrid planning model.

Table 6.6: Comparison of the AC and Hybrid Solutions

	AC Solution	**Hybrid Solution**
C_{AOM} at planning horizon year	6.4662 M$	6.3231 M$
Cost of network lines	1.7556 M$	1.4056 M$
Cost of system converters	2.2780 M$	2.0570 M$
Cost of breakers	1.5860 M$	1.5380 M$
Total investment cost (C_{INV})	5.6196 M$	5.0006 M$
Net present cost (C_{NPV})	60.690 M$	57.630 M$
EENS at planning horizon year	32.757 MWh	18.002 MWh
Total EENS	475.40 MWh	255.40 MWh

It is worth mentioning that the Pareto fronts obtained from the proposed planning framework provide a general solution for the case under study, and the DS planner can select the suitable system according to his/her preferences. For example, if the goal of the DS planner is to only minimize the DS costs, the weights can then be selected as ($w_1 = 1.0$ and $w_2 = 0.0$), and the optimal solution obtained from the Pareto fronts will be ($C_{NPV} = 60.18$ M$ and $EENS = 502.7$ MWh) for the AC system and ($C_{NPV} = 56.39$ M$ and $EENS = 312.2$ MWh) for the hybrid system. On the other hand, if the goal of the DS planner is to only minimize the EENS, the weights can then be selected as ($w_1 = 0.0$ and $w_2 = 1.0$), and the optimal solution obtained from the Pareto fronts will be ($C_{NPV} = 61.85$ M$ and $EENS = 469.1$ MWh) for the AC system and ($C_{NPV} = 59.11$ M$ and $EENS = 208.5$ MWh) for the hybrid system.

6.6 Conclusion

In this chapter, a stochastic multi-objective planning model has been proposed for determining the optimal network configuration of AC-DC hybrid DSs. The planning model goal is the simultaneous optimization of system costs and reliability. The model employs an MCS technique as a means of including consideration of the stochastic behavior of load demands and renewable DGs. The planning problem has been decomposed into a master

problem and a subproblem. The master problem is formulated using a multi-objective GA that generates different AC-DC configuration scenarios. The subproblem is formulated to solve the OPF problem for each MCS scenario for each GA chromosome. The trade-off between the DS costs and reliability is evaluated using the Pareto optimality concept, and an NSGA is used for generating the non-dominated Pareto front. The proposed model was employed for finding the optimal AC-DC network configuration for a 14-zone DS that included different types of AC and DC loads and DGs. The purely AC solution was obtained for the same case study and was compared with the AC-DC hybrid solution. A comparison of the Pareto fronts for the AC and hybrid solutions demonstrated that the hybrid solution resulted in a reduction in both the system costs and the EENS, which confirms the effectiveness of the proposed planning model. The investigation presented in this chapter proves that traditional AC systems may no longer be the best option for the design of future smart DSs.

Chapter 7

Summary, Contributions, and Directions for Future Work

7.1 Summary and Conclusions

The primary goal of the research presented in this thesis is to optimally accommodate the high penetration of DC loads and DC-based DGs in the current and future DSs. To achieve this goal, this thesis presents new approaches and techniques for the optimal planning and operation of AC-DC hybrid DSs. The research presented in this thesis includes four consecutive parts: 1) developing a unified AC-DC LF model to facilitate formulating the planning and operation algorithms for AC-DC hybrid DSs, 2) developing a two-stage EMS to guarantee optimal and reliable operation of AC-DC hybrid DSs, 3) developing a planning technique to determine the optimal AC-DC network configuration that minimizes the DS costs, and 4) developing a reliability-based planning framework for simultaneously optimizing the DS costs and reliability. A detailed summary of the four parts conducted in this thesis is highlighted below.

In the first part of this research, a unified LF model for AC-DC hybrid DSs was developed. Detailed analysis of this model was presented in Chapter 3. The developed model can solve the LF problem for the AC and DC portions of the hybrid DS simultaneously based on the integration of the AC and DC power equations into one unified model. VSCs

are used in the LF model for AC-DC power conversions. The LF model employs three binary matrices to describe the AC-DC configuration of any hybrid DS. These matrices enable a single configuration at a time to be activated in the unified power equations. In Chapter 3, the developed model was applied for solving the LF problem of grid-connected and isolated hybrid DSs that included a variety of types of loads, DGs, buses, and lines. As a means of evaluating the effectiveness and accuracy of the developed model, the LF solution was compared to the steady-state solution produced by PSCAD/EMTDC. The results demonstrate that the LF model can provide an accurate solution while also offering the flexibility and speed required for online smart-grid applications. The developed LF model is generic, flexible, and can be integrated in a variety of hybrid DS applications. Based on this unified LF model, a new EMS for hybrid DSs was developed in Chapter 4, and two novel planning techniques for the network configuration of AC-DC hybrid DSs were introduced in Chapters 5 and 6.

In the second part, a two-stage EMS is developed for achieving reliable and optimal operation of AC-DC hybrid DSs. In Stage 1 (i.e., the day-ahead stage), a reconfiguration algorithm is employed to determine the most efficient network configuration for each hour during the next day. The objective of the reconfiguration algorithm is to minimize DS energy losses, while considering the day-ahead forecasted data for load demands and renewable DGs. In Stage 2 (i.e., the real-time stage), an OPF-LCM technique is used to guarantee optimal operational schedule for the hybrid DS. The objective of the OPF-LCM technique is to minimize the DS operation costs and to guarantee reliable DS operation in the case of abnormal operating conditions. The proposed two-stage EMS was successfully tested on a case study of a hybrid DS that included different types of loads and DGs. The benefits provided by the proposed EMS were verified through a comparison of the EMS solution and the solution obtained from the base-case system.

Based on the unified LF model presented in Chapter 3, a novel planning approach for the network configuration of AC-DC hybrid DSs was developed in Chapter 5, which represents the third part of this research. The planning objective is to find the optimal network configuration of AC and DC buses and lines for the minimization of DS investment and operation costs. The developed planning model employs an MCS technique as a means of including consideration of the stochastic behavior of load demands and renewable DGs. The three binary matrices, which are used in Chapter 3 for describing the AC-DC hybrid

DS configuration, are employed as the decision variables of the planning model. These matrices facilitate the flexibility to treat all buses and lines as either AC or DC in order to achieve the planning objective. The developed planning model was tested on a case study of a hybrid DS that included different types of AC and DC loads and DGs. The solution derived by the model was then compared with the solution obtained using a traditional AC planning technique in order to evaluate the effectiveness of the developed model and the associated cost-savings.

The last part was directed to incorporate the DS reliability in the formulation of the planning problem, with the goal of determining the optimal network configuration of AC-DC hybrid DSs. The reliability-based planning model developed in Chapter 6 is formulated as a multi-objective optimization problem with two objectives: 1) minimizing the DS investment and operation costs, and 2) maximizing DS reliability, which can be achieved through minimization of the EENS. The model input includes the failure rate data for hybrid DS components as well as the stochastic variations associated with load demands and renewable DGs. Consideration of these stochastic variations is included in the model through the use of an MCS technique. The planning problem has been divided into two nested optimization problems: 1) the master problem is formulated using a multi-objective GA that generates different AC-DC configuration scenarios, and 2) the subproblem is formulated to solve the OPF problem for each MCS scenario for each GA chromosome. In the developed model, the Pareto optimality concept is applied, and an NSGA is used for generating the non-dominated Pareto front. The model was applied for solving the DS planning problem of a case study of a hybrid DS that included different types of AC and DC loads and DGs. As a means of evaluating the effectiveness of the proposed model, the AC-DC hybrid solution provided by the model was compared with a purely AC solution for the same case study. A comparison of the Pareto fronts for the AC and hybrid solutions demonstrated that the hybrid solution resulted in a reduction in both the system costs and the EENS, which confirms the effectiveness of the developed planning model.

The developed planning model provides a systematic approach for the design of a truly AC-DC hybrid DS and represents a powerful tool for DS planners that will enable them to identify the optimal AC-DC network configuration of future hybrid DSs.

7.2 Contributions

The main contributions of the work presented in this thesis can be highlighted as follows:

1. The development of a unified LF model for solving the LF problem of AC-DC hybrid DSs. The developed model can be applied in hybrid DSs with mixed configurations for AC/DC buses and AC/DC lines. The developed model is generic, versatile, and can be readily used for the planning and operation of AC-DC hybrid DSs.

2. The development of a two-stage EMS for the optimal operation of AC-DC hybrid DSs. In the first stage, a network reconfiguration algorithm is developed to determine the optimal day-ahead reconfiguration schedule for a hybrid DS. In the second stage, an OPF-LCM technique is employed for guaranteeing a reliable and optimal real-time operation of a hybrid DS.

3. The development of a novel stochastic planning model for the network configuration of AC-DC hybrid DSs. A connectivity profile has been introduced as a means of representing possible AC-DC hybrid bus and line configurations. The model searches for the optimal AC-DC network configuration that minimizes the DS investment and operation costs. The model incorporates consideration of the stochastic behavior of load demands and renewable DGs.

4. The development of a reliability-based stochastic planning model for AC-DC hybrid DSs. The developed model is formulated as a multi-objective optimization problem that has two objectives: 1) minimizing system costs, and 2) maximizing system reliability. The second objective is achieved through the minimization of the EENS in the system. Network buses and lines can become either AC or DC in order to achieve the planning objectives. The model features a Monte-Carlo simulation for addressing stochastic variations related to load demands and renewable DGs.

7.3 Directions for Future Work

Based on the work presented in this thesis, the following topics are suggested for future exploration:

1. Investigating and assessing the techno-economic impacts of battery storage systems on the planning and operation of AC-DC hybrid DSs. In this case, the planning and operation models should be developed to enable consideration of the charging and discharging cycles of battery storage systems.

2. The application of the reliability-based planning model for the design of isolated power systems (e.g., AC-DC hybrid microgrids).

3. The application of the developed planning model for the expansion of existing DSs using AC/DC interconnections.

4. The development of the introduced EMS to include consideration of different abnormal scenarios related to the failure of network lines and converters.

5. The development of the introduced EMS to include consideration of additional tools and techniques related to DSM programs as well as deregulated electricity markets (e.g., energy bidding and dynamic pricing).

References

[1] ABB-Canada. (2014, Dec.). Tesla vs Edison: the war of currents, 2011. [Online]. Available: http://www.abb.ca/cawp/seitp202/c646c16ae1512f8ec1257934004fa545.aspx.

[2] J. M. Guerrero, A. Davoudi, F. Aminifar, J. Jatskevich, and H. Kakigano, "Guest editorial: Special section on smart DC distribution systems," *IEEE Trans. Smart Grid*, vol. 5, no. 5, pp. 2473–2475, Sept 2014.

[3] T. Kaipia, P. Salonen, J. Lassila, and J. Partanen, "Possibilities of the low voltage DC distribution systems," *Nordac, Nordic Distribution and Asset Management Conference*, pp. 1–10, 2006.

[4] T. Kaipia, P. Salonen, J. Lassila, and J. Partanen, "Application of low voltage DC distribution system, a techno-economical study," *19th International Conference on Electricity Distribution, Vienna*, no. 0464, pp. 21–24, 2007.

[5] K. Kurohane, T. Senjyu, A. Yona, N. Urasaki, T. Goya, and T. Funabashi, "A hybrid smart AC/DC power system," *IEEE Trans. Smart Grid*, vol. 1, no. 2, pp. 199–204, Sept 2010.

[6] S. K. Chaudhary, J. M. Guerrero, and R. Teodorescu, "Enhancing the capacity of the AC distribution system using DC interlinks–A step toward future DC grid," *IEEE Trans. Smart Grid*, vol. 6, no. 4, pp. 1722–1729, 2015.

[7] M. S. ElNozahy and M. M. A. Salama, "Uncertainty-based design of a bilayer distribution system for improved integration of PHEVs and PV arrays," *IEEE Trans. Sustain. Energy*, vol. 6, no. 3, pp. 659–674, 2015.

[8] H. M. A. Ahmed, A. B. Eltantawy, and M. M. A. Salama, "A planning approach for the network configuration of AC-DC hybrid distribution systems," *IEEE Trans. Smart Grid*, vol. PP, no. 99, pp. 1–1, 2016.

[9] International Renewable Energy Agency (IRENA). (2015, May). Battery storage for renewables: market status and technology outlook, 2015. [Online]. Available: http://www.irena.org/DocumentDownloads/Publications/IRENA_Battery_Storage_report_2015.pdf.

[10] Solar Power Europe. (2016, Sept.). Global market outlook for solar power 2016-2020. [Online]. Available: http://www.solarpowereurope.org/insights/global-market-outllook/.

[11] National Resources Canada (nrcan). (2015, May). Energy Markets - Fact Book , 2014-2015. [Online]. Available: http://www.nrcan.gc.ca/sites/www.nrcan.gc.ca/files/energy/files/pdf/2014/14-0173EnergyMarketFacts_e.pdf.

[12] Canadian Solar Industries Association (CanSIA). (2017, June). Roadmap 2020: Powering Canada's future with solar electricity. [Online]. Available: http://www.cansia.ca/uploads/7/2/5/1/72513707/cansia_roadmap_2020_final.pdf.

[13] International Energy Agency (IEA). (2016, June). Global EV outlook 2016: Beyond one million electric cars. [Online]. Available: http://www.iea.org/publications/freepublications/publication/Global_EV_Outlook_2016.pdf.

[14] Ontario Power Authority. (2016, Feb.). Fit program. [Online]. Available: http://fit.powerauthority.on.ca/fit-program.

[15] Ministry of Transportation, Ontario, Canada. (2016, March). Electric vehicle incentive program (EVIP) guide. [Online]. Available: http://www.forms.ssb.gov.on.ca/mbs/ssb/forms/ssbforms.nsf/GetFileAttach/023-2096E~3/$File/2096E_Guide.pdf.

[16] D. Elliott, K. R. W. Bell, S. J. Finney, R. Adapa, C. Brozio, J. Yu, and K. Hussain, "A comparison of AC and HVDC options for the connection of offshore wind generation in Great Britain," *IEEE Trans. Power Del.*, vol. 31, no. 2, pp. 798–809, April 2016.

[17] A. Lotfjou, Y. Fu, and M. Shahidehpour, "Hybrid AC/DC transmission expansion planning," *IEEE Trans. Power Del.*, vol. 27, no. 3, pp. 1620–1628, 2012.

[18] S. A. Amamra, F. Colas, X. Guillaud, P. Rault, and S. Nguefeu, "Laboratory demonstration of a multi-terminal VSC-HVDC power grid," *IEEE Trans. Power Del.*, vol. PP, no. 99, pp. 1–1, 2017.

[19] E. Planas, J. Andreu, J. I. Garate, I. Martinez de Alegria, and E. Ibarra, "AC and DC technology in microgrids: A review," *Renewable and Sustainable Energy Reviews*, vol. 43, pp. 726–749, 2015. [Online]. Available: http://linkinghub.elsevier.com/retrieve/pii/S1364032114010065.

[20] J. J. Justo, F. Mwasilu, J. Lee, and J. W. Jung, "AC-microgrids versus DC-microgrids with distributed energy resources: A review," *Renewable and Sustainable Energy Reviews*, vol. 24, pp. 387–405, 2013. [Online]. Available: http://dx.doi.org/10.1016/j.rser.2013.03.067.

[21] F. Nejabatkhah and Y. W. Li, "Overview of power management strategies of hybrid AC/DC microgrid," *IEEE Trans. Power Electron.*, vol. 30, no. 12, pp. 7072–7089, Dec 2015.

[22] P. Salonen, T. Kaipia, P. Nuutinen, P. Peltoniemi, and J. Partanen, "An LVDC distribution system concept," *NORPIE, Nordic Workshop on Power and Industrial Electroncis*, 2008.

[23] G. Byeon, T. Yoon, S. Member, and S. Oh, "Energy management strategy of the DC distribution system in buildings using the EV service model," *IEEE Trans. Power Electron.*, vol. 28, no. 4, pp. 1544–1554, 2013.

[24] D. Dong, F. Luo, X. Zhang, D. Boroyevich, and P. Mattavelli, "Grid-interface bidirectional converter for residential DC distribution systems - Part 2: AC and DC interface design with passive components minimization," *IEEE Trans. Power Electron.*, vol. 28, no. 4, pp. 1667–1679, 2013.

[25] D. Salomonsson and A. Sannino, "Low-voltage DC distribution system for commercial power systems with sensitive electronic loads," *IEEE Trans. Power Del.*, vol. 22, no. 3, pp. 1620–1627, 2007.

[26] A. Sannino, G. Postiglione, and M. H. J. Bollen, "Feasibility of a DC network for commercial facilities," *IEEE Trans. Ind. Appl.*, vol. 39, no. 5, pp. 1499–1507, 2003.

[27] L. Powell, *Power System Load Flow Analysis*. McGraw Hill professional, 2004.

[28] A. R. Bergen, *Power Systems Analysis*. Pearson Education India, 2009.

[29] M. E. El-Hawary, *Electrical Power Systems: Design and Analysis*. John Wiley & Sons, 1995, vol. 2.

[30] J. Grainger and W. Stevenson, *Power system analysis*, ser. McGraw-Hill series in electrical and computer engineering: Power and energy. McGraw-Hill, 1994.

[31] D. R. R. Penido, L. R. de Araujo, S. Carneiro, J. L. R. Pereira, and P. Garcia, "Three-phase power flow based on four-conductor current injection method for unbalanced distribution networks," *IEEE Transactions on Power Systems*, vol. 23, no. 2, pp. 494–503, May 2008.

[32] L. R. de Araujo, D. R. R. Penido, S. C. Jnior, J. L. R. Pereira, and P. A. N. Garcia, "Comparisons between the three-phase current injection method and the forward/backward sweep method," *International Journal of Electrical Power & Energy Systems*, vol. 32, no. 7, pp. 825 – 833, 2010.

[33] M. F. AlHajri and M. El-Hawary, "Exploiting the radial distribution structure in developing a fast and flexible radial power flow for unbalanced three-phase networks," *IEEE Transactions on Power Delivery*, vol. 25, no. 1, pp. 378–389, 2010.

[34] W. H. Kersting and D. L. Mendive, "An application of ladder network theory to the solution of three phase radial load flow problem," in *the IEEE PES Winter Meeting, New York*, 1976.

[35] W. Kersting, "A method to teach the design and operation of a distribution system," *IEEE Transactions on Power Apparatus and Systems*, vol. PAS-103, no. 7, pp. 1945–1952, July 1984.

[36] J. Beerten, S. Cole, and R. Belmans, "Generalized steady-state VSC MTDC model for sequential AC/DC power flow algorithms," *IEEE Trans. Power Syst.*, vol. 27, no. 2, pp. 821–829, 2012.

[37] L. G. L. Gengyin, Z. M. Z. Ming, H. J. H. Jie, L. G. L. Guangkai, and L. H. L. Haifeng, "Power flow calculation of power systems incorporating VSC-HVDC," *2004 International Conference on Power System Technology*, vol. 2, pp. 21–24, 2004.

[38] C. Liu, B. Zhang, Y. Hou, F. F. Wu, and Y. Liu, "An improved approach for AC-DC power flow calculation with multi-infeed DC systems," *IEEE Trans. Power Syst.*, vol. 26, no. 2, pp. 862–869, May 2011.

[39] M. Baradar and M. Ghandhari, "A multi-option unified power flow approach for hybrid AC/DC grids incorporating multi-terminal VSC-HVDC," *IEEE Trans. Power Syst.*, vol. 28, no. 3, pp. 2376–2383, 2013.

[40] K. N. Narayanan and P. Mitra, "A comparative study of a sequential and simultaneous AC-DC power flow algorithms for a multi-terminal VSC-HVDC system," *2013 IEEE Innovative Smart Grid Technologies, ISGT Asia*, 2013.

[41] M. Baradar, M. R. Hesamzadeh, and M. Ghandhari, "Second-order cone programming for optimal power flow in VSC-type AC-DC grids," *IEEE Trans. Power Syst.*, vol. 28, no. 4, pp. 4282–4291, Nov 2013.

[42] Q. Li, M. Liu, and H. Liu, "Piecewise Normalized Normal Constraint Method Applied to Minimization of Voltage Deviation and Active Power Loss in an AC-DC Hybrid Power System," *IEEE Trans. Power Syst.*, vol. 30, no. 3, pp. 1243–1251, May 2015.

[43] R. Taghavi, A. R. Seifi, and M. Pourahmadi-Nakhli, "Fuzzy reactive power optimization in hybrid power systems," *International Journal of Electrical Power and Energy Systems*, vol. 42, no. 1, pp. 375–383, 2012.

[44] U. Kilic, K. Ayan, and U. Arifoglu, "Optimizing reactive power flow of HVDC systems using genetic algorithm," *International Journal of Electrical Power and Energy Systems*, vol. 55, pp. 1–12, 2014.

[45] A. A. Hamad, M. A. Azzouz, and E. F. E. Saadany, "A sequential power flow algorithm for islanded hybrid AC/DC microgrids," *IEEE Trans. Power Syst.*, vol. 31, no. 5, pp. 3961–3970, Sept 2016.

[46] A. A. Eajal, M. A. Abdelwahed, E. F. El-Saadany, and K. Ponnambalam, "Power flow analysis of AC/DC hybrid microgrids," in *2016 IEEE Electrical Power and Energy Conference (EPEC)*, Oct 2016, pp. 1–6.

[47] N. Eghtedarpour and E. Farjah, "Power control and management in a hybrid AC/DC microgrid," *IEEE Trans. Smart Grid*, vol. 5, no. 3, pp. 1494–1505, May 2014.

[48] S. Golshannavaz, S. Afsharnia, and F. Aminifar, "Smart distribution grid: Optimal day-ahead scheduling with reconfigurable topology," *IEEE Trans. Smart Grid*, vol. 5, no. 5, pp. 2402–2411, Sept 2014.

[49] C.-T. Su and C.-S. Lee, "Network reconfiguration of distribution systems using improved mixed-integer hybrid differential evolution," *IEEE Trans. Power Del.*, vol. 18, no. 3, pp. 1022–1027, July 2003.

[50] T. T. Nguyen and A. V. Truong, "Distribution network reconfiguration for power loss minimization and voltage profile improvement using cuckoo search algorithm," *International Journal of Electrical Power & Energy Systems*, vol. 68, pp. 233 – 242, 2015. [Online]. Available: http://www.sciencedirect.com/science/article/pii/S0142061514008023.

[51] R. Rajaram, K. S. Kumar, and N. Rajasekar, "Power system reconfiguration in a radial distribution network for reducing losses and to improve voltage profile using modified plant growth simulation algorithm with distributed generation (dg)," *Energy Reports*, vol. 1, pp. 116 – 122, 2015. [Online]. Available: http://www.sciencedirect.com/science/article/pii/S2352484715000165.

[52] S. Jena and S. Chauhan, "Solving distribution feeder reconfiguration and concurrent DG installation problems for power loss minimization by multi swarm cooperative PSO algorithm," in *2016 IEEE/PES Transmission and Distribution Conference and Exposition*, May 2016, pp. 1–9.

[53] S. Naveen, K. S. Kumar, and K. Rajalakshmi, "Distribution system reconfiguration for loss minimization using modified bacterial foraging optimization algorithm," *International Journal of Electrical Power & Energy Systems*, vol. 69, pp. 90

– 97, 2015. [Online]. Available: http://www.sciencedirect.com/science/article/pii/S0142061515000150.

[54] R. A. Jabr, R. Singh, and B. C. Pal, "Minimum loss network reconfiguration using mixed-integer convex programming," *IEEE Trans. Power Syst.*, vol. 27, no. 2, pp. 1106–1115, May 2012.

[55] H. M. Khodr, J. Martinez-Crespo, M. A. Matos, and J. Pereira, "Distribution systems reconfiguration based on OPF using Benders decomposition," *IEEE Trans. Power Del.*, vol. 24, no. 4, pp. 2166–2176, Oct 2009.

[56] M. Albadi and E. El-Saadany, "A summary of demand response in electricity markets," *Electric Power Systems Research*, vol. 78, no. 11, pp. 1989 – 1996, 2008. [Online]. Available: http://www.sciencedirect.com/science/article/pii/S0378779608001272.

[57] T. Logenthiran, D. Srinivasan, and T. Z. Shun, "Demand side management in smart grid using heuristic optimization," *IEEE Trans. Smart Grid*, vol. 3, no. 3, pp. 1244–1252, Sept 2012.

[58] M. Parvania, M. Fotuhi-Firuzabad, and M. Shahidehpour, "Iso's optimal strategies for scheduling the hourly demand response in day-ahead markets," *IEEE Trans. Power Syst.*, vol. 29, no. 6, pp. 2636–2645, Nov 2014.

[59] J. Liu, M. Kazemi, A. Motamedi, H. Zareipour, and J. Rippon, "Security-constrained optimal scheduling of transmission outages with load curtailment," *IEEE Trans. Power Syst.*, vol. PP, no. 99, pp. 1–1, 2017.

[60] A. Anastopoulou, I. Koutsopoulos, and G. D. Stamoulis, "Optimal targeting and contract offering for load curtailment in nega-watt markets," *IEEE Transactions on Control of Network Systems*, vol. PP, no. 99, pp. 1–1, 2016.

[61] A. A. Eajal, M. F. Shaaban, K. Ponnambalam, and E. F. El-Saadany, "Stochastic centralized dispatch scheme for AC/DC hybrid smart distribution systems," *IEEE Trans. Sustain. Energy*, vol. 7, no. 3, pp. 1046–1059, July 2016.

[62] P. T. Baboli, M. Shahparasti, M. P. Moghaddam, M. R. Haghifam, and M. Mohamadian, "Energy management and operation modelling of hybrid AC-DC microgrid," *IET Generation, Transmission and Distribution*, vol. 8, no. 10, pp. 1700–1711, October 2014.

[63] N. G. Boulaxis and M. P. Papadopoulos, "Optimal feeder routing in distribution system planning using dynamic programming technique and GIS facilities," *IEEE Trans. Power Del.*, vol. 17, no. 1, pp. 242–247, 2002.

[64] T. Fawzi, K. Ali, and S. El-Sobki, "A new planning model for distribution systems," *IEEE Trans. Power Appar. Syst.*, vol. PAS-102, no. 9, pp. 3010–3017, 1983.

[65] K. Aoki, K. Nara, T. Satoh, M. Kitagawa, and K. Yamanaka, "New approximate optimization method for distribution system planning," *IEEE Trans. Power Syst.*, vol. 5, no. 1, pp. 126–132, 1990.

[66] G. M. Delgado, J. Contreras, and J. M. Arroyo, "Joint expansion planning of distributed generation and distribution networks," *IEEE Trans. Power Syst.*, vol. 30, no. 5, pp. 2579–2590, Sept 2015.

[67] S. Haffner, L. Pereira, L. Pereira, and L. Barreto, "Multistage model for distribution expansion planning with distributed generation - part I: problem formulation," *IEEE Trans. Power Del.*, vol. 23, no. 2, pp. 915–923, 2008.

[68] H. Kuwabara and K. Nara, "Multi-year and multi-state distribution systems expansion planning by multi-stage branch exchange," *IEEE Trans. Power Del.*, vol. 12, no. 1, pp. 457–463, 1997.

[69] M. Gitizadeh, A. A. Vahed, and J. Aghaei, "Multistage distribution system expansion planning considering distributed generation using hybrid evolutionary algorithms," *Applied energy*, vol. 101, pp. 655–666, 2013.

[70] M. S. Nazar and M. R. Haghifam, "Multiobjective electric distribution system expansion planning using hybrid energy hub concept," *Electric Power Systems Research*, vol. 79, no. 6, pp. 899–911, 2009.

[71] E. G. Carrano, L. A. E. Soares, R. H. C. Takahashi, R. R. Saldanha, and O. M. Neto, "Electric distribution network multiobjective design using a problem-specific genetic algorithm," *IEEE Trans. Power Del.*, vol. 21, no. 2, pp. 995–1005, April 2006.

[72] O. A. Urquidez and L. Xie, "Smart targeted planning of VSC-based embedded HVDC via line shadow price weighting," *IEEE Trans. Smart Grid*, vol. 6, no. 1, pp. 431–440, 2015.

[73] H. Doagou-Mojarrad, H. Rastegar, and G. B. Gharehpetian, "Probabilistic multi-objective HVDC/AC transmission expansion planning considering distant wind/solar farms," *IET Science, Measurement Technology*, vol. 10, no. 2, pp. 140–149, 2016.

[74] W. Feng, S. Member, L. A. Tuan, L. B. Tjernberg, S. Member, A. Mannikoff, and A. Bergman, "A new approach for benefit evaluation of multi-terminal VSC-HVDC using a proposed mixed AC/DC optimal power flow," *IEEE Trans. Power Del.*, vol. 29, no. 1, pp. 432–443, 2014.

[75] S. S. Torbaghan, M. Gibescu, B. G. Rawn, and M. v. d. Meijden, "A market-based transmission planning for hvdc grid–case study of the north sea," *IEEE Trans. Power Syst.*, vol. 30, no. 2, pp. 784–794, March 2015.

[76] J. D. Glover, M. S. Sarma, and T. Overbye, *Power System Analysis and Design*. Cengage Learning, 2012.

[77] P. C. Loh, D. Li, Y. K. Chai, and F. Blaabjerg, "Autonomous operation of hybrid microgrid with AC and DC subgrids," *IEEE Trans. Power Electron.*, vol. 28, no. 5, pp. 2214–2223, May 2013.

[78] D. G. Holmes and T. A. Lipo, *Pulse Width Modulation for Power Converters: Principles and Practice*. John Wiley & Sons, 2003, vol. 18.

[79] A. Ravindran, K. M. Ragsdell, and G. V. Reklaitis, *Engineering Optimization: Methods and Applications*. John Wiley & Sons, New Jersey, 2006.

[80] GAMS Development Corp. (2015, Nov.). "GAMS–The Solver Manuals". [Online]. Available: http://www.gams.com/help/topic/gams.doc/solvers/allsolvers.pdf.

[81] M. M. A. Abdelaziz, H. E. Farag, E. F. El-Saadany, and Y. A. R. I. Mohamed, "A novel and generalized three-phase power flow algorithm for islanded microgrids using a newton trust region method," *IEEE Trans. Power Syst.*, vol. 28, no. 1, pp. 190–201, Feb 2013.

[82] M. E. Baran and F. F. Wu, "Network reconfiguration in distribution systems for loss reduction and load balancing," *IEEE Trans. Power Del.*, vol. 4, no. 2, pp. 1401–1407, Apr 1989.

[83] H. M. A. Ahmed, A. B. Eltantawy, and M. M. A. Salama, "A generalized approach to the load flow analysis of AC-DC hybrid distribution systems," *IEEE Trans. Power Syst.*, vol. PP, no. 99, pp. 1–1, 2017.

[84] D. E. Olivares, C. A. Caizares, and M. Kazerani, "A centralized energy management system for isolated microgrids," *IEEE Trans. Smart Grid*, vol. 5, no. 4, pp. 1864–1875, July 2014.

[85] North American Electric Reliability Corporation (NERC). (2017, May). Reliability Standards for the Bulk Electric Systems of North America. [Online]. Available: http://www.nerc.com/pa/stand/reliability%20standards%20complete%20set/rscompleteset.pdf.

[86] L. A. Tuan and K. Bhattacharya, "Competitive framework for procurement of interruptible load services," *IEEE Trans. Power Syst.*, vol. 18, no. 2, pp. 889–897, May 2003.

[87] MathWorks. (2016, July). Global Optimization Toolbox, User's Guide. [Online]. Available: http://www.mathworks.com/help/pdf_doc/gads/gads_tb.pdf.

[88] Hydro-Qubec. (2016, Jan.). Comparison of electricity prices in major north american cities. [Online]. Available: http://www.hydroquebec.com/publications/en/docs/comparaison-electricity-prices/comp_2015_en.pdf.

[89] Ontario Power Authority. (2016, Feb.). Fit/microfit price schedule. [Online]. Available: http://fit.powerauthority.on.ca/sites/default/files/version4/FIT-Price-Schedule-2016-01-01.pdf.

[90] M. E. Nassar and M. M. A. Salama, "Adaptive self-adequate microgrids using dynamic boundaries," *IEEE Trans. Smart Grid*, vol. 7, no. 1, pp. 105–113, Jan 2016.

[91] H. Mostafa, R. El Shatshat, and M. Salama, "Optimal distribution systems operation using smart matching scheme (SMS) for smart grid applications," *IEEE Trans. Smart Grid*, vol. 5, no. 4, pp. 1938–1948, July 2014.

[92] S. Sivanandam and S. Deepa, *Introduction to genetic algorithms.* Springer Science & Business Media, 2007.

[93] Y. M. Atwa and E. F. El-Saadany, "Optimal allocation of ESS in distribution systems with a high penetration of wind energy," *IEEE Trans. Power Syst.*, vol. 25, no. 4, pp. 1815–1822, Nov 2010.

[94] Solar Powered in Toronto. (2015, Nov.). [Online]. Available: http://www.yourturn.ca/solar/our-system/graphs-and-logs/.

[95] Y. T. Liao and C. N. Lu, "Dispatch of EV charging station energy resources for sustainable mobility," *IEEE Trans. Transport. Electrific.*, vol. 1, no. 1, pp. 86–93, June 2015.

[96] MathWave Technologies. (2015, Nov.). Data analysis and simulation. [Online]. Available: http://www.mathwave.com/.

[97] National Energy Board, Government of Canada. (2015, April). Canada's energy future 2013, energy supply and demand projections to 2035. [Online]. Available: https://www.neb-one.gc.ca/nrg/ntgrtd/ftr/2013/2013nrgftr-eng.pdf.

[98] General Electric (GE). (2015, March). Distribution Data Book. [Online]. Available: http://www.electricalmanuals.net/files/APP-MANUALS/GE/GET-1008L.pdf.

[99] M. Kirik, " VSC-HVDC for long-term voltage stability improvement ," Master's thesis, Royal Institute of Technology (KTH), School of Electrical Engineering, Department of Electric Power Systems, Stockholm, 2009.

[100] One Stop Buy. (2015, April). Prices for power cables. [Online]. Available: http://www.onestopbuy.co/wire-cable/PENGUIN-41245.asp.

[101] B. McConnell, "Applications of high temperature superconductors to direct current electric power transmission and distribution," *IEEE Trans. Appl. Supercond.*, vol. 15, no. 2, pp. 2142–2145, June 2005.

[102] A. B. Eltantawy and M. M. A. Salama, "Management scheme for increasing the connectivity of small-scale renewable DG," *IEEE Trans. Sustain. Energy*, vol. 5, no. 4, pp. 1108–1115, Oct 2014.

[103] H. M. A. Ahmed, A. B. Eltantawy, and M. M. A. Salama, "A stochastic-based algorithm for optimal feeder routing of smart distribution systems," in *2017 IEEE 30th Canadian Conference on Electrical and Computer Engineering (CCECE)*, April 2017, pp. 1–4.

[104] K. Deb, A. Pratap, S. Agarwal, and T. Meyarivan, "A fast and elitist multiobjective genetic algorithm: NSGA-II," *IEEE Trans. Evolut. Comput.*, vol. 6, no. 2, pp. 182–197, Apr 2002.

[105] W. H. Dickinson, "Report on reliability of electric equipment in industrial plants," *Transactions of the American Institute of Electrical Engineers, Part II: Applications and Industry*, vol. 81, no. 3, pp. 132–151, July 1962.

[106] K. Linden, B. Jacobson, and M. Bollen, "Reliability study methodology for HVDC grids," *Paper B4-108, CIGRE Session, Paris*, pp. 1–10, 2010.

[107] P. S. Hale and R. G. Arno, "Survey of reliability and availability information for power distribution, power generation, and HVAC components for commercial, industrial, and utility installations," *IEEE Industrial and Commercial Power Systems Technical Conference*, pp. 31–54, 2000.

[108] ABB Sales. (2016, Nov.). Budgetary quote for medium voltage circuit breakers. [Online]. Available: http://new.abb.com/medium-voltage/apparatus/circuit-breakers.